UNIVERSITY OF CALIFORNIA
RIVERSIDE

Study of Molecular and Biological Properties of *Citrus exocortis viroid* and Dweet mottle virus

A Dissertation submitted in partial satisfaction
of the requirements for the degree of

Doctor of Philosophy

in

Plant Pathology

by

Subhas Hajeri

June 2010

Dissertation Committee:

Dr. James Ng, Committee Chairperson
Dr. Georgios Vidalakis
Dr. Shou-Wei Ding

The Dissertation of Subhas Hajeri is approved:

_____

_____

_____

Committee Chairperson

University of California, Riverside

ACKNOWLEDGEMENTS

It is a pleasure to thank those who made this doctoral study a wonderful life experience.

I would like to express my sincere gratitude to my major professor, Dr. Georgios Vidalakis (Director of Citrus Clonal Protection Program (CCPP), University of California, Riverside) for providing the opportunity to work on the most exciting plant pathogens, viroids. His constant guidance and critical comments enabled me to develop an understanding of the subject.

I would like to thank my dissertation committee: Dr. James Ng and Dr. Shou-Wei Ding (UC Riverside) for their encouragement, insightful comments and advice. My sincere thanks to Dr. James Ng for training me in plant cell culture.

Special thanks to Dr. Richard Lee (USDA-ARS National Clonal Germplasm Repository for Citrus and Dates, Riverside CA) for introducing me to the doctoral research on intriguing citrus virus. I am grateful to Chandrika Ramadugu (Department of Botany and Plant Science, UCR) and Manjunath Keremane (USDA-ARS) for their critical comments, guidance and support throughout the dissertation work.

Many thanks to Dr. Mohammad Afunian and Tavia Rucker in Dr. Vidalakis lab, Nida, Angel and Chawin in Dr. Ng lab for their constant help, cooperation and support to my studies. Special thanks to the personnel of CCPP, John Bash, Greg Greer, James Diaz, and Ramon Serna for timely help and constant support with greenhouse experiments. Many thanks to the personnel of USDA-ARS NCGRCD, Robert Krueger,

Patricia Nielsen, Polly Balance, Vicki Newman, Jaclyn Sweet and Benjamin Rangel for their contribution to my studies.

I wish to express my warm and sincere thanks to Dr. Jude Grosser (Citrus Research and Education Center, Lake Alfred, FL) for providing me the training and supply of citrus callus culture.

My sincere thanks the Dean Fellowship (provided by the College of Natural and Agricultural Sciences and Department of Plant Pathology and Microbiology, UCR) for giving me an opportunity to pursue the doctoral program.

My special warm thanks to the lady in my life, Aruna Rawat for her support, encouragement, patience and unwavering love. Special thanks to Harish and Manu (all the way from Basel, Switzerland) for their encouragement and constant support. Many thanks to my friends, classmates and colleagues at UCR, Karthi, Shailu, Payal, Arinder, Venky, Kishor, Pushpa, Aman, Avneet, Ajay, Yusuf, Garima, Sandy, Ritu, Soon, Samer, Xiaofan, Niles, Alister, Douglas, Alisha and many friends for making the Riverside stay a wonderful experience.

Last but not the least; I would like to thank my parents: Radhabai and Shiva Singh; brothers: Siddu Singh & Sunil Singh; sister-in-laws: Rajashri & Supriya; the new member of the family Sanjana and extended family and friends in Bangalore, Belgaum, Bijapur, Delhi, Pauri and Rudrapur (India) for their unconditional love and support.

DEDICATION

To my father (late) Dr. Shivasingh Sangansingh Hajeri (Tonashyal) for being so influential with his genuine humane characteristics and true unconditional love for the family…..

ABSTRACT OF THE DISSERTATION

Study of Molecular and Biological Properties of
Citrus exocortis viroid and Dweet mottle virus

by

Subhas Hajeri

Doctor of Philosophy, Graduate Program in Plant Pathology
University of California, Riverside, June 2010
Dr. James Ng, Chairperson

Viroids are RNA-based infectious agents that are single-stranded, covalently closed circular, non-coding and naked. For a successful systemic infection, viroid must replicate in a cell, move systemically in whole-plant. The high genetic diversity observed at the cellular level for *Citrus exocortis viroid* (CEVd) might be due to the absence of proof-reading activity of the host RNA polymerases and the bottlenecks, associated with systemic movement of the virus, played an important role in the observed low genetic diversity at the plant level.

Study of molecular and biological properties of *in vivo* generated CEVd mutants has been approached by characterizing a single sequence variant and testing for its replication in citrus protoplasts, systemic accumulation in citron seedlings, biological properties in different experimental hosts and intra-population profile of progeny viroid within a single-host. *In vivo* generated CEVd mutant infection in a single plant resulted in a progeny population with distinct but closely related sequences composing a quasi-species. The study revealed the effects of mutation, selection, and genetic drift on the adaptation and extinction of CEVd RNA. The stability of the 62A+, U129A and U278A

variants in their respective progeny populations indicates the phenomenon of genetic drift and fixation of a mutation in the population. Genetic structure and diversity of CEVd progeny population altered significantly with replication in different hosts and understanding these interactions may facilitate the prediction and prevention of emerging virulent strains.

The nucleotide sequence of Dweet mottle virus (DMV) was determined and compared to sequences of *Citrus leaf blotch virus* (CLBV) and other members of the family *Alpha* and *Beta-flexiviridae*. The DMV genome has 8747 nt excluding the poly(A) tail at the 3' end of the genome. DMV genomic RNA contains three putative open reading frames (ORFs) and untranslated regions of 73 nt at the 5' and 541 nt at 3' termini. ORF1 potentially encoding a 227.48 kDa polyprotein, which has methyltransferase, oxygenase, endo-peptidase, helicase, and RNA-dependent RNA polymerase (RdRP) domains. ORF2 encodes a movement protein of 40.25 kDa while ORF3 is the coat protein of 40.69 kDa. Phylogenetic analysis, based on RdRP core domain revealed that DMV and CLBV are closely related.

TABLE OF CONTENTS

LIST OF TABLES

LIST OF FIGURES

GENERAL INTRODUCTION

The dissertation work is focused on two pathogens of citrus namely, *Citrus exocortis viroid* (CEVd) and Dweet mottle virus (DMV). The effect of genetic bottlenecks associated with the systemic movement of CEVd was studied by comparing the genetic structure and diversity of CEVd at the cellular level with the plant level. In addition, the molecular and biological properties of *in vivo* generated CEVd mutants were studied following four major aspects of viroid biology. i) Replication in citrus protoplasts; ii) Systemic accumulation in citron seedlings; iii) Biological properties (disease symptom expression) in different host species; iv) *De novo* generated viroid progeny population from a single sequence variant within a single-plant. Molecular study of DMV was carried out by unraveling the complete nucleotide sequence of the virus and comparing it with genomes of members of the *Betaflexiviridae* family. Since two different citrus pathogens were studied, this dissertation is divided into two parts. Part A is focused on studies related to the citrus viroid and Part B on the citrus virus. Part A is again subdivided in to two parts, A1 and A2 to address the different aspects of CEVd study separately. Each part consists of Introduction, Materials and Methods, Results, and Discussion. A common list of Reference is presented at the end of the dissertation.

PART A1

Genetic diversity of *Citrus exocortis viroid* at the cellular level and plant level

INTRODUCTION

A viroid infection in a single plant results in a progeny population with distinct but closely related sequences (Gandia *et al*., 2000; Owens *et al*., 2000; Gandia and Duran-Vila, 2004). The systemic infection process of a viroid can be divided into two major steps: (i) replication in individual cells and (ii) movement throughout the plant (Ding *et al*., 2009). Viroids completely rely on the host RNA polymerase II for replication (Diener, 1979; Muhlbach & Sanger, 1979; Schindler & Muhlbach, 1992; Warrilow and Symons, 1999). The plant RNA polymerase II lacks proof-reading activity, which leads to the introduction of errors into nascent RNA (Styer, 1995; Gandia *et al*., 2000). The high genetic diversity in viroids, like other RNA genomes, is believed to be due to the absence of proof-reading activity of the host RNA polymerases, the large population size and rapid rate of replication (Holland *et al*., 1982; Domingo and Holland, 1997; Garcia-Arenal *et al*., 2001). A model has been proposed, in which the replication of viroid RNA would generate a population of similar but non-identical sequence variants (termed as quasi-species) (Eigen, 1971 and 1993).

Genetic diversity of viroid populations at the whole-plant level has been identified in isolates of *Citrus exocortis viroid* (CEVd) (Visvader and Symons, 1985; Gandia *et al*.,

2005; Bernard et al., 2009), *Potato spindle tuber viroid* (PSTVd) (Gora *et al*., 1994; Gruner *et al.*, 1995; Gora-Sochacka *et al*., 1997), *Hop stunt viroid* (Kofalvi *et al*., 1997; Palacio-Bielsa *et al*., 2004), *Grapevine yellow speckle viroid 1* (Rigden & Rezaian, 1993; Polivka *et al*., 1996), *Citrus dwarfing viroid* (Owens *et al*., 2000), *Citrus bent leaf viroid* (Foissac & Duran-Vila, 2000; Gandıa & Duran-Vila, 2004), *Avocado sunblotch viroid* (Rakowski & Symons, 1989), *Peach latent mosaic viroid* (Ambros *et al*., 1998, 1999), and *Chrysanthemum chlorotic mottle viroid* (Codoner *et al*., 2006). However, little is known about the genetic diversity of replicating viroid at the cellular level.

It is conceivable that the selection pressure is much greater and the dynamics of viroid replication and movement is more complex at the plant level as compared to the cellular level in protoplasts. An obvious difference in protoplasts is the absence of both cell to cell and long distance movement. Thus protoplasts transfected with viroid molecules offer a synchronous system to study the population profile at the cellular level (Aoki & Takebe, 1969; Marton *et al*., 1982; Qi & Ding, 2002; Zhong *et al*., 2005; Flores *et al*., 2008). Cocking was the first to isolate plant protoplast enzymatically (Cocking, 1960), and transfect tomato protoplasts with *Tobacco mosaic virus* (Cocking, 1966) establishing the single-cell system to study plant viruses. The pioneer work showed that virus infection was synchronous and its replication was supported by the efficient uptake of viral particle/RNAs by protoplasts (Aoki & Takebe, 1969; Takebe & Otsuki, 1969; Warren *et al*., 1989). Since then, protoplasts have been extensively used for the study of replication of plant viruses and viroids at the cellular level (Murakishi *et al*., 1970; Sztuba-Solinska & Bujarski, 2008; Ding, 2009).

The main objective of the present work was to characterize the genetic diversity of a CEVd clone at the cellular level and compare it with the genetic diversity at the plant level.

MATERIALS AND METHODS

Viroid source. A cDNA clone of CEVd preserved as bacterial glycerol stock at -80 ^{0}C (Dr. Vidalakis Laboratory, University of California, Riverside) was used in the present study. The *in vitro* transcripts of CEVd have been shown to be infectious on citrus plants upon slash inoculation (Rigden and Rezaian, 1992; Szychowski *et al*., 2005). The plasmid pSTBlue-1 (EMD Chemicals Inc.), containing a full-length CEVd cDNA (Figure 1), was isolated from *Escherichia coli* strain JM109 (Promega Corp.) using QIAprep Miniprep Kit (Qiagen) following the manufacturer's instructions. Presence of cloned insert DNA was tested by a diagnostic digestion of the plasmid DNA with *Bam*HI restriction enzyme (New England Biolabs Inc.) and further confirmed (GenBank Accession number GU295988) by sequencing at the core facility of the University of California, Riverside. For the generation of plus-sense CEVd RNA transcripts, pSTBlue-1 DNA was linearized with *Sal*I restriction enzyme (New England Biolabs Inc.). Linearized plasmid was used as a template for run-off transcription with T7 RNA polymerase using MEGAscript Kit (Ambion, Inc.). Freshly prepared transcripts, free of template DNA, were spectrometrically quantified and used for protoplast and plant inoculations.

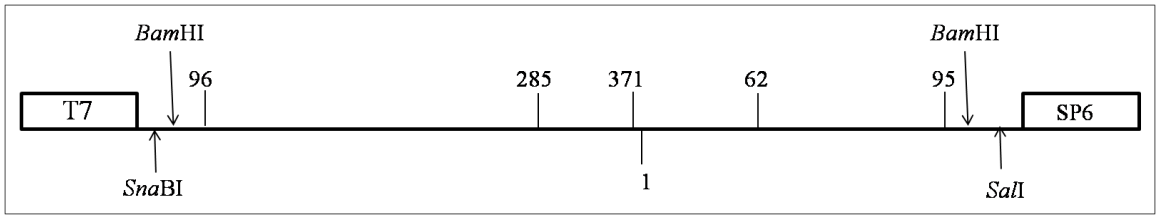

Figure 1. Cartoon showing important features of Citrus *exocortis viroid* in pST-Blue1 plasmid used for the study of intra-population profile. Promoters and selected restriction sites are indicated. Thick line indicates the genomic region of CEVd. The numbers correspond to the genomic sequence of CEVd (Accession number GU295988).

Source of citrus protoplast material. A suspension culture of the citrus cultivar Amblycarpa mandarin (*Citrus amblycarpa* Ochse.) was developed from callus culture. Callus culture was generously provided by Dr. Jude Grosser (Citrus Research and Education Center, Lake Alfred, Florida). Suspension culture was maintained in medium H+H (Grosser and Gmitter, 1990). Suspension cell culture was maintained at room temperature with constant shaking (150 rpm). Every alternate week, the culture was diluted in equal volume of fresh H+H medium and split in to half (two cultures) in 250 ml Erlenmeyer flasks. One of the two flasks was used for isolating protoplast while other flask was kept for maintain the suspension cell culture.

Isolation of citrus protoplasts. Protoplasts were isolated from suspension culture by the procedure of Grosser and Gmitter (1990) with minor modifications. An enzyme solution composed of 13% mannitol, 2% Cellulase "Onozuka"RS and 2% Macerozyme R10 (Yakult Pharmaceutical, Tokyo, Japan), was used to digest the cell culture. One flask (40 ml) of 4-10 day-old suspension cell culture was divided and added to four sterile

disposable Petri plates. The medium was removed using a Pasteur pipet and to each plate, a 5 ml of the enzyme solution (described above) and 7.5 ml of 0.6M BH3 protoplast medium (Grosser and Gmitter, 1990) were added to the cells and incubated for overnight digestion (~16 h) in dark at 28 °C with slow shaking (30-40 rpm).

Digested suspension cell culture from all the four plates was filtered through a sterile 70 µm disposable Cell Strainer (BD Falcon), to remove undigested cell clumps and debris. The purified protoplasts were centrifuged at 100 g for 5 min in four 15 ml Falcon tubes. Supernatant was removed with a Pasteur pipette, and the pellets were gently resuspended in 5 ml each of SucroseM solution (Grosser and Gmitter, 1990). Two ml of 13% mannitol solution was slowly added on top without disturbing the sucroseM-protoplast suspension. The tube was centrifuged at 100 g for 10 min. The protoplasts located in the interface between the sucroseM and mannitol layers were collected from all the four tubes into one tube using a sterile glass Pasteur pipette. Protoplasts were washed twice, gently with 0.6M BH3 medium, and resuspended in 10 ml volume of the same medium.

The number of viable protoplasts was counted on a haemocytometer by staining the protoplasts with flourescein diacetate (FDA) dye (Widholm, 1972). The dye was prepared by dissolving 5 mg FDA in 1 ml acetone and storing at 4°C in the dark. FDA stains viable cells green visible under blue light excitation (Figure 3). The dye solution (1-2 µl) was added to 20-30 µl of protoplast suspension and incubated for 1-2 min. Stained protoplasts suspension was applied to a haemocytometer and viewed under a microscope equipped with UV light (Epifluorescent Zeiss Axioplan Microscope). The

viable protoplasts, which fluoresce bright green, were counted in five (5) of the chambers and number of viable protoplasts was calculated by using following equation:

Viable protoplasts=Average x Dilution x Total volume x the factor of the chamber (10^4).

An aliquot of half a million protoplasts was prepared in a snap cap tube for each transfection experiment.

Transfection of citrus protoplasts. 5 µg of *in vitro* transcripts from CEVd plasmid in 50 µl DEPC water (0.1% diethylpyrocarbonate) and 0.5 million citrus protoplast pellet in 10 ml snap cap tubes were used to perform the viroid transfection assay (Price *et al*., 1996; Albiach-Marti *et al*., 2004). To the protoplast and transcript RNA mixture, 400 µL of 30% polyethylene glycol, MW 8000 (PEG 8000) solution was added drop by drop with instant gentle mixing which was continued for 25 seconds. Immediately 4 ml of 0.6 MMCPW plus 10 mM $CaCl_2$ buffer (Grosser and Gmitter, 1990) was added and mixed gently and incubated for 5 min at room temperature. Transfected protoplasts were carefully washed in 4 ml of 0.6M BH3 and cultured in a final volume of 2 ml of 0.6M BH3 solution in 6 well tissue culture plates. The plates were incubated for 1 to 5 days in dark without shaking at 28 ^oC.

Time course experiment. Replication of CEVd in citrus protoplast was monitored over the period of five days (Table 1). At every 24 h interval, transfected protoplasts were harvested from three wells (replicates) as described below. Mock-transfected protoplasts and protoplasts transfected in the absence of PEG served as controls.

Table 1. Details of time course experiment to analyze the replication of *Citrus exocortis viroid* (CEVd) in citrus protoplasts. Pellets of 0.5 million protoplasts were transfected by polyethylene glycol (PEG) method with appropriate inocula in 50 µl volumes and incubated for 1-5 days post inoculation and harvested for analysis of CEVd population.

Treatment	Incubation period	Inoculation			Remarks
		Source	Amount (µg)	Volume (µL)	PEG treatment
1	1 dpi	CEVd	5	50	Yes
2	2 dpi	CEVd	5	50	Yes
3	3 dpi	CEVd	5	50	Yes
4	4 dpi	CEVd	5	50	Yes
5	5 dpi	CEVd	5	50	Yes
Control 1	5 dpi	water	NA	50	Yes
Control 2	5 dpi	CEVd	5	50	No

dpi, days post inoulation; PEG, Polyethylene Glycol; NA, not applicable.

Total RNA was extracted from the transfected protoplasts using Trizol (Invitrogen Corp.) extraction method (Chomczynski and Sacchi 1987). To the protoplast pellet of 2 ml culture, 1 ml of Trizol was added, vortexed for 15 sec and incubated for 5 min at room temperature. Samples were vortexed again and incubated with 200 µl of chloroform followed by centrifugation at 4 ^{0}C for 15 min at 12000 g. Aqueous phase was carefully transferred to a fresh microfuge tube and the nucleic acid was precipitated with 0.5 volumes of isopropanol at room temperature for 10 min. Following precipitation, the tubes were centrifuged at 12000 g for 10 min. The pellet was washed with 1 ml of 70% ethanol, dried and resuspended in 40 µl DEPC water. Total RNA preparation was treated

with RQ1 RNase-Free DNase I (Promega Corp.) following the manufacturer's instructions and stored at -80 ^{0}C.

Real-Time RT-PCR assay. The amounts of CEVd in total RNA preparations from transfected citrus protoplasts were estimated by reverse transcription followed by SYBR Green I based quantitative PCR assay. Six sets of primers (Table 2) were tested for optimization by both conventional PCR (using Taq polymerase) and SYBR Green I based real-time RT-PCR assay using the CEVd/pSTBlue-1 plasmid (Figure 1) as template.

Table 2. List of primer pairs employed for the optimization of SYBR Green I based real-time PCR assay with CEVd/pSTBlue-1 plasmid. The nucleotide numbering is based on the genomic sequence of CEVd from the NCBI Accession number GU295988.

Set	Primer	Sequence 5' to 3'	Location*	Polarity	Product size (bp)
1	1F	TGGCGTCCAGCGGAGAA	157-173	Forward	100
	1R	AGAGAAGCTCCGGGCGA	242-258	Reverse	
2	2F	TCGCCCGGAGCTTCTCTC	242-259	Forward	191
	2R	CTTTTTTCTTTTCCTGCCTGCA	41-62	Reverse	
3	3F	GAAGCTTCAACCCCAAACC	285-303	Forward	148
	2R	CTTTTTTCTTTTCCTGCCTGCA	41-62	Reverse	
4	1F	TGGCGTCCAGCGGAGAA	157-173	Forward	146
	3R	GGTTTGGGGTTGAAGCTTC	285-303	Reverse	
5	4F	GAAACCTGGAGGAAGTCG	100-117	Forward	208
	4R	AAGCGGTTTGGGGTTGAAG	289-307	Reverse	
6	4F	GAAACCTGGAGGAAGTCG	100-117	Forward	159
	1R	AGAGAAGCTCCGGGCGA	242-258	Reverse	

Quantification of CEVd in transfected protoplasts required normalization of host RNA using an internal control. Microarray analysis has shown that the nuclear gene of citrus, Phospholipase isoform Delta or ankyrin gene (GenBank Accn. No. CX074707) had very similar levels of expression under different phylsiological conditions (Tomassini

et al., 2009). In the present study, this gene was used as an internal control to normalize template volumes prior to quantification of CEVd.

cDNA preparations using forward and reverse primers of two sets of cDNA syntheses were made for each sample, one with a combination of primer specific to the internal control, ankyrin gene (5′-CAACAT ATCAGGAAGACTCATG -3′) and CEVd specific forward primer, 3F (Table 2), and another with the same ankyrin specific primer and CEVd specific reverse primer, 2R (Table 2). The serial dilutions of cDNA were then used for real time PCR of internal control gene for normalization of templates. The normalized templates were then used for quantitative assay of CEVd.CEVd (3F and 2R respectively, Table 2) were used in for quantification of replicative intermediate (negative sense) and progeny viroid molecules (positive sense) respectively, at different post inoculation periods.

First strand cDNA synthesis. Two sets of first-strand cDNA were synthesized from each of total RNA preparations from transfected protoplasts using SuperScript^{TM} III Reverse Transcriptase (Invitrogen Corp.) following the manufacturer's protocol. Total RNA of 2 µl, 0.5 µl (10 µM conc.) each of two appropriate primers (ankyrin reverse primer with either 3F or 2R) as described above and 1 µl of 10 mM dNTPs (deoxyribonucleoside triphosphates) were mixed in DEPC-water to a total volume of 10 µl and the mixture was incubated at 65°C for 5 min for denaturing RNA template, and then placed on ice for at least 1 min. To this reaction mixture, 2 µl of 10x RT-buffer (Invitrogen Corp.), 4 µl of 25 mM $MgCl_2$, 2 µl of 0.1 M DTT, 1 µL of RNaseOUT (40 U/µl) and 1 µL of SuperScript^{TM} III reverse transcriptase (200 U/µl) were added and the

mixture (final volume of 20 µl) was incubated at 50 ^{o}C for 50 min. The reaction was stopped by incubating at 80° C for 10 min and the reactions were stored at -20° C and used for real time PCR assays.

Normalization of template volumes. Two-fold dilution series of the cDNA products from each batch of protoplast transfections were prepared (1:2, 1:4, 1:8, 1:16, 1:32, 1:64, and 1:128). Real-Time PCR assay was performed in a MX3005P qPCR Machine **(**Stratagene) using RT² SYBR® Green qPCR Master Mix (SABiosciences Corp.). The master mix contained a high-performance HotStart Taq DNA polymerase, ROX® as a reference dye and other necessary optimized PCR components. In a PCR tube, 12.5 µl RT² SYBR® Green qPCR Master Mix, 0.6 µl ankyrin-specific forward (5'-ATCCTCTGCAAGTAGATGC -3') and 0.6 µl of ankyrin-specific reverse (5′-CAACAT ATCAGGAAGACTCATG -3′) primers (10 µM each) and 2 µl template cDNA to a final volume of 25 µl were mixed and used in real-time PCR with the following program. Initial denaturation of 10 min step at 95 ^{0}C was required also to activate the HotStart Taq DNA polymerase. Amplification of the target gene was done in 40 cycles of 95ºC, 15 sec and 60ºC, 60 sec. This was followed by a run of melt curve analysis, from 60° C to 95° C with measurement of fluorescence taken at every 0.5 °C.

Quantitative PCR assay of normalized templates for CEVd. Quantitative assay for CEVd was done using appropriate dilutions of templates which expressed similar quantities of ankyrin gene product as determined in normalization assays. After normalization of the cDNA preparations with an internal control, appropriate cDNA dilutions were used in the real time PCR assay of CEVd. A 2 µl of cDNA was used in the

real-time PCR with CEVd specific forward primer 3F and reverse primer 2R (Table 2) following the procedure described above.

Standard curve. Standard curve was constructed using serial dilutions of CEVd plasmid over a range six dilutions from 10^{-1} to 10^{-6} of target DNA.

Analysis of real-time RT-PCR data. The real-time PCR results were analyzed with MX3005P data analysis software (Stratagene). Quantification of CEVd in the protoplast samples was performed by plotting the Ct value of each sample on the standard curve. The amount of starting template in a PCR reaction, expressed as the copy number of the target CEVd cDNA was determined by this method.

Source of citrus plant material. 'Etrog' citron (*Citrus medica* L.) selection 'Arizona 861-S1', free of all known graft transmissible pathogens of citrus, was propagated on rough lemon (*C. jambhiri* Lush.) rootstock seedlings. These plants were used as hosts for intra-population study of CEVd at the plant level.

Citrus plant infectivity assay. Three citrus plants (citron bud-grafted on rough lemon root-stock) were used for infectivity assay. Each plant was slash inoculated with an aliquot of 10 µg *in vitro* transcripts using a razor blade. All plants were maintained at elevated greenhouse temperatures (32-38^{o}C) optimum for citrus viroid replication and symptom expression.

Monitoring symptom expression. Plants inoculated with CEVd transcript RNAs were observed for symptom expression at weekly intervals. Infectivity was also tested by tissue imprint hybridization using PCR-digoxigenin (DIG) labeled DNA probes as described by (Palacio-Bielsa *et al.*, 1999) for tissue cuttings at weeks intervals from week 1 to 4.

Recovery of progeny viroids from citrus plants. Five grams of young tissue from viroid inoculated plants was homogenized in presence of three volume of water-saturated neutralized phenol and one volume of extraction buffer, 0.4 M Tris-HCl, pH 8.9, 1% (w/v) sodium dodecyl sulfate (SDS), 5 mM ethylenediaminetetraacetic acid (EDTA), pH 7.0, 4% (v/v) β-mercaptoethanol. The aqueous solution was recovered by centrifugation at 7,000-12,000 g for 20 minutes at 4 ^{0}C, and mixed with three volumes of cool 95% ethanol and 10% v/v of 3 M sodium acetate for overnight precipitation at -20 ^{0}C. The precipitated nucleic acids were pelleted by centrifugation at 7,000-12,000 g for 20 minutes at 4 ^{0}C and the pellet was resuspended in 1 ml of TKM-buffer (10 mM Tris-HCl, 10 mM KCl, 0.1 mM $MgCl_2$, pH 7.4). The nucleic acid suspension was dialyzed overnight against TKM buffer at 4 ^{o}C. The dialyzed nucleic acid preparation was precipitated with one volume of 4 M Lithium chloride (LiCl). After incubating at least 4 hours at 4 ^{o}C, the solution was centrifuged at 7,000-12,000 g for 20 minutes at 4 ^{o}C and followed by precipitation with three volume of cool 95-100% ethanol (Semancik *et al*., 1988). The pelleted nucleic acids were resuspended in 1 ml of TKM-buffer and used for CF-11 column chromatography. The CF-11 cellulose column saturated with 35% ethanol

in 1x STE. The nucleic acid preparation was prepared with 35% ethanol in 1x STE buffer and loaded onto the column. Column was washed with 30% ethanol in 1x STE twice (Semancik, 1986). The viroid RNA was eluted with 1x STE, ethanol precipitated and finally resuspended in 300 µl TKM-buffer. Eluted viroid RNA was stored at -20 ^{0}C.

Reverse Transcriptase-Polymerase Chain Reaction (RT-PCR). The first-strand of cDNA was synthesized using SuperScript™ III Reverse Transcriptase (Invitrogen Corp.) following the manufacturer's protocol. CEVd specific 24-mer primer C3c (5′ -CAAGGATCCCTGAAGGACTTCTTC- 3′) complementary to bases 73 to 94 of CEVd genome with a unique restriction site *Bam*HI (underlined) and three extra nucleotides unrelated to viroid sequence at the 5′ end was used. The reverse transcription reaction (RT) mixture was prepared in two steps at a final volume of 20 µl. Viroid RNA of 2 µL, 2µM of the reverse primer and 1 µl of 10 mM dNTPs (deoxyribonucleoside triphosphates) were mixed in DEPC-water (0.1% diethylpyrocarbonate) at total volume of 10 µl. RNA template and complementary primer were denatured at 80 ^{o}C for 5 minutes, annealed at 37 ^{o}C for 15 minutes and placed on ice for at least 1 min. To the RT mixture, 2 µl of 10x RT-buffer (Invitrogen Corp.), 4 µl of 25 mM $MgCl_2$, 2 µl of 0.1 M DTT, 1 µL of RNaseOUT and 1 µL of SuperScript™ III RTase were added and incubated at 50 ^{o}C for retrotranscription for 50 min.

Second-strand synthesis and amplification of dsDNA was performed using *Pfu* DNA Polymerase (Biovision Research Products) in the presence of reverse primer and the 21-mer forward primer (5′ -CTCGGATCCCCGGGGAAACCT- 3′) homologous to

bases 89-106 of CEVd genome with a unique restriction site *Bam*HI (underlined) and three extra nucleotides unrelated to viroid sequence at the 5′ end. Both forward and reverse primers lie in the central conserved region of CEVd secondary structure.

The polymerase chain reaction (PCR) mixture of 100 µL containing, 8 µL of the RT reaction product served as the DNA template for amplification, 10 µL of 10x PCR-buffer (Biovision Research Products), 4 µL dNTPs, 4 µL each of the 10µM forward and reverse primers, 2.5 unit of *Pfu* DNA Polymerase and DEPC-water up to the final volume. The PCR was performed as initial denaturation step at 95 ^{o}C for 2 min, 35 cycles of 95 ^{o}C for 30 seconds, 55 ^{o}C for 30 seconds, and 72 ^{o}C for 1 minutes plus a final cycle of 10 minutes at 72 ^{o}C.

Cloning and Sequencing. RT-PCR products from citrus plant and protoplast (5 dpi treatment) were purified according to the High Pure PCR Product Purification Kit by Roche (Roche Applied Science). As *Pfu* DNA polymerase creates blunt end products, purified PCR product was used for 3'A-tailing reaction using *Taq* Polymerase (Promega Corp.) at 72 °C for 25 min. In a 0.5 ml nuclease-free centrifuge tube, 7.7 µl of purified DNA fragment, 1 µl Mg-free 10x PCR buffer, 1 µl of 25 mM $MgCl_2$, 0.2 µl of 10 mM dNTPs and 0.1 µl of *Taq* DNA polymerase were used to add adenine nucleotide at the 3' end of the PCR product, which facilitates in TA cloning system.

Ligation of the A-tailed DNA Fragment to the pGEM-T easy plasmid vector (Promega Corp.), which has a single 3′-T overhangs at the insertion site greatly improve the efficiency of ligation of a PCR product into the plasmids by preventing

recircularization of the vector and providing a compatible overhang for PCR products generated by *Taq* DNA polymerase. In a 0.5 ml nuclease-free centrifuge tube, 5 µl of 2x rapid ligation buffer, 1 µl of pGEM-T easy vector (50 ng), 1 µl of T4 DNA ligase enzyme (Promega Corp.), and 2 µl of A-tailed DNA were mixed in DEPC-water to the final volume of 10 µl. Ligation reaction was incubated at 4 ^{o}C for overnight (~16 h).

The ligated plasmid vector was used to transform *E. coli* cells by the method described in Sambrook & Russell, 2001. Ligated plasmid DNA (2 µL) was added into a 50 µL suspension of Z-Competent™ *E. coli* Strains - JM109 (Zymo Research Corp.) in a sterile plastic tube mixed gently and held on ice for 30 minutes then heat shock transformation was performed at 42 ^{o}C for 45 sec and returned to ice for 2 minutes. LB-media (450 µl) was added into the tube and incubated for 60 minutes at 37 ^{o}C without shaking. A total volume (50 µL) of the LB-*E. coli* solution was placed on four LB-Agar petri plates containing 50 µg/ml ampicillin and 100 µl of ChromoMax™ IPTG/X-Gal Solution (Fisher Bioreagents) and then placed inverted at 37 ^{o}C for overnight.

96-well format plasmid preparation and DNA sequencing. The Genomics Core (Institute for Integrative Genome Biology, Noel T. Keen Hall, University of California Riverside) offers the service of 96-well format plasmid preparation and DNA sequencing. The selected white colonies (from blue/white screening) were grown in a 96-well block containing 1ml of LB medium under 50 µg/ml ampicillin selections. The 96-well block was divided into two and used for 48 colonies from citrus plant material and 48 colonies from citrus protoplast material. The 96-well block was incubated overnight in the core facility. For the 96-well format plasmid prep, Perfectprep Plasmid 96 Vac Kit (5

PRIME, Inc.) was employed, which utilizes alkaline lysis following by DNA binding and washing. Subsequently, the recombinant plasmids were sequenced (unidirectional) using SP6 promoter primer.

C**omputer analysis.**

Manual rearrangement of the viroid molecule and multiple sequence alignment. Sequence files were copied using Chromas 1.55 (Technelysium Pty Ltd 1998, Queensland, Australia) and used for manual rearrangement in Microsoft Office Word document (Microsoft Corp.). Since the primers designed for RT-PCR were located at the central conserved region of the viroid molecule, cDNA of the viroid molecule was not extended from the conventionally accepted first nucleotide position (Figure 1). Therefore, the viroid sequence was rearranged manually and the extra nucleotides that the primers added to the viroid sequences were removed. The rearranged viroid sequences from the Word documents were converted to text file. The text files were used for multiple sequence alignment using ClustalX 1.81 (Thompson, *et al.* 1997) and the alignment output file was saved in nexus format. Using DnaSP software (Librado and Rozas, 2009), nexus format was converted to phylip format (Felsenstein, 1989, Felsenstein, 1991.).

Genealogical analysis. The genealogical analysis of intra-population profile of CEVd was performed by utilizing TCS software v1.21 (Clement *et al.*, 2000). This software is based on principles of the coalscent theory (Kingman, 1982a, Kingman, 1982b) and uses cladistic analysis and nested statistical design for the cladogram

construction (Templeton *et al.*, 1992, Templeton & Sing, 1993). The phylip file produced from the viroid sequences alignment was the input for the TCS software.

Statistical analysis. The categorical data were analyzed using $\chi 2$ contingency analysis (Zar, 1984).

RESULTS

Diagnostic digestion of the CEVd/pSTBlue-1 plasmid with *Bam*HI (Figure 2) confirmed the presence of cloned insert DNA.

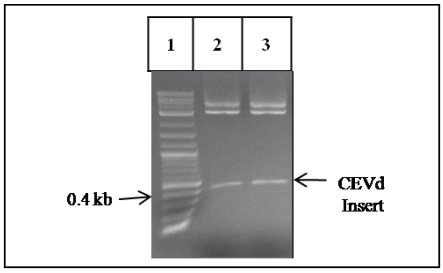

Figure 2. Presence of *Citrus exocortis viroid* (CEVd) insert DNA was confirmed by a diagnostic digestion of the plasmid DNA with BamHI restriction enzyme. Lane 1. 2-log DNA ladder (0.1-10.0 kb), Lane 2 & 3. released CEVd insert DNA.

Citrus protoplasts. Using an established suspension culture of citrus cultivar Amblycarpa mandarin (*C. amblycarpa*), up to 40 million protoplasts from 40 ml suspension culture could be reliably obtained with the protocol mentioned above. Based on staining with FDA, the viability of freshly isolated protoplasts was over 90% (Figure 3). Transfected protoplasts could be kept alive in 0.6M BH3 protoplast culture medium for at least five days.

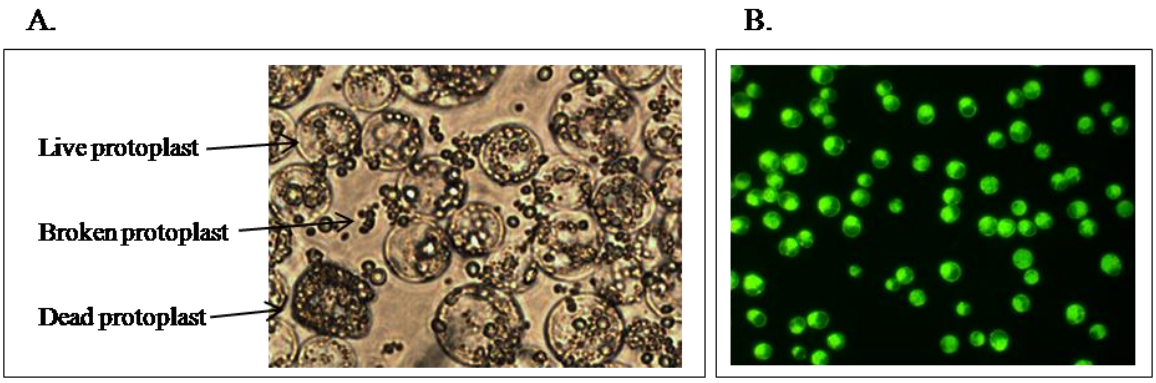

Figure 3. Protoplasts isolated from the suspension cell culture of *C. amblycarpa* (1h post-isolation). (A) Inverted optical microscope image (40x). Live protoplasts typically assume a spherical shape. Irregular shaped, darker looking protoplasts are usually dead protoplasts. Mechanically damaged protoplast debris was found to be floating in the buffer. (B) Fluorescein diacetate (FDA) stained live protoplasts fluoresce green as observed under Epifluorescent Zeiss Axioplan Microscope (10x) equipped with 485/535 excitation/emission filter combination.

Primers for real-time RT-PCR. Among six primer pairs tested for the optimization by both conventional PCR (using Taq polymerase) (Figure 4) and SYBR Green I based real-time RT-PCR assay using the CEVd/pSTBlue-1 plasmid (Figure 1) as template, primer pair set 3 (3F & 2R) (Table 2) performed better in the real-time RT-PCR assay and subsequently used in the following experiments.

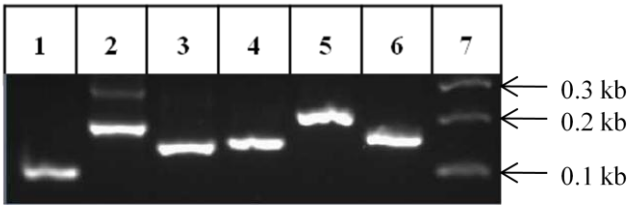

Figure 4. Examination of the primer pairs for real-time RT PCR experiments. Lane 1-6 corresponds to PCR products of CEVd generated by using following primer combinations (Table 2) on 2% TBE agarose gel. Lane 1. 1F/1R, Lane 2. 2F/2R, Lane 3. 3F/2R, Lane 4. 1F/3R, Lane 5. 4F/4R, Lane 6. 4F/1R, Lane 7. Arrows indicate the corresponding molecular marker sizes.

Real-time RT-PCR assay. Normalization of host RNA using an internal control, ankyrin gene, was performed before the quantification of CEVd in transfected protoplasts. The serial dilutions of cDNA were used for real time PCR of ankyrin gene for normalization of templates (Figure 5 and 6). The normalized templates were then used for quantitative assay of CEVd.

A standard linear regression line was obtained by plotting the Ct values for the DNA standards versus log of their starting copy number of each of the six dilutions (Figure 7). Quantification of CEVd in the protoplast samples was performed by plotting the Ct value of each sample on the standard curve. The amount of starting template in a PCR reaction, expressed as the copy number of the target CEVd cDNA was determined by this method. Melt curve analysis generated a first derivative dissociation curve which helped in analysis of the specificity of real time PCR product. The specificity of real-time PCR product was observed as two separate specific melt curve generated for ankyrin and CEVd (Figure 8).

A.

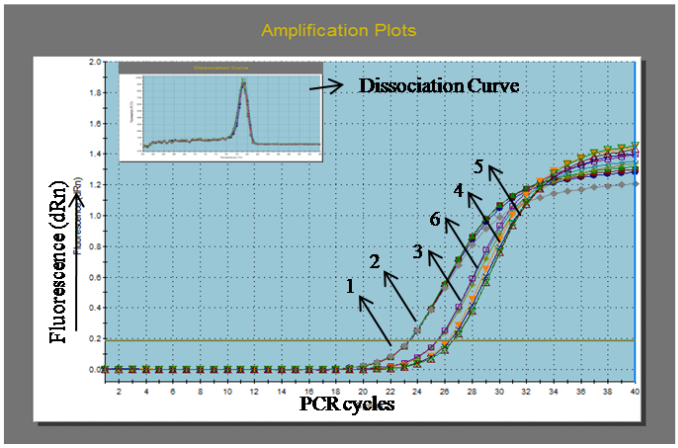

B. **Before normalization of internal control**

No.	Protoplast Sample	Dilution of cDNA	cDNA Vol. (µL)
1	1 dpi/CEVd	1:2	2
2	2 dpi/CEVd	1:2	2
3	3 dpi/CEVd	1:2	2
4	4 dpi/CEVd	1:2	2
5	5 dpi/CEVd	1:2	2
6	5 dpi/H_2O	1:2	2

Figure 5. Real-time RT-PCR amplification plots of ankyrin (before normalization). Panel (A) on the left shows the variation in the Ct of normalizer (ankyrin) for all samples. Dissociation curve generated for this experiment is presented in the left corner. Panel (B) on the right shows the information of numbers 1-6, which corresponds to samples of protoplast experiment. The dilution factors and amount of cDNA used for real-time PCR are mentioned for each sample.

A.

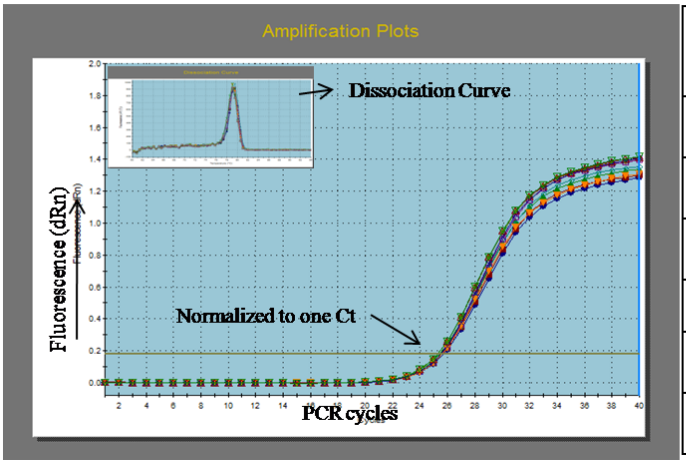

B. After normalization of internal control

No.	Protoplast Sample	Dilution of cDNA	cDNA Vol. (µL)
1	1 dpi/CEVd	1:16	1
2	2 dpi/CEVd	1:16	1
3	3 dpi/CEVd	1:2	8
4	4 dpi/CEVd	1:4	2
5	5 dpi/CEVd	1:4	2
6	5 dpi/H_2O	1:2	8

Figure 6. Real-time RT-PCR amplification plots of ankyrin (after normalization). Panel (A) on the left shows the normalized Ct of ankyrin for all samples. Dissociation curve generated for this experiment is presented in the left corner. Panel (B) on the right represents the adjusted dilution factors and corresponding volumes of cDNA used for real-time PCR with CEVd specific primers.

A.

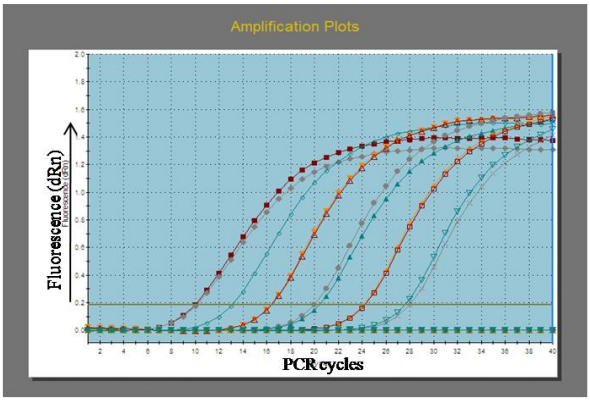

B.

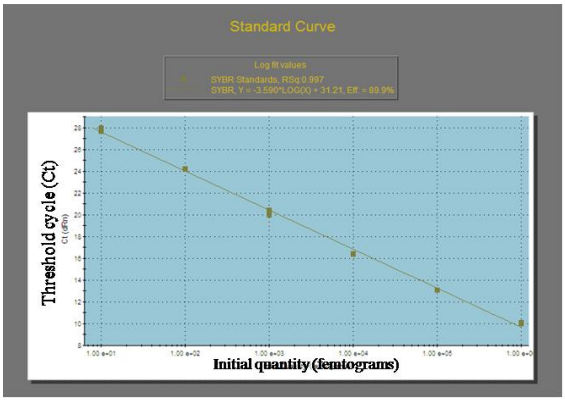

Figure 7. Real-time PCR amplification plot generated from known amounts of template DNA to construct standard curves for quantification of unknown samples. (A) Linear plot of the increase in fluorescence versus PCR cycle number of DNA standards ranging from 11 x 10^9 to 11 x 10^3 molecules per µl with corresponding Ct values for each of the amplified standards. (B) A standard linear regression line was obtained by plotting the Ct values for the DNA standards versus log of their starting copy number of each six-fold dilution.

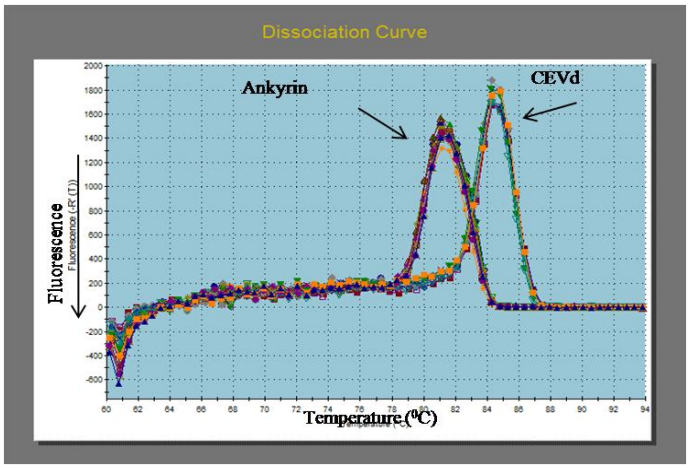

Figure 8. The dissociation curve generated for ankyrin (internal control) and CEVd separately on the same real-time PCR plate.

Replication of CEVd in citrus protoplasts. A time course experiment was carried out to investigate the CEVd replication in citrus protoplasts transfected with transcript RNAs. SYBR Green I based real-time RT-PCR was used to monitor the viroid RNA accumulation over the five days at every 24 hours post-inoculation (Figure 9). The average of the three replications per treatment was used in comparing the relative levels of viroid accumulation in the protoplasts over the period of five days. The numerical value data was converted to chart data (Figure 9). For the ease of comparison, the

accumulation levels of CEVd RNA after 1 dpi was arbitrarily set to a value of 1 and the levels of CEVd RNA from subsequent days were presented as relative values to this reference value.

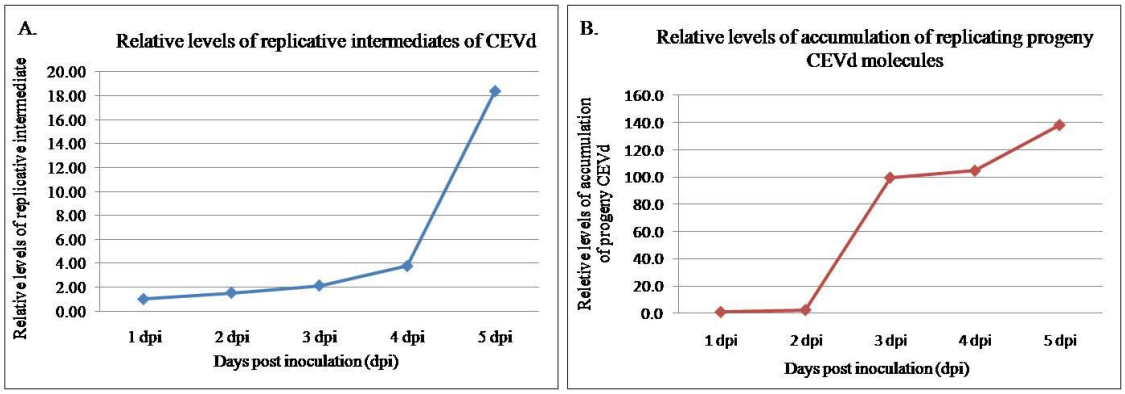

Figure 9. Replication of CEVd in citrus protoplast (*C. amblycarpa*) was monitored by quantitative real-time RT-PCR. The panel (A) on the left shows the relative levels of replicative intermediates of CEVd over the period of five days. The panel (B) on the right shows the relative levels of accumulation of replicating CEVd progeny molecules. For the ease of comparison, the accumulation levels of CEVd RNA after 1 dpi was arbitrarily set to a value of 1 and the levels of CEVd RNA from subsequent days are presented as relative values to this reference value.

The replicative intermediate of viroid RNA was detected by using forward (sense) primer during cDNA synthesis step. A 2.5 fold increase in the progeny CEVd RNA level at 2 dpi compared to 1 dpi (Figure 9B). The level of accumulation of progeny CEVd RNA leaped at 3dpi to 40 fold. Similar trend of increasing levels of accumulation was observed for the next two days. The levels of accumulation of replicative intermediate and newly generated progeny viroid RNA differ significantly, but both show similar trend of increase in accumulation over the period of five days (Figure 9).

The characteristic symptoms induced by CEVd such as rugosity, leaf epinasty and stunting in citron could be observed in 8-10 weeks post inoculations (Figure 10).

Figure 10. The characteristic symptoms induced by CEVd, rugosity and leaf epinasty, were prominent by 8-10 weeks post inoculation.

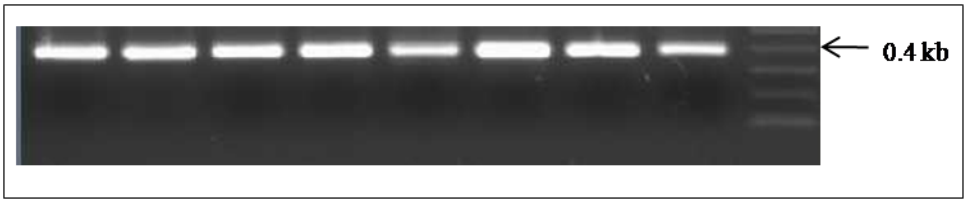

Figure 11. *Citrus exocortis viroid* (CEVd) PCR product in ethidium bromide stained 1.2% TBE agarose gel. Arrowhead indicates molecular marker band 0.4 kb.

The amplified RT-PCR product from both protoplasts and citron plant samples was analyzed with 1.2% Tris-borate-EDTA (TBE) agarose gel electrophoresis (Figure 11) (Sambrook & Russell, 2001) with standard molecular weight markers after staining with ethidium bromide. This RT-PCR product was further used for cloning and sequencing.

Genetic diversity of CEVd progeny. The effect of selection pressures on the progeny population diversity of CEVd generated from a single sequence variant within a single-plant was compared to the population variability at the cellular at level. The population variability was tested by analyzing the genome sequences of approximately 43 progeny viroid cDNA clones each from infected plant and the protoplasts (Table 3).

Table 3. Genetic diversity of *Citrus exocortis viroid* (CEVd) at the plant and the cellular levels.

Host	CEVd clones					
	Master Sequence	No. of sequences	Master sequence	Fitness peaks	Variants	
					Total	Unique[¥]
Citron/'Rough' lemon plant	wild-type	43	33	108G+	10	7 (16%)
Citrus Protoplast	wild-type	43	15	G50A & A130U	28	13 (30%)

[¥] Multiple clones with the same mutations; Values in the bracket are Percent of unique clones in the population.

De novo generated viroid progeny population of CEVd in citron plant and citrus protoplasts is presented in Table 3. The wild-type CEVd found to be the master sequence as well as the most recent common ancestor in both viroid progeny profiles. A sequence variant with addition of G at position 108 (108G+) induced fitness peak in the viroid progeny profile at the plant level. While the mutations at positions 50 and 130 resulted in fitness peaks at the cellular level. There was statistically significant difference in the haplotype frequency of the master sequence and the variants within the progeny population at the plant (χ^2=12.30, two-tailed P value=0.0005, df=1) as well as at the cellular level (χ^2=3.93, two-tailed P value=0.047, df=1) (Table 3). However, the

haplotype frequency of variants was predominant at the cellular level in contrary to the plant level. Variants with unique sequences were up to 30% in the viroid progeny profile at the cellular level, which was almost double than the plant level (Table 3).

The intra-population variability of CEVd at the cellular level exhibit statistically significant difference (χ^2= 29.16, two-tailed P value=0.0001, df=1) than the whole-plant level. At the cellular level, replicating CEVd progenies display more diverse population compared to the whole-plant level (Table 3). The number of mutations induced in the viroid genome at the cellular level was significantly higher than the whole-plant (χ^2=9.52, two-tailed P value=0.002, df=1) (Table 4). However, there were two sites of mutation on the CEVd genome those were found in the viroid progeny populations at both plant and cellular level. The common mutations 108G+ and A130U reside in the central conserved region and the variable domain respectively (Table 5). At the cellular level, there was a significant difference in the type of mutations induced (χ^2=25.38, two-tailed P value=0.0001, df=3). Transition mutations were more common in the progeny populations followed by transversion (Table 4). However, at the whole-plant level, statistically no significant difference was observed (χ^2=3.90, two-tailed P value=0.271, df=3) (Table 4).

Table 4. Type of mutations induced by the citrus plant and the protoplasts with CEVd infection.

Hosts	Number of mutations	Type of Mutation			
		Addition	Deletion	Transition	Transversion
Citron plant	11	4	0	4	3
Protoplasts	31	2	0	17	12

Table 5. Specific mutations of *Citrus exocortis viroid* progeny in citrus plant material.

Citrus Plant Material	Nucleotide position and viroid structural domains (Upper Strand)							
	TL[a]			**P**		**CCR**	**V**	**TR**
	19	22	30	50	59	108	130	163
Citron plant			C>U			G+	A>U	
Protoplasts	U>C	U>C		G>A	A>G	G+	A>U	U>C

Citrus Plant Material	Nucleotide position and viroid structural domains (Lower Strand)							
	TR	**CCR**	**P**				**TL**	
	194	265	301	302	303	308	335	339
Citron Plant			U>A		C>U	U>C		
Protoplasts	U>C	U>A		A>G			C>U	A>U

[a] TL; left terminal, P; pathogenic, CCR; central conserved region, V; variable, and TR; right terminal.
[b] Highlighted sites mutated in both citron plant and protoplasts and also mutation occurred more than once.

DISCUSSION

Increasing levels of accumulation of viroid RNA in protoplast over the period of five days (Figure 9) and the intra-population profile of CEVd (Table 3) indicates the successful replication of CEVd in citrus protoplasts. Asymmetry in synthesis of replicative intermediate (negative-strand in viruses) and progeny molecules (positive-strand in viruses) is observed (Figure 9). The ratio of positive-strand to negative-strand varied from 1 dpi to 5 dpi. At 3 dpi, the ratio was 50:1 (Figure 9). Asymmetry in replication was for *Potato spindle tuber viroid* (Qi and Ding, 2002) and it is characteristically found in all positive-strand RNA viruses investigated (Mandahar, 2006). The ratio of synthesis of positive-strand to negative-strand genomic RNAs is 10:1

for flaviviruses (animal viruses), 40:1 for *Citrus tristeza virus* (Satyanarayana *et al*., 1999 & 2002b), 100:1 for *Brome mosaic virus* and *Tobacco mosaic virus* (Mandahar, 2006).

De novo generated viroid progeny population from a single sequence variant within a single-plant have been identified in viroids (Visvader and Symons, 1985; Gora *et al*., 1994; Ambros *et al*., 1998; Foissac & Duran-Vila, 2000, Gandia *et al.*, 2000, Ito *et al.*, 2000, Owens *et al.*, 2000, Gandía & Duran-Vila, 2004). For a successful systemic infection, viroid must replicate in a cell, move both cell-to-cell and systemically in whole-plant (Ding, 2009). The presence of selection pressure at whole-plant level from the plant tissue and the environment yielded a less diverse progeny viroid population compared to the cellular level, where the selection pressure is minimal (Table 3). The high genetic diversity observed at the cellular level might be due to the absence of proof-reading activity of the host RNA polymerases and less selection pressure on the replicating progeny viroid molecules (Holland *et al*., 1982; Domingo and Holland, 1997; Garcia-Arenal *et al*., 2001).

Schneider and Roossinck (2001) found much higher mutation frequencies for both *Cucumber mosaic virus* (CMV) and *Tobacco mosaic virus* in isolated protoplasts than in intact plants. Li and Roossinck (2004) observed that the systemic infection induced a significant bottleneck on the CMV population structure. The bottlenecks, associated with systemic movement of the virus, played an important role in the observed low genetic diversity at the plant level.

PART A2

Molecular and Biological Properties of *in vivo* Generated *Citrus exocortis viroid* Mutants

INTRODUCTION

Viroids are the smallest known infectious, single stranded, circular, highly structured non-protein-coding, non-encapsidated RNA molecules (Diener, 1971a & 1971b; Semancik & Weathers, 1972; Sanger *et al*., 1976; Gross *et al*., 1978). Non-coding does not mean non-functional (Diener, 1979; Flores *et al*., 2005). Viroid genome has genetic information for replication, movement from cell-to-cell and long distance, host specificity by inducing specific pathogenic effect in a host. The disease process is initiated by the direct interaction of genomic RNA and or structural determinants of viroid molecule with the host factors (proteins or nucleic acids) due to the apparent absence of pathogen-specified proteins (Keese & Symons, 1985; Visvader & Symons, 1986; Schmitz & Riesner, 1998; Diener, 1999; Flores *et al*., 2005).

The systemic infection process of a viroid can be divided into two major steps: (i) replication in individual cells and (ii) movement throughout the plant (Ding *et al*., 1999). *De novo* generated viroid progeny population from a single sequence variant within a single-plant show distinct pathogenicity and host range effects (Foissac & Duran-Vila, 2000, Gandia *et al.*, 2000, Ito *et al.*, 2000, Owens *et al.*, 2000, Gandía & Duran-Vila, 2004). Therefore, the determination of sequence and or structural features of viroid

genome responsible for the biological functions can enhance the understanding of the infectious nature of viroids.

Systemic movement is one of the fundamental requirements of viroids to achieve successful infection (Tabler and Tsagris, 2004; Flores *et al*., 2005). Unlike viruses, viroid RNA is non-coding and not encapsidated and unlike satellite RNAs, they do not require helper viruses for infection. Thus, they must interact directly with cellular factors to accomplish all of the functions needed for infection (Ding *et al*., 2005). The long distance movement of viroids was considered to be a passive movement mechanism (source-to-sink) through the phloem (Palukaitis, 1987; Gafny *et al*., 1995) but, the current evidences indicate that the systemic trafficking of viroid is regulated (Zhu *et al*., 2001; Zhu *et al*., 2002). PSTVd failed to invade the shoot apical meristem of infected *N. benthamiana* or tomato plants, (Zhu *et al*., 2001). Intriguingly, PSTVd RNA was selectively transported into sepals but not into petals, stamens, styles, or ovaries, even though the phloem tissue was present and floral organs are strong sink for photoassimilates (Zhu *et al*., 2001; Zhu *et al*., 2002). These observations indicate that the viroid trafficking is regulated within the phloem and viroid movement does not occur by simple diffusion mechanism (Zhu *et al*., 2001; Zhu *et al*., 2002).

A model for rod-like viroid molecule was proposed on the basis of comparative pairwise sequence analysis of members of the PSTVd group (Keese & Symons, 1985). The viroid molecule has been divided into five distinct structural and functional domains (Figure 12): i. left terminal (TL), ii. Pathogenic (P), iii. central conserved (CCR), iv. variable (V), and v. right terminal (TR). Earlier studies with *Citrus exocortis viroid*

(CEVd) and *Potato spindle tuber viroid* (PSTVd) mapped the nucleotide changes in the pathogenic domain of viroid secondary structure to the different degree of symptom expression (Visvader & Symons, 1985 & 1986; Schnolzer *et al*., 1985; Sano *et al*., 1992; Owens *et al*., 1995 & 1996; Gora *et al*., 1996). The subsequent studies showed that the variable domain (Hu *et al*., 1996), left and right terminal domains (Sano *et al*., 1992) and central conserved domain (Qi & Ding, 2003) also play important role in symptom expression. Recently, Zhong *et al*. (2008) showed a genomic map of PSTVd RNA motifs critical for replication and systemic trafficking in *Nicotiana benthamiana*.

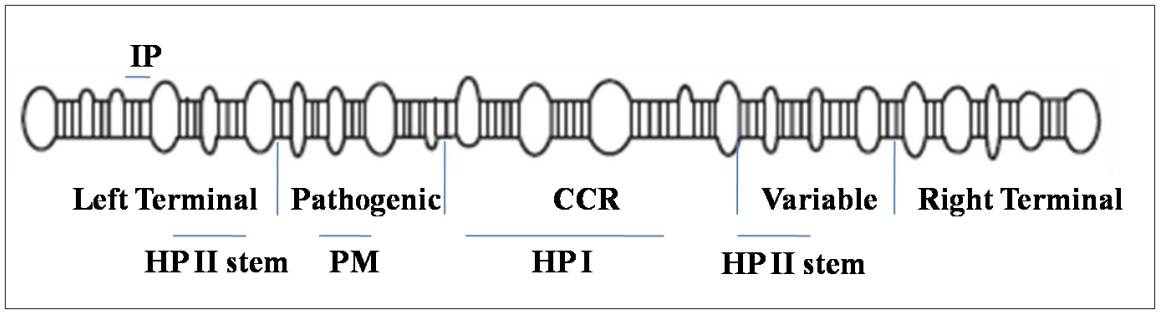

Figure 12. Schematic model of rod-like secondary structure proposed for *Pospiviroidae* family members. [CCR: Central Conserved Region; HP I: Hairpin loop; HP II: Hairpin Stem; IP: Imperfect palindrome; PR: Pre-melting Region].

Like other single-stranded RNAs, viroids can take on a variety of secondary structures. During thermal denaturation of PSTVd secondary structure (Henco *et al*. 1979; Riesner *et al*. 1979), the native structure are disorganized and a metastable structure with three hairpins (HP I, HP II and HP III) is observed. HP I is formed in the CCR domain, HP II is formed in the pathogenicity and variable domains of the majority

of the *Pospiviroidae* members (Figure 12) while, HP III is only found in PSTVd (Gora-Sochacka, 2004; Daros *et al*., 2006). Functionality for HP II has been established as it is essential for infectivity (Loss *et al*. 1991) and restoration of HP II was associated with the restoration of infectivity of a nonviable recombinant viroid (Candresse *et al*., 2001). The loop E motif located in the CCR domain of PSTVd has been found to play an important role in regulating symptom expression (Wassenegger *et al*., 1996; Zhu *et al*., 2002; Qi & Ding 2002) apart from involving in RNA–RNA, RNA–protein interactions and processing reaction of longer-than-unit length viroid RNA transcripts (Baumstark *et al*. 1997). Replication of PSTVd was increased by 5 to 10 fold in the cultured cells of tobacco BY2, but not in *N. benthamiana* due to a single nucleotide substitution (C259U) in loop E. (Qi and Ding 2002). The U257A substitution engineered in loop E of a PSTVd strain caused flat-top lethal symptoms (Qi and Ding 2003).

Numbers of studies have been conducted, where structural features of viroid have been linked to its infectivity, transmissibility and pathogenesis, in which viroid strains were created by site-directed mutagenesis. But little work is done on the biological properties of *in vivo* generated mutants or sequence variants. In the present study, an attempt was made to understand how the sequence and/or structural features of a single sequence variant affect the replication, movement, and within-plant progeny population profile to bring about distinct symptoms. In addition, the biological properties of *in vivo* generated viroid sequence variant were studied by characterizing a single sequence variant. The replication efficiency of *in vivo* generated CEVd variant was studied at the cellular level, systemic accumulation at the seedling level, intra-population profile at the

plant level and the biological properties were addressed at the disease symptom expression level in different hosts. This study was focused on four major aspects of the viroid biology: i) Replication of *in vivo* generated CEVd mutants in citrus protoplasts, ii) Systemic accumulation of *in vivo* generated CEVd mutants in citron seedlings, iii) Biology (i.e. disease symptom expression) of *in vivo* generated CEVd mutants in different experimental hosts, and iv) *De novo* generated viroid progeny population from a single sequence variant within a single-plant.

MATERIALS AND METHODS

Viroid sources. The original inoculums of CEVd, which is referred as wild-type (WT) in this present study, was obtained from the viroid collection of the Citrus Clonal Protection Program (CCPP) at the University of California, Riverside (UCR). The disease collection source tree, sweet orange (*Citrus sinensis*) for CEVd isolate E-811, was positive for a single disease agent as confirmed by repeated testing over 25 years. CEVd RNA from the reservoir tree was retro-transcribed and the amplified full length cDNA was cloned into plasmid pSTBlue-1 (EMD Chemicals). The nucleotide sequence of the full-length CEVd cDNA was determined by the University of California Riverside genomics core facility (NCBI GenBank accession GU295988).

For the study of molecular and biological properties of *in vivo* generated CEVd mutants, cDNA clones of *in vivo* generated CEVd mutants (preserved as bacterial glycerol stock in -80 ^{0}C at Dr. Vidalakis Lab, UC Riverside) were used.

Table 6. List of selected *in vivo* generated CEVd mutants.

Mutant	Domain*	Strand	Location	Mutation**	Type of Mutation[¥]	Secondary Structures[Γ]
Single Mutation	Left Terminal (TL)	Upper	17	G>A	TS	IP
		Upper	30	U>C	TS	
		Lower	344	A-	DEL	
	Pathogenic (P)	Upper	50	G>A	TS	
		Upper	62	A+	ADD	
		Lower	320	C>U	TS	HP II Loop
	Central Conserved Region (CCR)	Upper	108	U+	ADD	HP I
		Lower	264	U>A	TV	Loop E
		Lower	265	A>G	TS	Loop E
		Lower	278	U>A	TV	HP II Loop
		Lower	289	C>U	TS	HP II Loop
	Variable (V)	Upper	128	G-	DEL	
		Upper	128	G>A	TS	
		Upper	129	U>A	TV	
	Right Terminal (TR)	Upper	159	G>U	TV	
		Upper	182	U>C	TS	
		Lower	185	A>U	TV	
Double Mutation	P	Upper	41	U>A	TV	
	CCR	Upper	107	G>U	TV	HP I
Double Mutation	P	Upper	61	A>G	TS	PM
	CCR	Upper	107	G>U	TV	HP I
Double Mutation	P	Upper	62	A+	ADD	
	CCR	Lower	278	U>A	TV	HP II Loop
Double Mutation	TR	Upper	155	A>G	TS	
	CCR	Lower	263	C>A	TV	Loop E
Double Mutation	CCR	Lower	278	U>A	TV	HP II Loop
	P	Lower	316	U>C	TS	PM
Triple Mutation	TL	Upper	15	A>G	TS	
	TL	Lower	366	G>U	TV	IP
	V	Upper	130	U>A	TV	
Triple Mutation	TL	Upper	19	U>C	TS	IP
	P	Upper	67	G>A	TS	
	P	Lower	321	A>U	TV	
Triple Mutation	CCR	Upper	106	G>U	TV	HP I
	V	Lower	228	A>G	TS	
	CCR	Lower	263	C>A	TV	Loop E

* TL, Terminal Left; TR, Terminal Right;P, Pathogenic; CCR, Central Conserved Region; V, Variable.
** A, Adenine; C, Cytosine; G, Guanine; TS, Transition; TV, Transversion; U, Uracil; ">" symbol indicates "to"; "+" indicates "addition"; "-" indicates "deletion".
[¥] ADD, addition; DEL, deletion; TS, transition; TV, transversion.
[Γ] IP, imperfect palindrome; PM, pre-melting region; HP-I, hairpin loop; HP-II, hairpin stem.

The selection of CEVd mutant or sequence variants (Table 6) was based on the mutation type (transition, transversion, addition, or deletion) and site of the mutation in relation to the different structural domains of secondary structure of CEVd genome (Figure 12) (Keese and Simons 1985).

For the production of plus sense CEVd RNA transcripts, pSTBlue-1 DNA was linearized with *Sal*I and *SnaB*I restriction enzymes (New England Biolabs Inc.) for the clones with T7 and SP6 promoters respectively (Figure 1). Linearized plasmids were used as a template for the *in vitro* transcription using MEGAscript Kit (Ambion, Inc./Applied Biosystems). Freshly (1-8 hours) prepared transcripts were used for the experiments.

Characterization of *in vivo* generated CEVd mutants. Plasmid pSTBlue-1 (EMD Chemicals Inc.), containing a full-length CEVd cDNA, was isolated from *Escherichia coli* strain JM109 (Promega Corp.) using QIAprep Miniprep Kit (Qiagen) following the manufacturer's instructions. Presence of a mutation or mutations in a cDNA clone was confirmed by restriction digestion of the plasmid cDNA clone (Figure 14), followed by *in vitro* transcription, reverse transcription polymerase chain reaction (Sambrook & Russell, 2001) and finally sequencing. RNAdraw V1.1, an integrated program for RNA secondary structure calculation and analysis (Matzura & Wennborg, 1996), was used to predict the viroid RNA thermodynamic secondary structure (temperature ranging 25-37 ^{0}C).

Four major aspects of viroid biology were addressed to understand the molecular and biological properties of *in vivo* generated CEVd mutants, i) replication in citrus protoplasts, ii) systemic accumulation in citron seedlings, iii) biological properties (disease symptom expression) in different experimental hosts, and iv) *de novo* generated viroid progeny population from a single sequence variant within a single-plant. Methodology for each aspect is provided separately.

i) Replication of in vivo generated CEVd mutants in citrus protoplasts

Methodology for isolation and transfection of protoplasts was followed as mentioned in the chapter A1. For each mutant, three biological replications were used. WT-CEVd was used as a positive control while DEPC-water as a mock inoculation. Transfected protoplasts were incubated for 5 days in the dark without shaking at 28 ^{o}C. After 5 days post inoculation (dpi), total RNA was extracted from the transfected protoplasts using Trizol (Invitrogen Corp.) extraction method (Chomczynski and Sacchi 1987) as mentioned in the chapter A1. Total RNA preparation was treated with RQ1 RNase-Free DNase I (Promega Corp.) following the manufacturer's instructions and stored at -80 ^{0}C.

ii) Systemic accumulation of in vivo generated CEVd mutants in citron seedlings

Source of citron seedling material. Three week old 'Etrog' citron (*Citrus medica* L.) selection 'Arizona 861-S1' seedlings growing *in vitro* were used for the study of systemic accumulation of *in vivo* generated CEVd mutants. Seed germinating media

(pH 5.7) constituted MS salts (Murashige & Skoog, 1962) with GELRITE® Gellan Gum (CP Kelco applications, USA) as solidifying agent. Seed coat of healthy citron seeds were peeled off manually and sterilized in 10% solution of household bleach. Under aseptic conditions, three peeled and sterilized seeds were cultured in 25×150 mm culture tubes containing 25 ml seed germinating medium. Cultures were incubated in plant growth chamber with 16 h photoperiod at 32 ºC and 8 h darkness at 28 ºC (Navarro *et al*., 1975). Three-to-four week old seedlings, which measured 7-8 cm in length with 4-5 leaflets, were inoculated and the systemic accumulation of the viroid was monitored (Figure 13).

Study of Systemic accumulation with WT-CEVd. To make a comparative analysis of systemic accumulation of *in vivo* generated CEVd mutants with WT-CEVd, it was necessary to perform a control experiment with wild-type viroid clone to know the optimum days post inoculation for the analysis.

Systemic accumulation of CEVd was monitored over the period of five days (Table 7). For each day treatment, three biological replicas were used. Under sterilization conditions, three-to-four week old seedling was slash inoculated on to the lower part of the stem region with an aliquot of 500 ng *in vitro* transcripts using a razor blade (Figure 13).

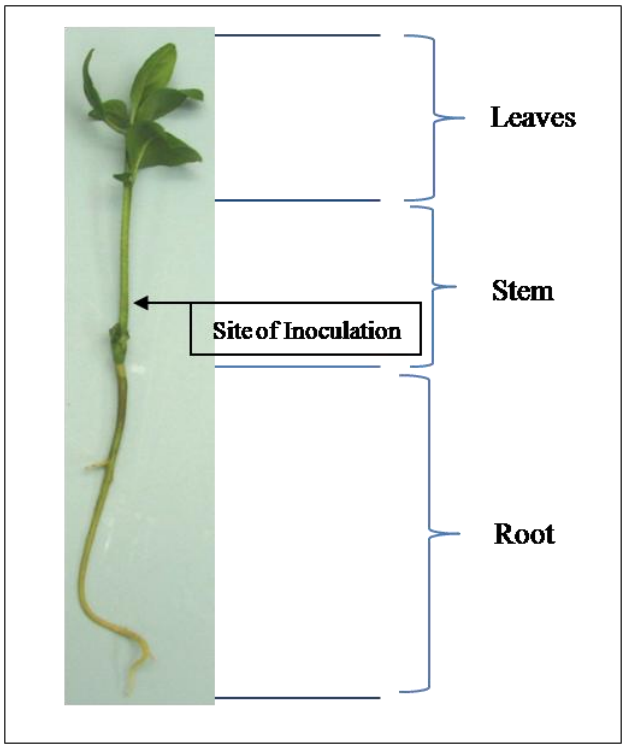

Figure 13. Citron seedling used for the study of systemic accumulation of CEVd. As shown in the figure, the lower part of stem was the site of inoculation of CEVd transcript RNA. For the analysis, seedling was divided in to three parts namely leaves, stem and root.

Upon inoculation, the seedlings were transferred to 25×150 mm culture tubes containing liquid medium. The liquid medium contained 4.33 g/l MS salts, White's vitamins (1 mg/l nicotinic acid, 1 mg/l pyridoxine, 0.2 mg/l thiamine HCl) (White, 1943 & 1963), 100 mg/l inositol, and 75 g/l sucrose. All seedlings were maintained under plant growth chamber with 16 h photoperiod at 32 ºC and 8 h darkness at 28 ºC (Navarro *et al*., 1975).

Table 7. Time course experiment to analyze the systemic accumulation of CEVd in citron seedlings.

No.	Seedling Sample	Inoculation	
	Days post inoculation (dpi)	Amount of transcript RNA (μg)	Volume (μL)
1	1 dpi/CEVd	0.5	10
2	2 dpi/CEVd	0.5	10
3	3 dpi/CEVd	0.5	10
4	4 dpi/CEVd	0.5	10
5	5 dpi/CEVd	0.5	10
6	5 dpi/H_2O	NA	10

NA, not applicable.

Total RNA extraction. For the analysis of systemic accumulation of WT-CEVd, citron seedling was divided in to three parts; leaf, stem and root (Figure 13). Total RNA was extracted by using a commercial kit (Spectrum Plant Total RNA Kit-Sigma Aldrich) with slight modifications. Initial tissue disruption was performed in Mini-BeadBeater-96® Homogenizer (Daintree Scientific, Australia). This homogenizer is ideal for avoiding cross-contamination. Cell disrupter utilizes sterilized ceramic beads for complete cell breakage in three minutes. Initial tissue grinding was performed in the Lysis Solution plus β-mercaptoethanol mixture from the Spectrum Plant Total RNA Kit (Sigma Aldrich). Rest of the protocol was performed according to the manufacturer's

instructions. The total RNA preparation was aliquot and stored at -80 ^{0}C until used for further analysis.

Real-Time RT-PCR assay. The systemic accumulation of CEVd in citron seedlings was monitored by SYBR Green I based real-time RT-PCR assay. The procedure for real-time RT-PCR assay was followed as mentioned in the chapter A1. Total RNA preparation was normalized to the internal control (citrus Phospholipase-Delta gene). After the normalization of the samples with an internal control, the adjusted dilution factors of total RNA were used to make cDNA specific to CEVd. A 2 µl of cDNA was used in the real-time PCR with CEVd specific forward primers 3F (5'-GAAGCTTCAACCCCAAACC-3') and reverse primer 2R (5'-CTTTTTTCTTTTCCTGCCTGCA-3') following the manufacturer's (SABiosciences) instructions.

The real-time PCR results were analyzed with MX3005P data analysis software (Stratagene). Quantification of CEVd in citron seedling samples was performed by comparing the Ct value of each sample to the Ct values of the standard curve. The amount of starting template in a PCR reaction, expressed as the copy number of the target CEVd cDNA, could be determined. The average of the three biological replications per treatment was used in comparing the relative levels of viroid accumulation in different parts of citron seedling over the period of five days. The numerical value data was converted to chart data (Figure 16). For the ease of comparison, the accumulation level of CEVd RNA in stem at 1 dpi was arbitrarily set to a value of 1. The levels of CEVd RNA

from other parts of the seedlings from subsequent days were presented as relative values to this reference value.

Study of systemic accumulation of *in vivo* generated CEVd mutants with WT-CEVd. Based on the control experiment results, 5 dpi was set as the standard days post inoculation for the comparative analysis of systemic accumulation of *in vivo* generated CEVd mutants with the WT-CEVd. For each day treatment, three biological replicas were used. Inoculation procedure followed as mentioned above with an aliquot of 500 ng *in vitro* transcripts. Upon inoculation, the seedlings were maintained under plant growth chamber with 16 h photoperiod at 32 ºC and 8 h darkness at 28 ºC (Navarro *et al*., 1975).

Total RNA extraction. Since one of the objectives of the present study was to correlate the specific mutation of CEVd to its effect on systemic accumulation and disease symptom expression, for the analysis of systemic accumulation of *in vivo* generated CEVd mutants, the upper systemic part of the citron seedling, leaf, was used (Figure 13). Total RNA was extracted by using a commercial kit (Spectrum Plant Total RNA Kit-Sigma Aldrich) with slight modifications as mentioned above. The total RNA preparation was aliquot and stored at -80 ^{0}C until used for further analysis.

Real-Time RT-PCR assay for the study of replication and systemic accumulation of *in vivo* generated CEVd mutants. A comparative analysis of replication and systemic accumulation of *in vivo* generated CEVd mutants and the WT-CEVd was performed by SYBR Green I based real-time RT-PCR assay. The total RNA extracted after 5 dpi, from

the study of replication in citrus protoplasts and systemic accumulation study in citron seedlings, were employed in the real-time RT-PCR assay. The procedure for real-time RT-PCR assay was followed as mentioned in the chapter A1.

Analysis of real-time RT-PCR data. The real-time PCR results were analyzed with MX3005P data analysis software (Stratagene). Quantification of CEVd in the protoplast samples and leaves of citron seedlings was performed by comparing the Ct value of each sample to the Ct values of the standard curve. The amount of starting template in a PCR reaction, expressed as the copy number of the target CEVd cDNA, could be determined. The average of the three replications per treatment was used in comparing the relative levels of *in vivo* generated CEVd mutant's accumulation in comparison with WT-CEVd after 5 dpi. The numerical value data was converted to chart data. For the ease of comparison, the accumulation levels of WT-CEVd RNA after 5 dpi was arbitrarily set to a value of 1 and the levels of accumulation of *in vivo* generated CEVd mutants after 5 dpi were presented as relative values to this reference value.

iii) Biological properties of in vivo generated CEVd mutants in different experimental hosts

Sources of Plant Material. Citrus and herbaceous hosts employed in the study of biological properties of *in vivo* generated mutants of CEVd were listed in Table 8.

Table 8. Citrus and herbaceous hosts employed in study of biological properties of *in vivo* generated mutants of *Citrus exocortis viroid* (CEVd).

Common name	Family	Genus	Species
Citrus hosts			
'Etrog' citron*	*Rutaceae*	*Citrus*	*medica*
Herbaceous hosts			
Rutgers tomato	*Solanaceae*	*Lycopersicon*	*esculentum*
Eggplant		*Solanum*	*melongena*
Datura		*Datura*	*stramonium*
Gynura	*Asteraceae*	*Gynura*	*aurantiaca*
Chrysanthemum		*Dendranthema*	*grandiflora*

* Bioamplification host for CEVd

'Etrog' citron (*Citrus medica* L.) selection 'Arizona 861-S1' propagated by bud grafting onto the rough lemon (*C. jambhiri* Lush.) rootstock, was used as a citrus host. Gynura (*Gynura aurantiaca* DC), chrysanthemum (*Dendranthema grandiflora* Tzvelev.) cv. "Bonnie Jean", tomato 'Rutgers' (*Lycopersicon esculentum* Mill.), eggplant (*Solanum melongena* L.), and datura (*Datura stromanium* L.), were used as herbaceous host plants. All the herbaceous hosts were propagated as seedlings except gynura and chrysanthemum. Clonal propagations of gynura and chrysanthemum were prepared by rooted cuttings from healthy sources. All plants were maintained under standard glasshouse conditions.

Infectivity assays. Each plant was slash inoculated with an aliquot of 10 µg *in vitro* transcripts using a razor blade. Host range of each mutant was tested by inoculating to three experimental hosts such as citron, gynura and chrysanthemum apart from inoculating to the original host of the mutant. Biological properties of the *in vivo* generated CEVd mutants at the disease symptom expression level was monitored as mentioned in the chapter A1.

iv) De novo generated viroid progeny population from a single sequence variant within a single-plant

The host plants, which were positive from the tissue imprint and slot-blot hybridization assays, were further used for the study of intra-population profile of CEVd within a single-plant. Extraction of progeny viroid RNA and RT-PCR procedures were followed as mentioned in chapter A1.

Cloning and Sequencing. RT-PCR products from different experimental hosts were purified according to the High Pure PCR Product Purification Kit by Roche (Roche Applied Science) and used for cloning and sequencing. 96-well format plasmid preparation and DNA sequencing was employed for this purpose. Cloning and sequencing protocols were followed as mentioned in the chapter A1.

Statistical analysis. The categorical data were analyzed using $\chi 2$ contingency analysis. Larger contingency tables (greater than 3x3) were reduced to smaller sizes by combining cells in a meaningful way to enhance the statistical power of the $\chi 2$ test (Zar, 1984).

RESULTS

Diagnostic digestion of the CEVd/pSTBlue-1 plasmid with *Bam*HI (Figure 14) confirmed the presence of cloned insert DNA. The confirmed CEVd/pSTBlue-1 plasmids were further used for the study of molecular and biological properties.

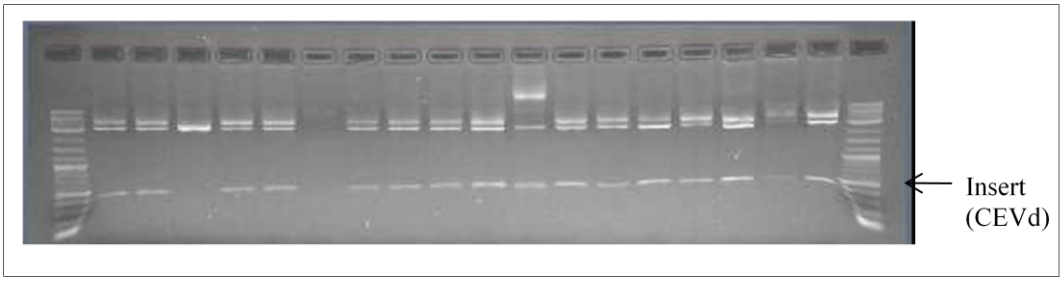

Figure 14. Presence of *Citrus exocortis viroid* (CEVd) insert DNA was confirmed by a diagnostic digestion of the plasmid DNA with BamHI restriction enzyme. Ethidium bromide stained 2% TBE agarose gel.

The purified RT-PCR product from different experimental hosts was analyzed with 1.2% Tris-borate-EDTA (TBE) agarose gel electrophoresis (Figure 17) with standard molecular weight markers after staining with ethidium bromide.

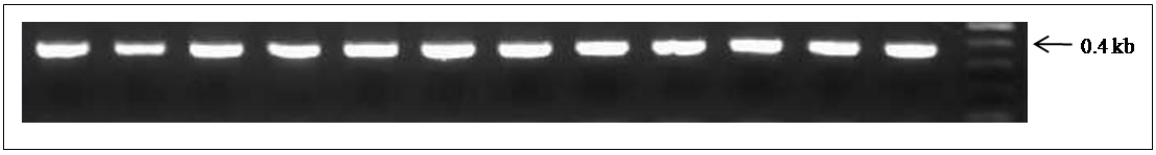

Figure 15. *Citrus exocortis viroid* (CEVd) PCR product in ethidium bromide stained 1.2% TBE agarose gel. Arrowhead indicates molecular marker band 0.4 kb.

WT-CEVd could be detected in stem, which was the site of inoculation, from all five day samples. There was gradual increase in the accumulation level of CEVd in stem region. After 5 dpi, CEVd could be detected in leaves of the seedling (Figure 16). Based on this control experiment results, 5 dpi was set as the standard days post inoculation for the comparative analysis of systemic accumulation of *in vivo* generated CEVd mutants.

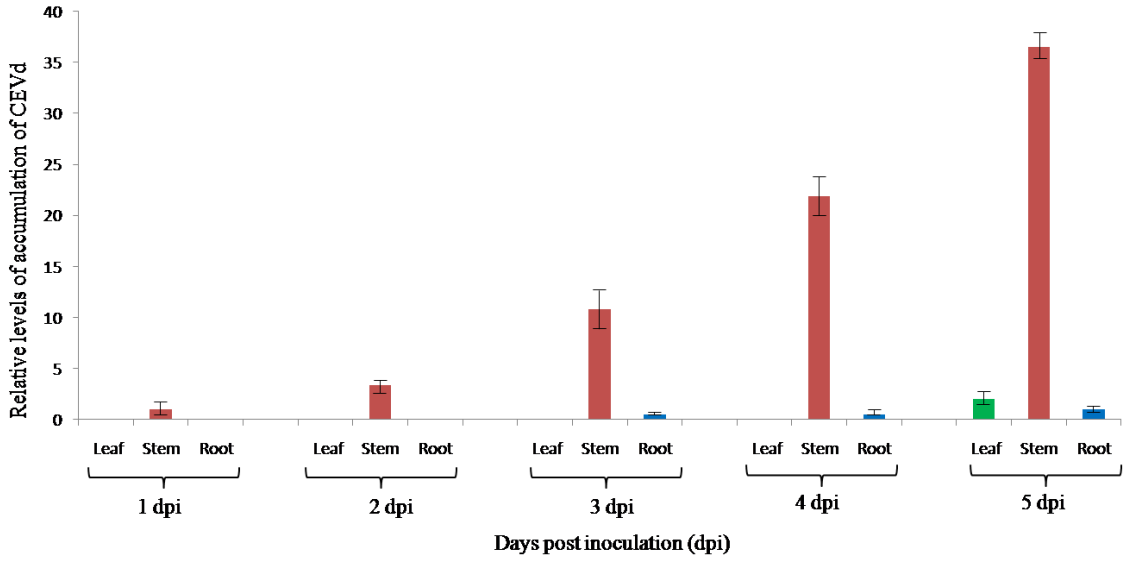

Figure 16. Relative levels of accumulation of CEVd in different parts of citron seedling. Base of the stem was the site of inoculation (Refer Figure 13). The accumulation level of CEVd RNA in stem at 1 dpi was arbitrarily set to a value of 1. The levels of CEVd RNA from other parts of the seedlings from subsequent days were presented as relative values to this reference value.

To understand the molecular and biological properties of *in vivo* generated CEVd mutants, each mutant was tested for its replication in citrus protoplasts, systemic accumulation in citron seedlings, biological properties in different experimental hosts and

intra-population profile of progeny viroid within a single-host. Host range of each mutant was tested by inoculation of three experimental hosts namely 'Etrog' citron, gynura, and chrysanthemum.

***Mutants with a single mutation*:**

***Mutant G17A*:**

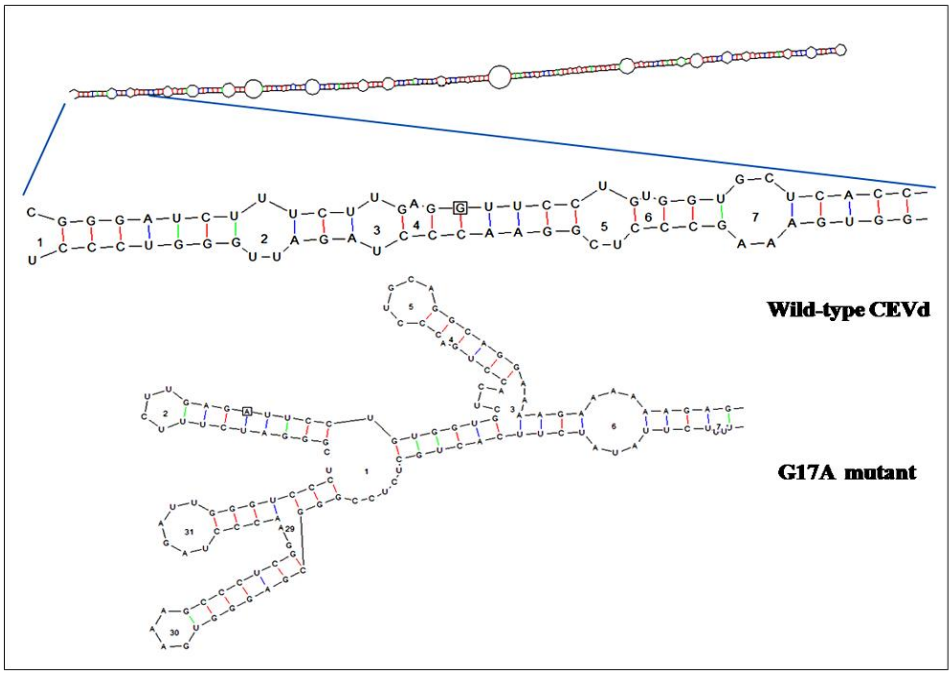

Figure 17. Primary and thermodynamic secondary structures of CEVd RNA (-137.84 at 37 ^{0}C) as predicted by RNAdraw V1.1 RNA secondary structure calculation and analysis algorithm. Mutated nucleotide site is presented in the square box. The transition, from G to A at position 17 (G17A), lead to an alternative secondary structure.

A CEVd mutant generated in 'Sweet' orange (*Citrus sinensis*) with transition mutation G17A in left terminal domain (Figure 17) could not infect the experimental hosts citron, gynura, and chrysanthemum (Table 9). Even after 5 dpi, the mutant G17A was not detected in citrus protoplasts when compared to WT-CEVd. Similarly, it was not detected in the systemic leaves of citron seedlings after 5 dpi.

***Mutant U30C*:**

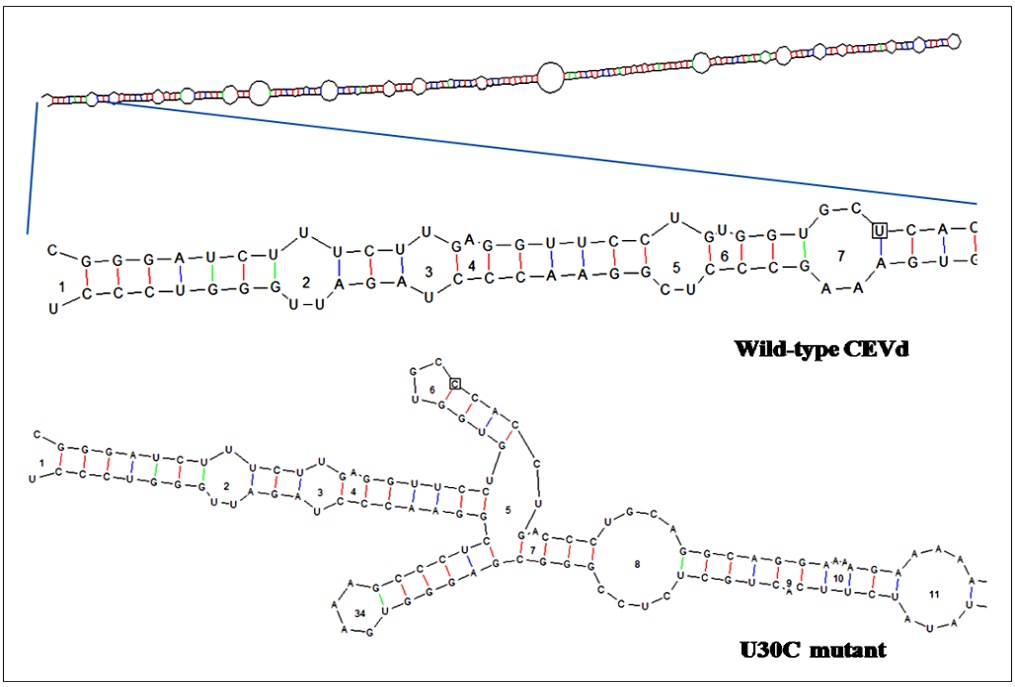

Figure 18. Primary and thermodynamic secondary structures of CEVd RNA (-139.5 at 37 ^{0}C) as predicted by RNAdraw V1.1 RNA secondary structure calculation and analysis algorithm. Mutated nucleotide site is presented in the square box. The transition, from U to C at position 30 (U30C), lead to an alternative secondary structure.

A CEVd mutant generated in eggplant (*Solanum melongena*) with the transition mutation U30C in the left terminal domain (Figure 18) could infect eggplant but not the other experimental hosts citron, gynura and chrysanthemum (Table 9) The mutant U30C did not induce any visible symptoms in eggplant (Figure 19). After 5 dpi, the mutant was not detected in citrus protoplast or in the systemic leaves of citron seedlings (Table 11).

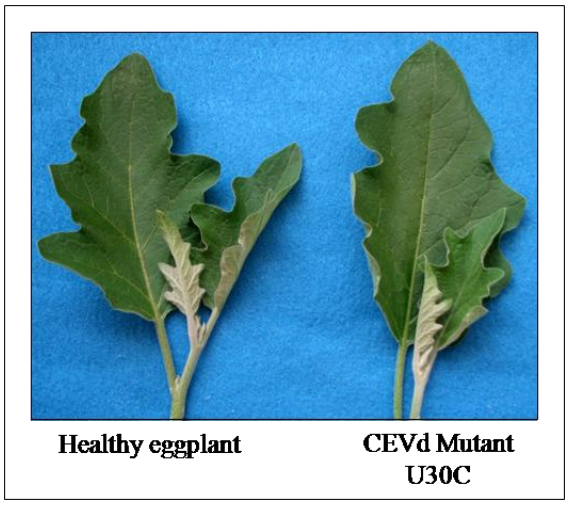

Figure 19. Biological properties of *in vivo* generated CEVd mutant U30C. Eggplant inoculated with CEVd mutant U30C exhibited no symptoms.

In the viroid progeny profile, the wild-type CEVd found to be the master sequence as well as the most recent common ancestor. The effect of host processing on the inoculated CEVd mutant clone U30C resulted in the reversion of the mutation to the wild-type sequence (Table 12). There was no statistically significant difference (χ^2=1.88, two-tailed P value=1.69, df=1) between the haplotype frequency of the master sequence and the variants population (Table 12).

A CEVd mutant generated in datura (*Datura stramonium*) with the deletion of adenine 344A- in the left terminal domain (Figure 20) could infect datura and gynura but not citron, and chrysanthemum (Table 9). The mutant 344A- induced milder symptoms in gynura than the WT-CEVd, (Figure 21-B).The original host, datura, was symptomless for both CEVd types (Figure 21-A). The mutant was not detected, after 5 dpi, in citrus protoplasts or systemically in the leaves of citron seedlings (Table 11).

***Mutant 344A-*:**

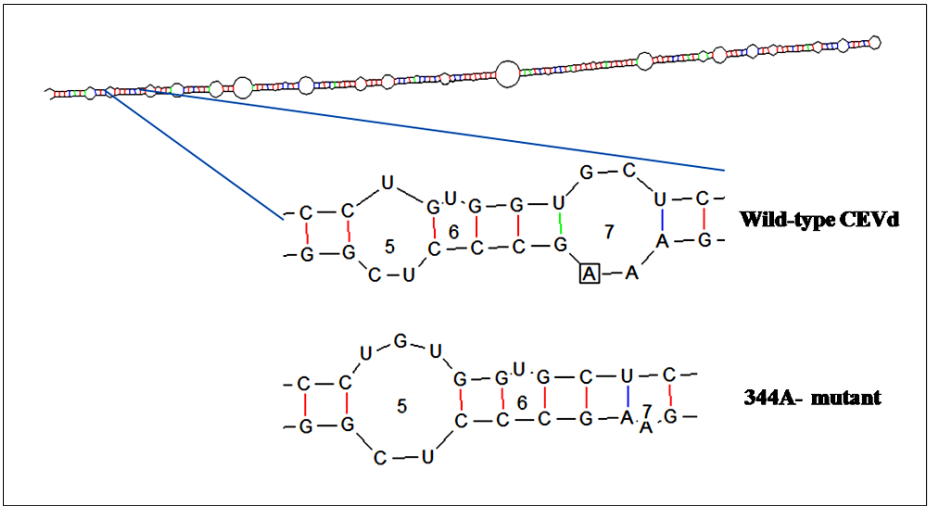

Figure 20. Primary and thermodynamic secondary structures of CEVd RNA (-139.85 at 37 ^{0}C) as predicted by RNAdraw V1.1 RNA secondary structure calculation and analysis algorithm. Mutated nucleotide site is presented in the square box. The deletion of adenine nucleotide at position 344 (344A-) resulted in change in the size of the loop number 7 of the predicted secondary structure.

In both viroid progeny profiles, WT-CEVd found to be the master sequence as well as the most recent common ancestor. The viroid processing in both hosts inoculated with the CEVd mutant 344A- resulted in the reversion of the mutation to the wild-type sequence (Table 12). In datura, a unique variant with a transversion mutation at position 130 generated a fitness peak. There was no statistically significant difference (χ^2=0.023, two-tailed P value=0.878, df=1) between the frequency of the master sequence and the progeny variants in datura. On the contrary, the frequency of the master sequence was significantly higher (χ^2= 9.38, two-tailed P value=0.002, df=1) than the progeny variants in the gynura population.

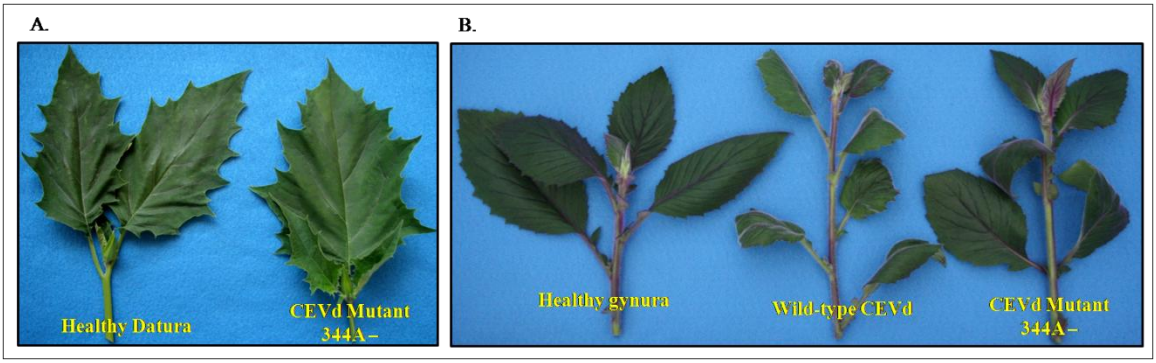

Figure 21. Biological properties of *in vivo* generated CEVd mutant 344A-. Mutant did not induce symptoms in its original host datura (A), while it manifested symptoms like that of the WT-CEVd, leaf rugosity and epinasty, in gynura (B).

***Mutant G50A*:**

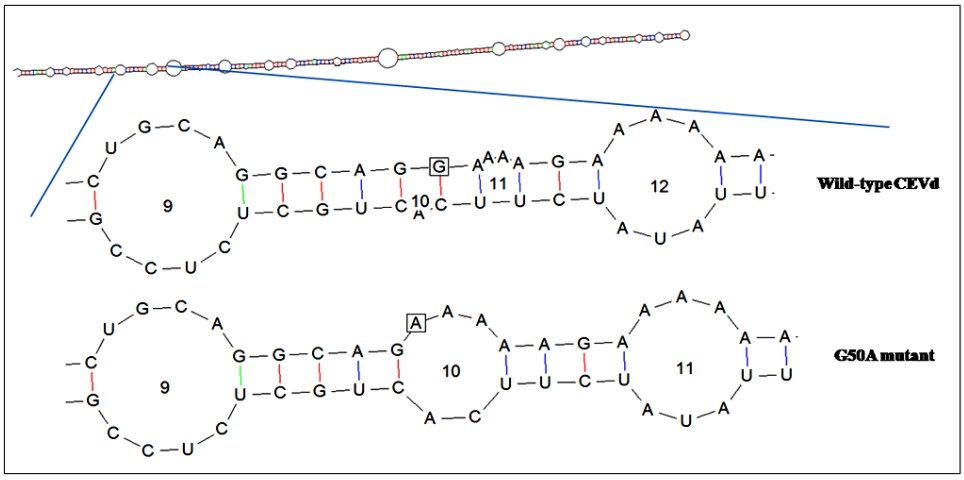

Figure 22. Primary and thermodynamic secondary structures of CEVd RNA (-137.95 at 37 ^{0}C) as predicted by RNAdraw V1.1 RNA secondary structure calculation and analysis algorithm. Mutated nucleotide site is presented in the square box. The transition at position 50 (G50A) resulted in merging and enlargement of the loop number 10.

A CEVd mutant generated in citron (*Citrus medica*) with the transition mutation G50A in the pathogenic domain (Figure 22) could infect all the three experimental hosts (Table 9). The mutant G50A could induce symptoms in gynura similar to the WT-CEVd, while in citron, the symptoms appeared less severe than the WT (Figure 23).

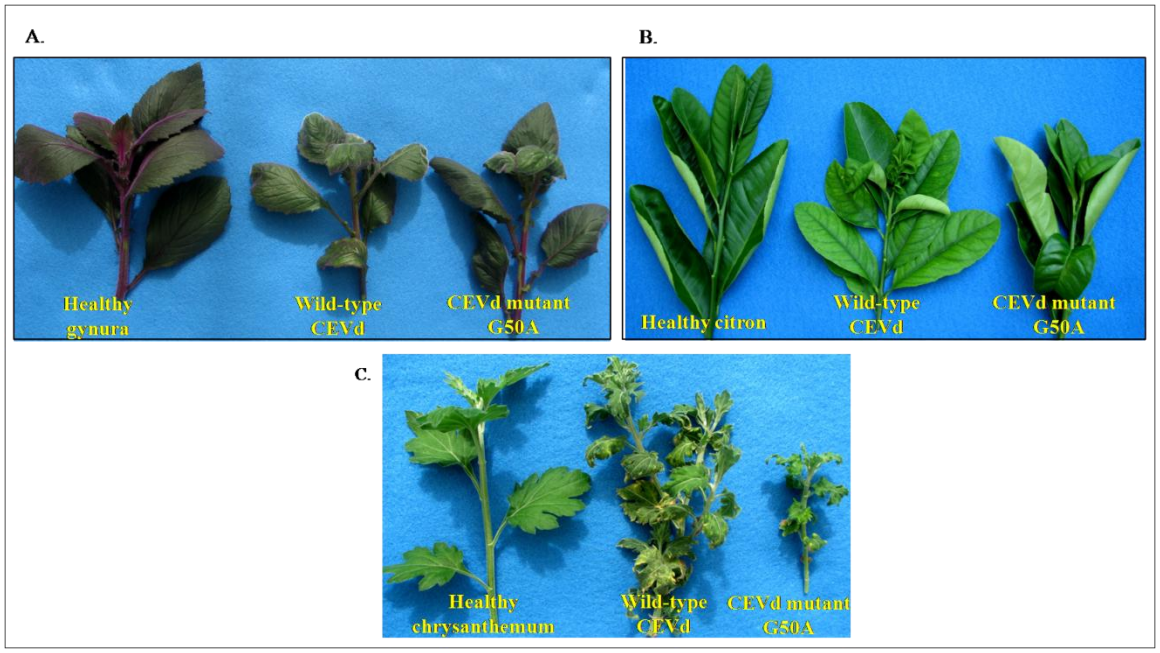

Figure 23. Biological properties of *in vivo* generated CEVd mutant G50A. Mutant induced symptoms like that of WT-CEVd clone, leaf rugosity and epinasty, in all the three experimental hosts, gynura (A) and citron (B) and chrysanthemum (C).

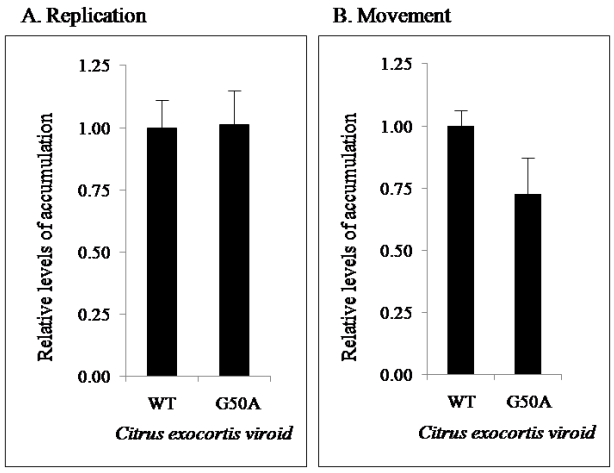

Figure 24. Relative levels of accumulation of wild-type CEVd and *in vivo* generated CEVd mutant G50A in citrus protoplasts (A) and systemic leaves of citron seedling (B).

Citrus protoplasts supported replication of the CEVd mutant G50A and systemic accumulation was verified on leaves of citron seedlings after 5 dpi (Table 11). No significant difference was found in the levels of accumulation of the mutant G50A and WT-CEVd in the citrus protoplasts or the systemic leavesof citron seedlings after 5 dpi (Figure 24). In the viroid progeny profile, the WT-CEVd found to be the master sequence as well as the most recent common ancestor (Table 9) in both hosts. The effect of host processing on the CEVd mutant G50A resulted in the reversion of the mutation to the wild-type sequence in all the three cases (Table 12). No significant difference was observed between the number of master sequences and the variants in both hosts (Table 12).

***Mutant 62A+*:**

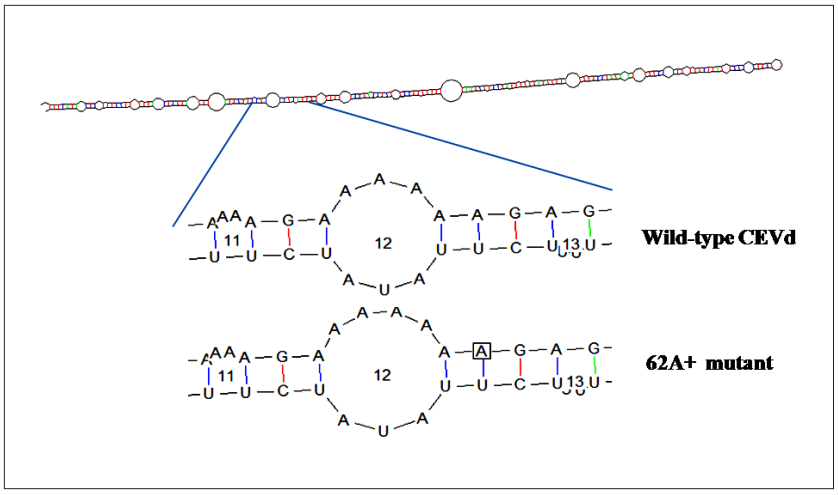

Figure 25. Primary and thermodynamic secondary structures of CEVd RNA (-138.75 at 37 ^{0}C) as predicted by RNAdraw V1.1 RNA secondary structure calculation and analysis algorithm. Mutated nucleotide site is presented in the square box. The addition of adenine nucleotide at position 62 (62A+) did result in the enlargement of the loop number 12 of the predicted secondary structure.

The CEVd mutant generated in citron (*Citrus medica*) with the addition of an adenine (62A+) in the pathogenic domain (Figure 25) infected all expermental hosts tested (Table 9). The mutant 62A+ was able to induce symptoms, like that of WT-CEVd clone (Figure 26-A), in gynura. However, it induced more severe symptoms, compared to the WT-CEVd, in citron and chrysanthemum (Figure 26-B & 26-C). Levels of accumulations of the mutant 62A+ in citrus protoplast was significantly higher than the WT-CEVd after 5 dpi (χ^2= 14.2, two-tailed P value=0.0002, df=1). However, its systemic presence in the leaves of citron seedling after 5 dpi was not significantly different when compared to the WT-CEVd levels (χ^2=0.52, two-tailed P value=0.46, df=1) (Figure 27).

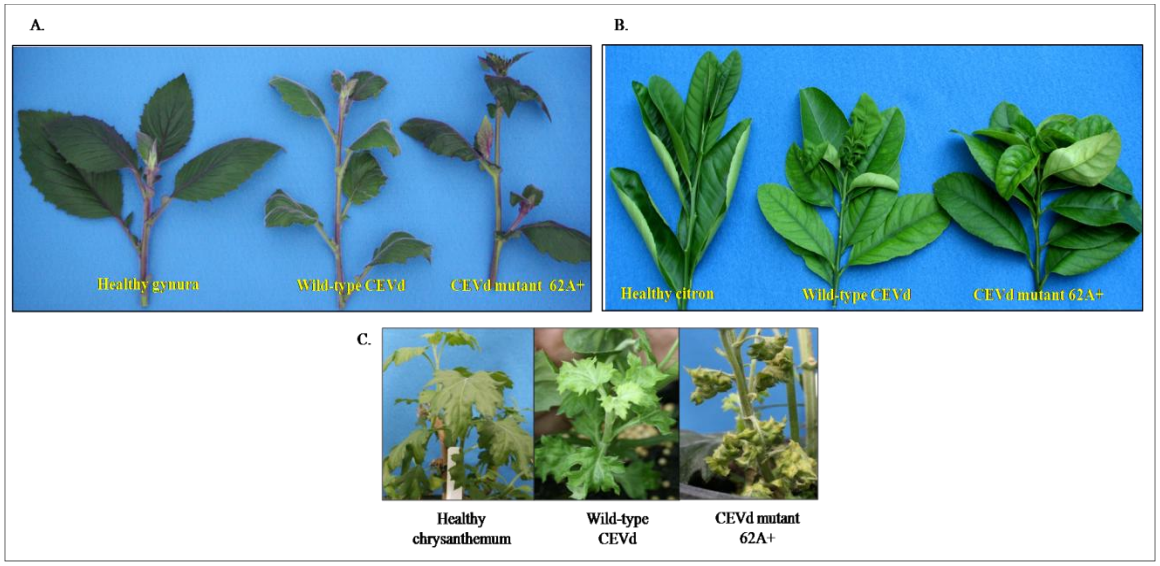

Figure 26. Biological properties of *in vivo* generated CEVd mutant 62A+. Mutant induced severe symptoms, leaf rugosity and epinasty, than the WT in gynura (A), citron (B) and chrysanthemum (C).

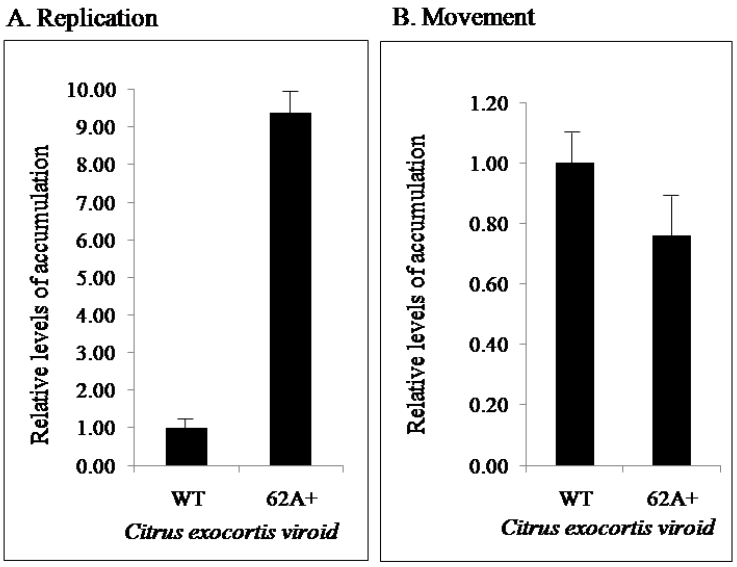

Figure 27. Relative levels of accumulation of wild-type CEVd and *in vivo* generated CEVd mutant 62A+ in citrus protoplasts (A) and systemic leaves of citron seedling (B).

In the viroid progeny profile of citron and chrysanthemum hosts, the WT-CEVd found to be the master sequence as well as the most recent common ancestor. Whereas, a new sequence variant (61A-) found to be the master sequence as well as the most recent common ancestor in the viroid progeny population of gynura (Table 12). The wild-type sequence was found to be the second-most frequent sequence in the CEVd gynura population (Table 12).

Viroid replication in citron resulted in the reversion of the mutation 62A+ to the wild-type sequence. The inoculated mutant sequence 62A+ was found to be the second highest in frequency (8/47) in the population (Table 12). The difference in the haplotype frequency of the master sequences and the variants in the viroid population was not statistically significant in gynura (χ^2=1.68, two-tailed P =0.19, df=1) as well as in citron (χ^2=3.59, two-tailed P =0.058, df=1) (Table 12).

Like in gynura, a new sequence variant (61A-) induced fitness peak in chrysanthemum. The host processing on the CEVd mutant (62A+) resulted in reversion of the mutation to the wild-type sequence in chrysanthemum (Table 12). However, the sequence (62A+) was not eliminated from the progeny population since it induced a fitness peak. The difference in the haplotype frequency of master sequences and the variants in the viroid population of chrysanthemum host was statistically significant (χ^2=15.24, two-tailed P =0.0001, df=1) as more variants were found compared to citron and gynura (Table 12).

***Mutant C320U*:**

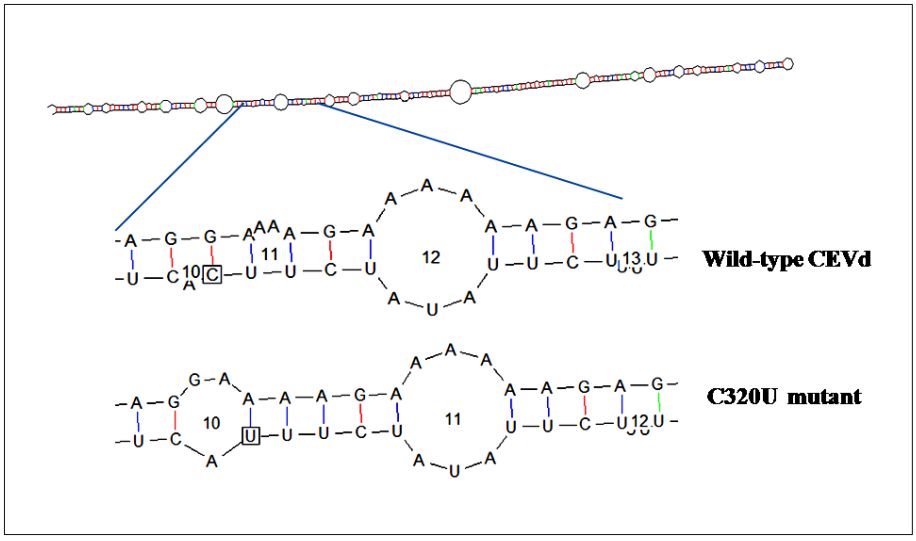

Figure 28. Primary and thermodynamic secondary structures of CEVd RNA (-140.34 at 37 ^{0}C) as predicted by RNAdraw V1.1 RNA secondary structure calculation and analysis algorithm. Mutated nucleotide site is presented in the square box. The transition, from C to U at position 320 (C320U), resulted in the merging and enlargement of a loop in the predicted secondary structure.

A CEVd mutant generated in hybrid tomato (*Lycopersicon esculentum* x *L. peruvianum*) with the transition mutation C320U in the pathogenic domain (Figure 28) did not infect the experimental hosts' citron, gynura and chrysanthemum (Table 9). The mutant C320U was able to replicate in citrus protoplast but in lower levels when compared to WT-CEVd after 5 dpi. On the contrary, the mutant was not detected systemically in the leaves of citron seedlings after 5 dpi (Table 11).

***Mutant 108U+*:**

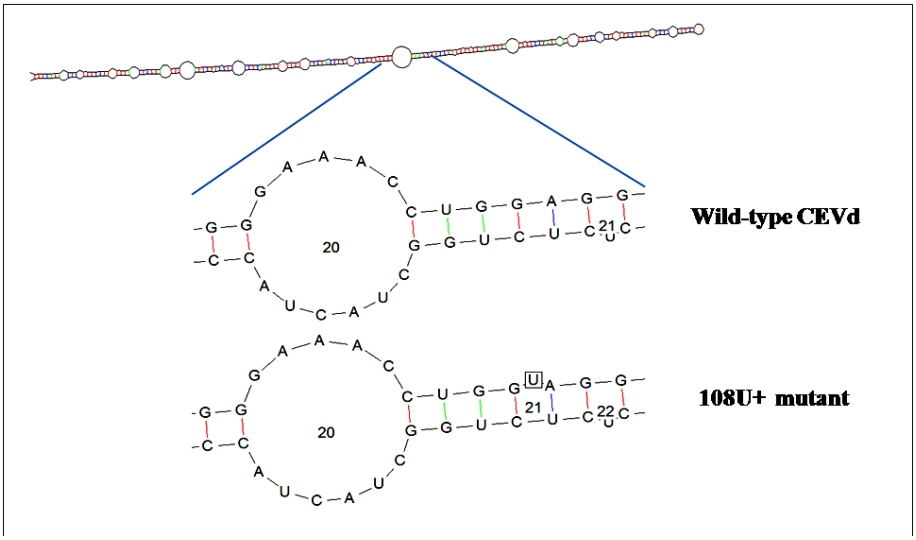

Figure 29. Primary and thermodynamic secondary structures of CEVd RNA (-135.22 at 37 ^{0}C) as predicted by RNAdraw V1.1 RNA secondary structure calculation and analysis algorithm. Mutated nucleotide site is presented in the square box. The addition of uridine nucleotide at position 108 (108U+) did introduce a small loop in the predicted secondary structure.

A CEVd mutant generated in chrysanthemum (*Dendranthema grandiflora*) with the addition of uridine (108U+) in the central conserved region of CEVd (Figure 29) infected all expermental hosts tested (Table 9). The mutant 108U+ induced symptoms,

like that of WT-CEVd, in all the three hosts (Figure 30). Levels of accumulations of mutant 108U+ in citrus protoplas and systemically in leaves of citron seedlings were statistically not different from the levels of WT-CEVd after 5 dpi (χ^2= 1.00, two-tailed P value=0.317, df=1) (Table 11).

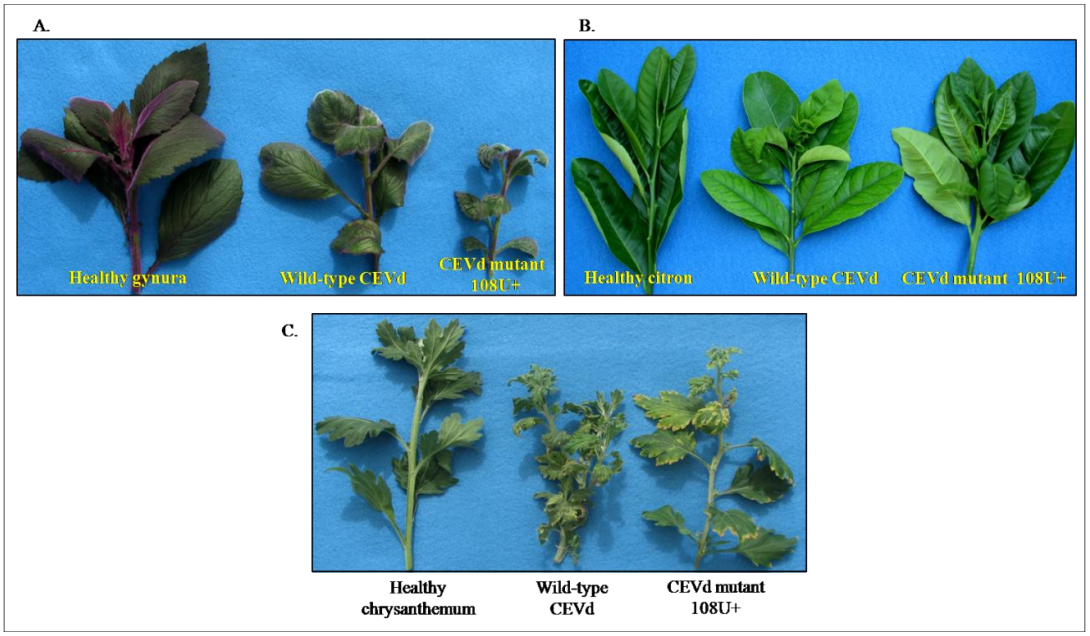

Figure 30. Biological properties of *in vivo* generated CEVd mutant 108U+. Mutant induced symptoms like that of WT-CEVd clone, leaf rugosity and epinasty, in gynura (A), citron (B) and chrysanthemum (C).

In the viroid progeny profile, the WT-CEVd found to be the master sequence as well as the most recent common ancestor in all three hosts. Viroid processing in all three experimental hosts resulted in the reversion of the mutant to wild-type sequence. Mutations at positions 107, 108, 153 and 186 induced fitness peaks (Table 12). The difference in the number of master sequences and the variants in the viroid population of

all experimental hosts tested were considered to be statistically significant (χ^2= 1.47, two-tailed P value=0.367, df=1) (Table 12).

***Mutant U264A*:**

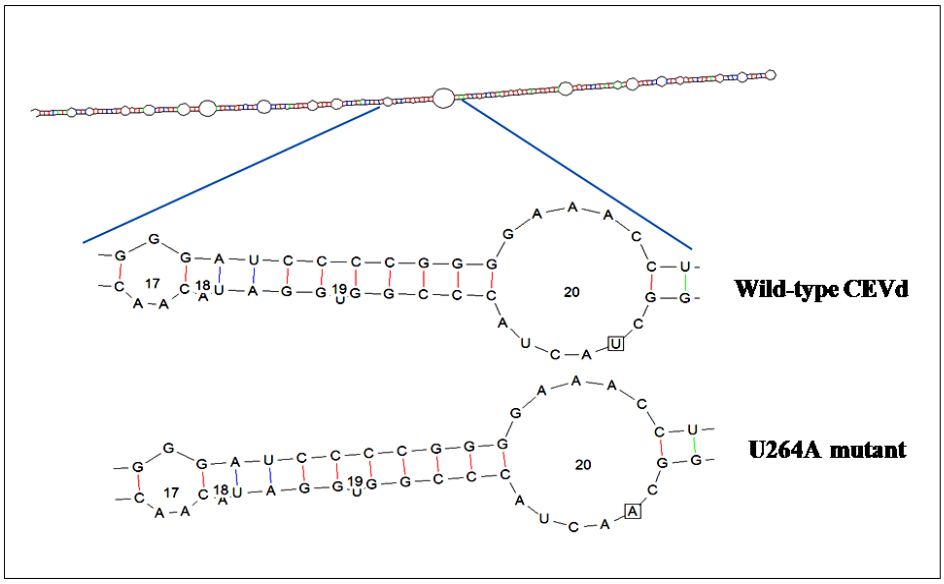

Figure 31. Primary and thermodynamic secondary structures of CEVd RNA (-139.12 at 37 ^{0}C) as predicted by RNAdraw V1.1 RNA secondary structure calculation and analysis algorithm. Mutated nucleotide site is presented in the square box. The transversion, from U to A at position 264 (U264A) did not result in change of the predicted secondary structure.

A CEVd mutant generated in luffa (*Luffa aegyptiaca*) with the transversion mutation U264A in the central conserved region of CEVd (Figure 31) infected only gynura from the expermental hosts tested (Table 9). The mutant U264A induced milder symptoms than the WT-CEVd, in gynura (Figure 32). After 5 dpi, the mutant U264A was not detected in citrus protoplast as well as systemically in the leaves of citron seedlings (Table 11).

The inoculated mutant sequence U264A found to be the master sequence as well as the most recent common ancestor in gynura. Viroid replication and processing in gynura resulted in the stability of the U264A mutation (Table 12). The difference in the haplotype frequency of the master sequence and the variants in the viroid population was not statistically significant (χ^2= 3.42, two-tailed P value=0.064, df=1) (Table 12).

Figure 32. Biological properties of *in vivo* generated CEVd mutant U264A in gynura. Mutant induced symptoms milder than that of WT-CEVd clone.

A CEVd mutant generated in eggplant (*S. melongena*) with the transition mutation (A265G) in the central conserved region of CEVd (Figure 33) could infect all expermental hosts tested (Table 9). The mutant A265G induced more severe symptoms, compared to the WT-CEVd, in chrysanthemum while, symptoms induced in gynura and citron were similar to the WT-CEVd. The original host eggplant was symptomless for both CEVd types (Figure 34). Levels of accumulations of the A265G mutant in citrus protoplast and systemically in the leaves of citron seedlings was not statistically

significant from the levels of the WT-CEVd after 5 dpi (χ^2= 1.38, two-tailed P value=0.23, df=1) (Figure 35).

***Mutant A265G*:**

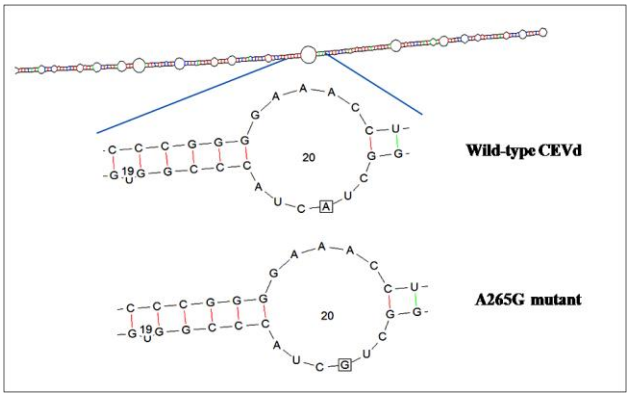

Figure 33. Primary and thermodynamic secondary structures of CEVd RNA (-139.12 at 37 ^{0}C) as predicted by RNAdraw V1.1 RNA secondary structure calculation and analysis algorithm. Mutated nucleotide site is presented in the square box. The transition, from A to G at position 265 (A265G) did not result in change of the predicted secondary structure.

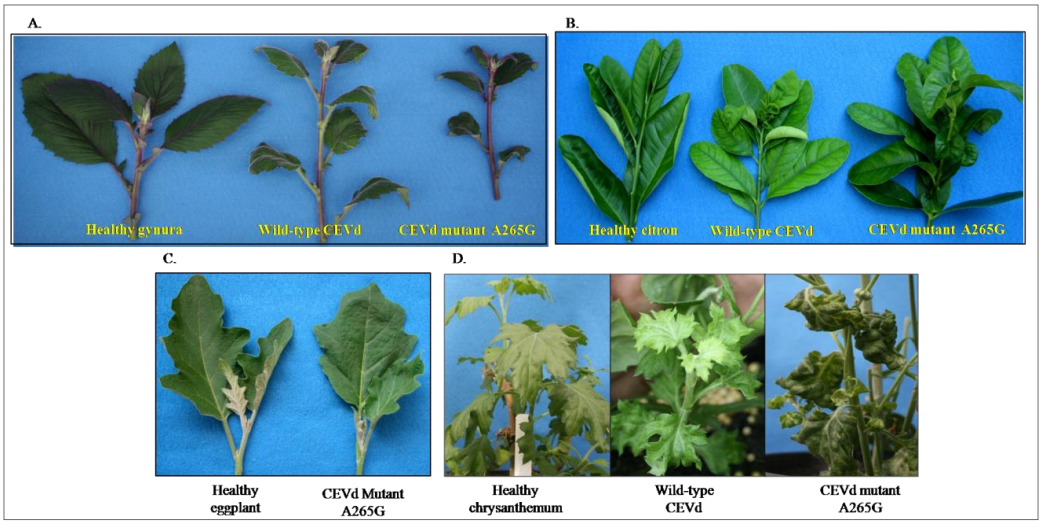

Figure 34. Biological properties of *in vivo* generated CEVd mutant A265G. Mutant induced symptoms like that of WT-CEVd clone, leaf rugosity and epinasty, in gynura (A). It induced severe symptoms, compared to the symptoms induced by WT-CEVd, in citron (B) and chrysanthemum (D). The original host, eggplant, did not show any visible symptoms (C).

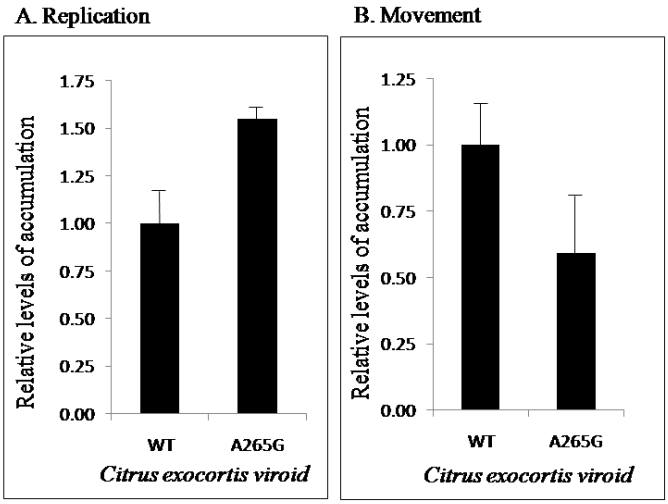

Figure 35. Relative levels of accumulation of wild-type CEVd and *in vivo* generated CEVd mutant A265G in citrus protoplasts (A) and systemic leaves of citron seedling (B).

In the viroid progeny profiles, the WT-CEVd found to be the master sequence as well as the most recent common ancestor in all four experimental hosts (Table 12). Viroid processing in all four hosts resulted in the reversion of the mutant to wild-type sequence. However, the inoculated sequence is maintained in the progeny populations of citron and chrysanthemum. In eggplant, a sequence variant with a mutation at position 108 & 129 induced fitness peak (Table 12). The difference in the haplotype frequency of the master sequence and the variants population was statistically significant in eggplant and gynura (χ^2= 6.72, two-tailed P value=0.0095, df=1) as well as in chrysanthemum (χ^2= 19.20, two-tailed P value=0.0001, df=1). However, in citron, there were no statistically significant differences (χ^2= 0.90, two-tailed P value=0.34, df=1) (Table 12) observed. In chrysanthemum, mutations at position 62 and 131 induced fitness peak in the viroid progeny population (Table 12).

***Mutant U278A*:**

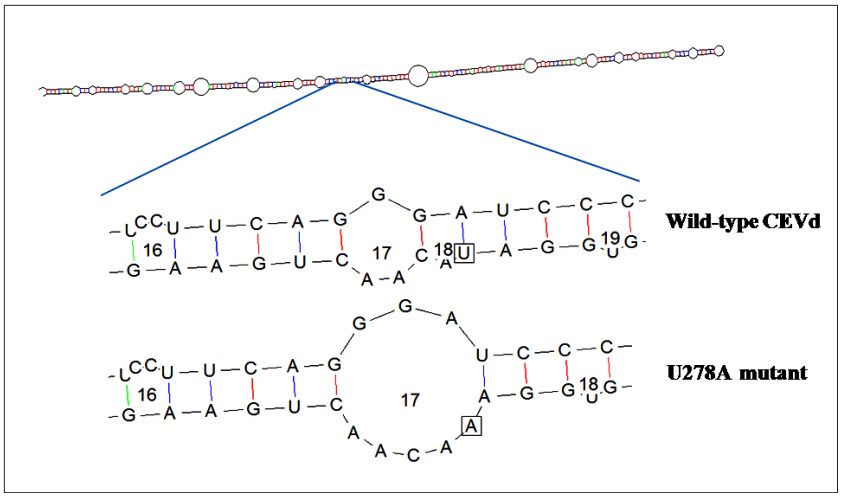

Figure 36. Primary and thermodynamic secondary structures of CEVd RNA (-137.24 at 37 ^{0}C) as predicted by RNAdraw V1.1 RNA secondary structure calculation and analysis algorithm. Mutated nucleotide site is presented in the square box. The transversion from U to A at position 278 (U278A) resulted in the elimination of a loop leading to the enlargement of the loop in the predicted secondary structure.

A CEVd mutant generated in Rutgers tomato (*L. esculentum*) with the transversion mutation (U278A) in the central conserved region of CEVd (Figure 36) could infect all expermental hosts tested (Table 9). The mutant U278A induced more severe symptoms, compared to the symptoms induced by WT-CEVd, in tomato, citron, gynura, and chrysanthemum (Figure 37). The levels of accumulations of mutant U278A in citrus protoplast was significantly higher than the WT-CEVd after 5 dpi. However, both the mutant and the wild-type accumulated to similar levels systemically in leaves of citron seedlings after 5 dpi (χ^2= 0.22, two-tailed P value=0.63, df=1) (Figure 38).

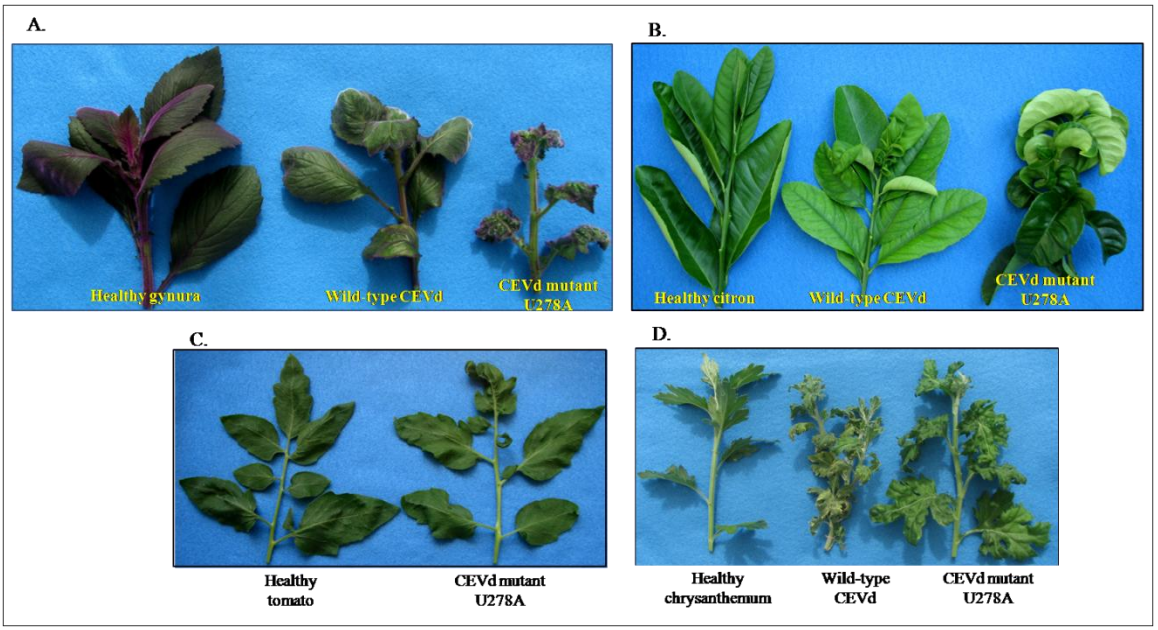

Figure 37. Biological properties of *in vivo* generated CEVd mutant U278A. Mutant induced severe symptoms, compared to the symptoms induced by WT-CEVd, in gynura (A), citron (B), tomato (C) and chrysanthemum (D). Symptoms ranging from leaf rugosity, epinasty and stunting were observed in all the experimental hosts.

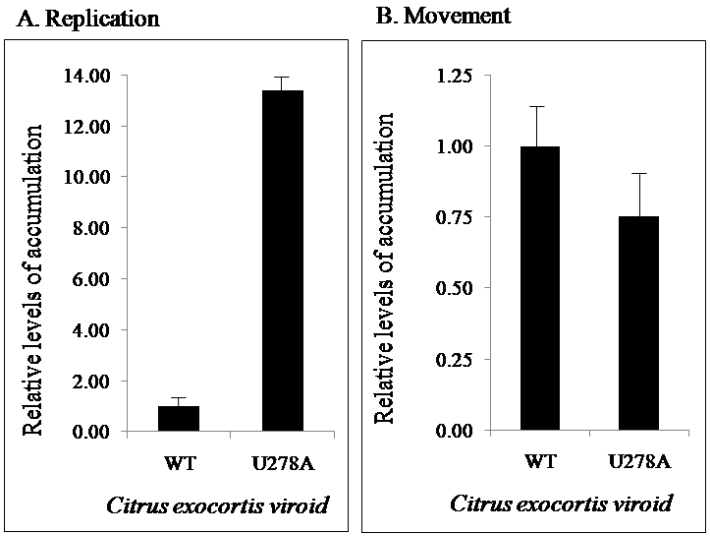

Figure 38. Relative levels of accumulation of wild-type CEVd and *in vivo* generated CEVd mutant A265G in citrus protoplasts (A) and systemic leaves of citron seedling (B).

The inoculated mutant U278A found to be the master sequence as well as the most recent common ancestor in gynura, chrysanthemum and tomato and in citron, where the WT-CEVd was the master sequence as well as the most recent common ancestor (Table 12). Viroid processing in all the hosts resulted in the stability of the mutation. The difference in the haplotype frequency of the master sequences and the variants in the viroid population were not statistically significant in citron (χ^2= 0.81, two-tailed P value=0.36, df=1) and gynura (χ^2= 1.60, two-tailed P value=0.20, df=1), but significant in tomato (χ^2= 12.30, two-tailed P value=0.0005, df=1) and chrysanthemum (χ^2= 29.45, two-tailed P value=0.0001, df=1) (Table 12). In chrysanthemum, mutations at positions 131 and 187 induced fitness peaks in the progeny viroid population (Table 12).

***Mutant C289U*:**

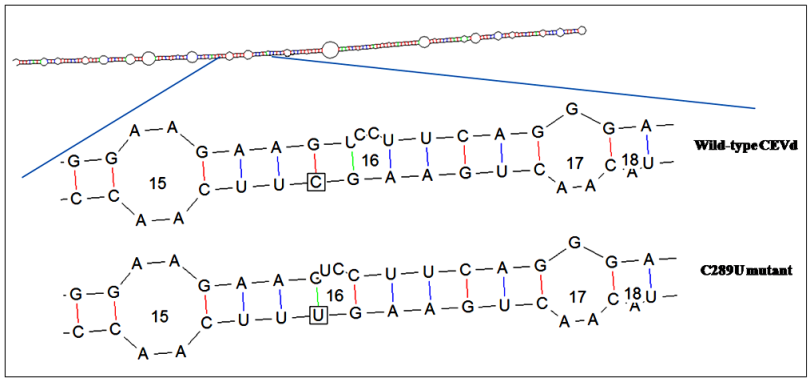

Figure 39. Primary and thermodynamic secondary structures of CEVd RNA (-137.53 at 37 ^{0}C) as predicted by RNAdraw V1.1 RNA secondary structure calculation and analysis algorithm. Mutated nucleotide site is presented in the square box. The transition, from C to U at position 289 (C289U), shifted the position of the loop number 16.

The CEVd mutant generated in 'Sweet' orange with the transition mutation C289U in the central conserved region (Figure 39) could not infect the expermental hosts tested. After 5 dpi, the mutant C289U was not detected in citrus protoplast as well as systemically in the leaves of citron seedlings (Table 11).

***Mutant G128A*:**

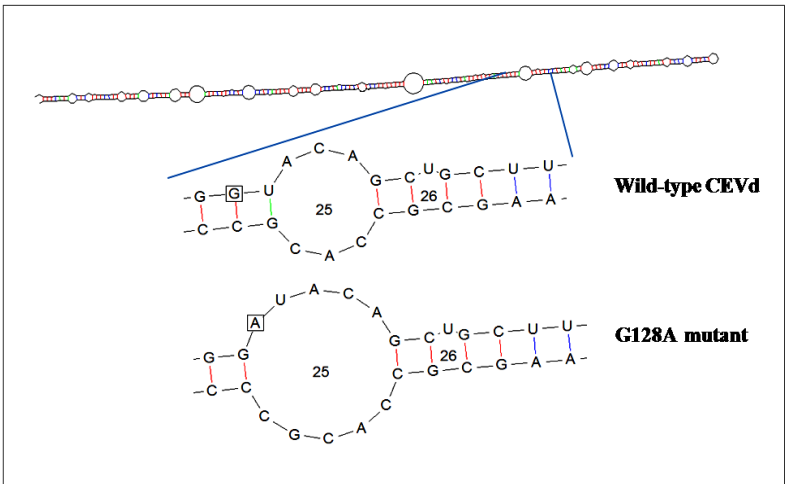

Figure 40. Primary and thermodynamic secondary structures of CEVd RNA (-133.41 at 37 ^{0}C) as predicted by RNAdraw V1.1 RNA secondary structure calculation and analysis algorithm. Mutated nucleotide site is presented in the square box. The transition, from G to A at position 128 (G128A) resulted in the enlargement of loop number 25 of the predicted secondary structure.

A CEVd mutant generated in Rutgers tomato (*L. esculentum*) with the transition mutation G128A in the variable domain (Figure 40) could not infect citron, gynura and chrysanthemum (Table 9). After 5 dpi, the mutant G128A was not detected in citrus protoplast or systemically on leaves of citron seedlings (Table 11).

***Mutant 128G-*:**

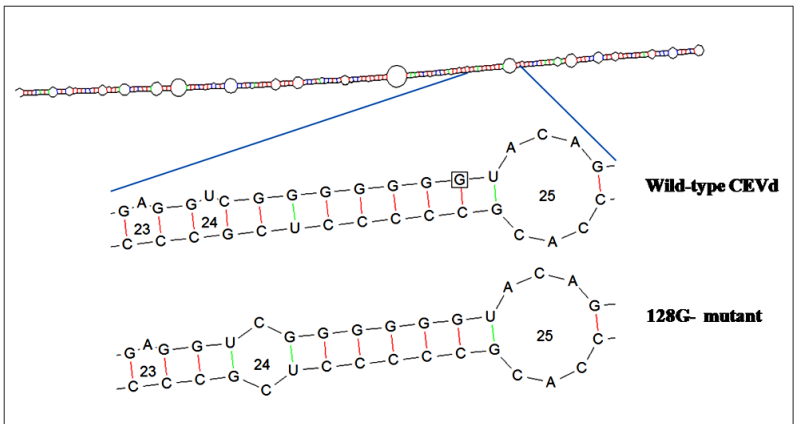

Figure 41. Primary and thermodynamic secondary structures of CEVd RNA (-136.06 at 37 ^{0}C) as predicted by RNAdraw V1.1 RNA secondary structure calculation and analysis algorithm. Mutated nucleotide site is presented in the square box. The deletion of guanidine at position 128 (128G-) did result in the enlargement and position shift of the loop number 24 of the predicted secondary structure.

A CEVd mutant generated in datura (*D. stramonium*) with the deletion of guanidine 128G- in the variable domain (Figure 41) could infect only gynura and datura (Table 9). The mutant 128G- induced more severe symptoms, than the WT-CEVd in gynura. The original host, datura did not show any visible symptoms (Figure 42). The replication of the mutant (128G-) in citrus protoplast could be detected at 5 dpi, at similar levels to the WT-CEVd (χ^2= 0.52, two-tailed P value=0.46, df=1) but, its systemic presence in the leaves of citron seedlings could not be detected after 5 dpi (Table 11).

The WT-CEVd was the master sequence as well as the most recent common ancestor in both hosts. Viroid processing in both datura and gynura resulted in the reversion of the mutation to wild-type sequence (Table 12). The difference in the haplotype frequency of the master sequence and the variants in the viroid population was

statistically significant in datura (χ^2= 6.14, two-tailed P value=0.031, df=1) as well as in gynura (χ^2= 7.04, two-tailed P value=0.0079, df=1) (Table 12).

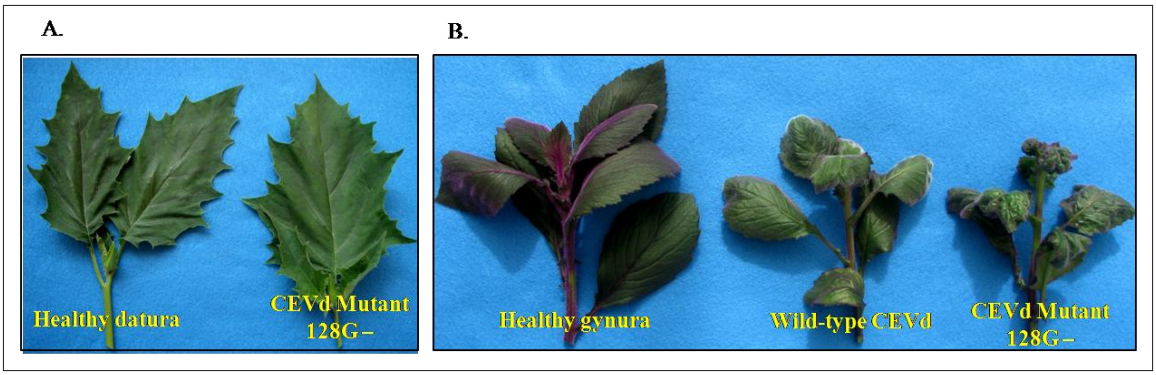

Figure 42. Biological properties of *in vivo* generated CEVd mutant 128G-. The original host, datura, did not show any visible symptoms (A). Mutant induced severe symptoms than that of WT-CEVd clone in gynura (B).

***Mutant U129A*:**

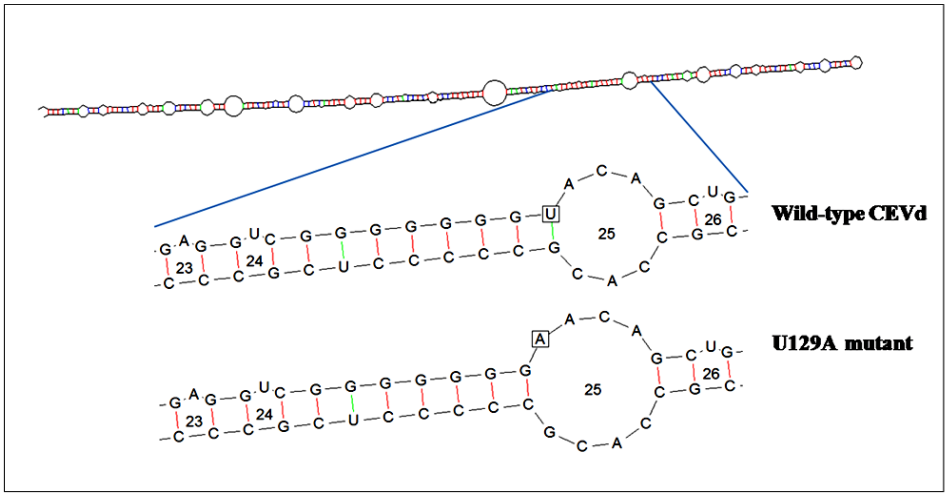

Figure 43. Primary and thermodynamic secondary structures of CEVd RNA (-136.63 at 37 ^{0}C) as predicted by RNAdraw V1.1 RNA secondary structure calculation and analysis algorithm. Mutated nucleotide site is presented in the square box. The transversion, from U to A at position 129 (U129A) did result in the enlargement of the loop number 25 of the predicted secondary structure.

A CEVd mutant generated in citron (*C. medica*) with the transversion mutation U129A in the variable domain (Figure 43) could infect all experimental hosts tesed (Table 9). The mutant U129A induced severe symptoms than the WT-CEVd in all hosts tested (Figure 44). The replication of the mutant U129A in citrus protoplast could be detected at 5 dpi, similarly to the levels of WT-CEVd (χ^2= 0.53, two-tailed P value=0.47, df=1). However, it accumulated to higher levels than the WT-CEVd systemically in the leaves of citron seedlings after 5 dpi (χ^2= 9.00, two-tailed P value=0.0027, df=1) (Figure 45).

The WT-CEVd was the master sequence as well as the most recent common ancestor in citron and chrysanthemum hosts. However, in gynura, the inoculated mutant sequence U129A was the master sequence as well as the most recent common ancestor (Table 12). Viroid processing in all the three hosts resulted in the stability of the mutation in the progeny population. The WT-CEVd sequence induced a fitness peak in gynura while the inoculated sequence induced a fitness peak in chrysanthemum. The difference in the haplotype frequency of the master sequences and the variants in the viroid population was statistically significant in citron (χ^2= 0.209, two-tailed P value=0.647, df=1), in gynura (χ^2= 3.57, two-tailed P value=0.0588, df=1), and in chrysanthemum (χ^2= 3.13, two-tailed P value=0.076, df=1) (Table 12).

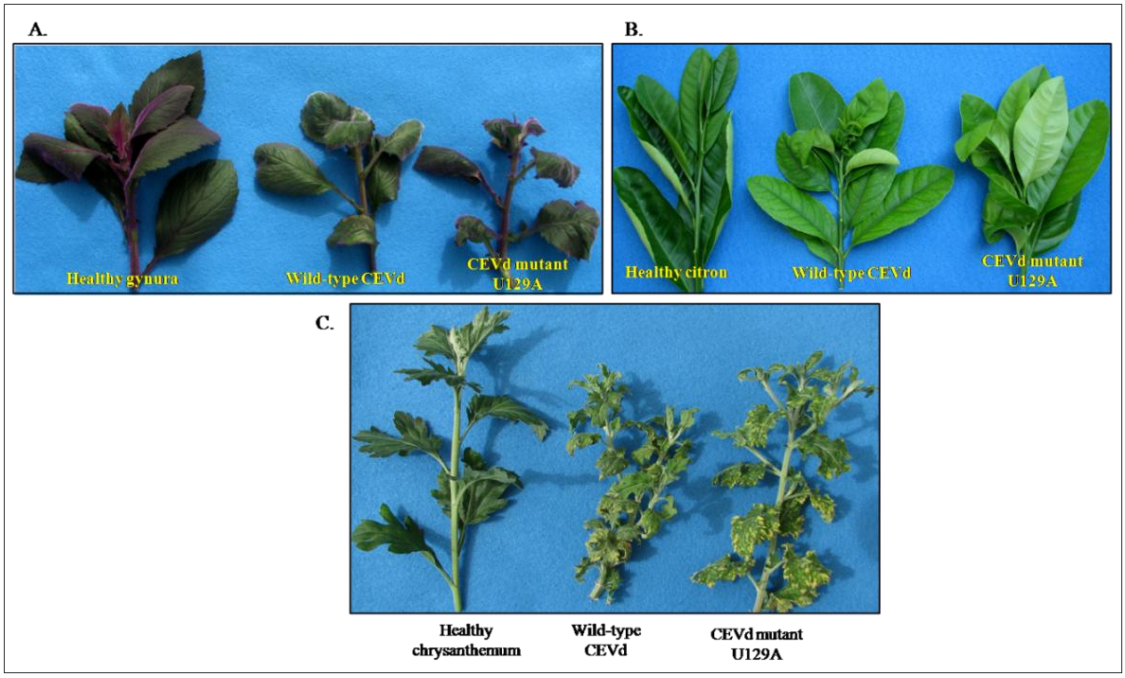

Figure 44. Biological properties of *in vivo* generated CEVd mutant U129A. Mutant induced severe symptoms, compared to the symptoms induced by WT-CEVd, in gynura (A) citron (B) and chrysanthemum (C).

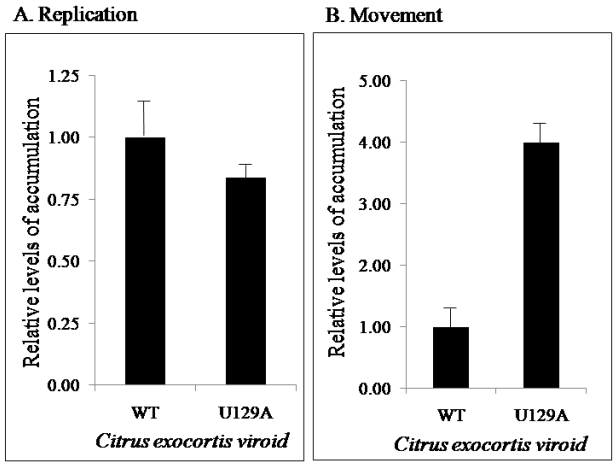

Figure 45. Relative levels of accumulation of wild-type CEVd and *in vivo* generated CEVd mutant U129A in citrus protoplasts (A) and systemic leaves of citron seedling (B).

Two mutants in the right terminal domain of CEVd generated in citron (*C. medica*) namely, transversion mutant G159U (Figure 46) and a transition mutation U182C (Figure 47) were not able to infect the experimental hosts citron, gynura and chrysanthemum (Table 9). No significant difference was observed in the accumulation levels of the mutants and WT-CEVd in citrus protoplast after 5 dpi. However, systemic accumulation was not observed even after 5 dpi in the leaves of citron seedlings (Table 11).

***Mutant G159U*:**

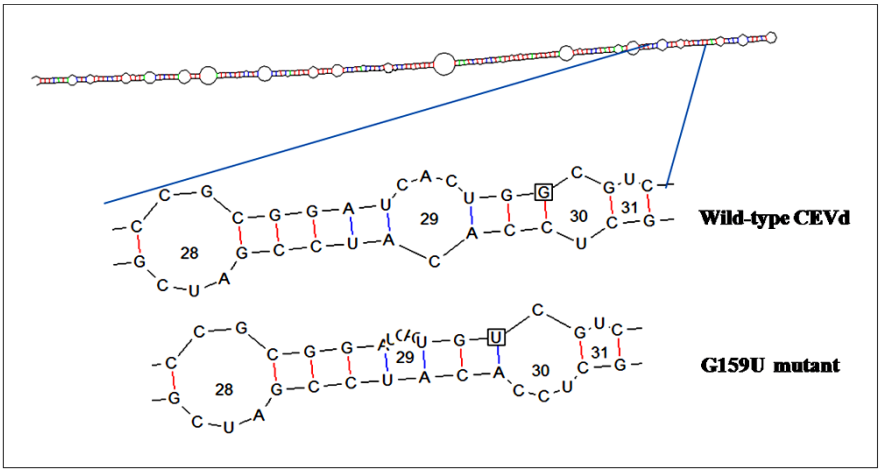

Figure 46. Primary and thermodynamic secondary structures of CEVd RNA (-136.22 at 37 ^{0}C) as predicted by RNAdraw V1.1 RNA secondary structure calculation and analysis algorithm. Mutated nucleotide site is presented in the square box. The transversion, from G to U at position 159 (G159U) did result in change in the size of loops of the predicted secondary structure.

***Mutant U182C*:**

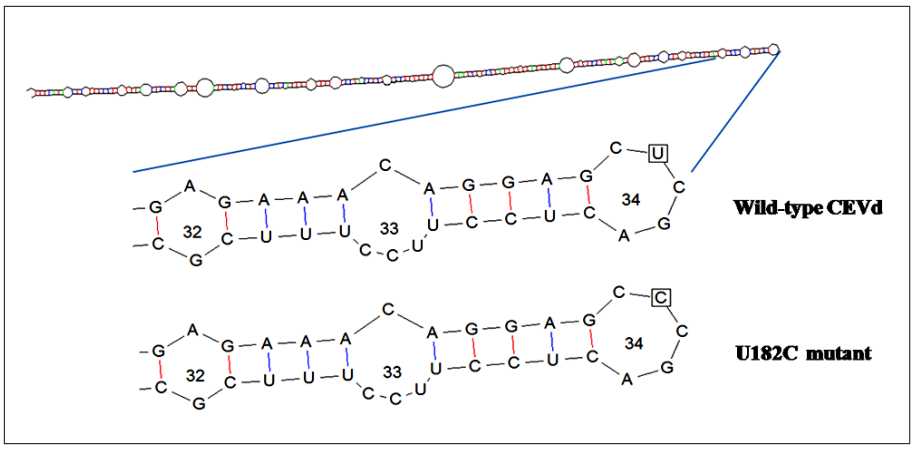

Figure 47. Primary and thermodynamic secondary structures of CEVd RNA (-139.12 at 37 ^{0}C) as predicted by RNAdraw V1.1 RNA secondary structure calculation and analysis algorithm. Mutated nucleotide site is presented in the square box. The transition, from U to C at position 182 (U182C) did not result in change of the predicted secondary structure.

***Mutant A185U*:**

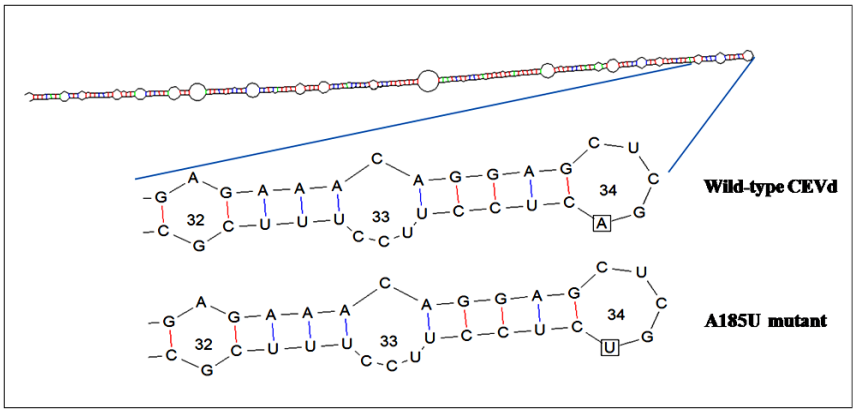

Figure 48. Primary and thermodynamic secondary structures of CEVd RNA (-138.52 at 37 ^{0}C) as predicted by RNAdraw V1.1 RNA secondary structure calculation and analysis algorithm. Mutated nucleotide site is presented in the square box. The transversion, from A to U at position 185 (A185U) did not result in change of the predicted secondary structure.

A CEVd mutant generated in luffa (*Luffa aegyptiaca*) with the transversion mutation A185U in the right terminal domain (Figure 48) could infect citron and gynura (Table 9). The mutant A185U induced milder symptoms, than WT-CEVd, in citron and gynura (Figure 49). The replication of the mutant A185U in citrus protoplasts could be detected at 5 dpi, which was similar to the levels of WT-CEVd (χ^2= 0.18, two-tailed P value=0.66, df=1). No significant difference was observed in the levels of systemic accumulation of the mutant A185U and the WT-CEVd in the leaves of citron seedlings after 5 dpi (χ^2= 0.52, two-tailed P value=0.46, df=1) (Figure 50).

The WT-CEVd was the master sequence as well as the most recent common ancestor in both gynura and citron. Viroid processing in both gynura and citron resulted in the reversion of the mutation to wild-type sequence (Table 12). The difference in the number of master sequences and the variants in the viroid population was statistically significant in citron (χ^2= 5.81, two-tailed P value=0.0159, df=1) and as well as in gynura (χ^2= 3.93, two-tailed P value=0.047, df=1) (Table 12).

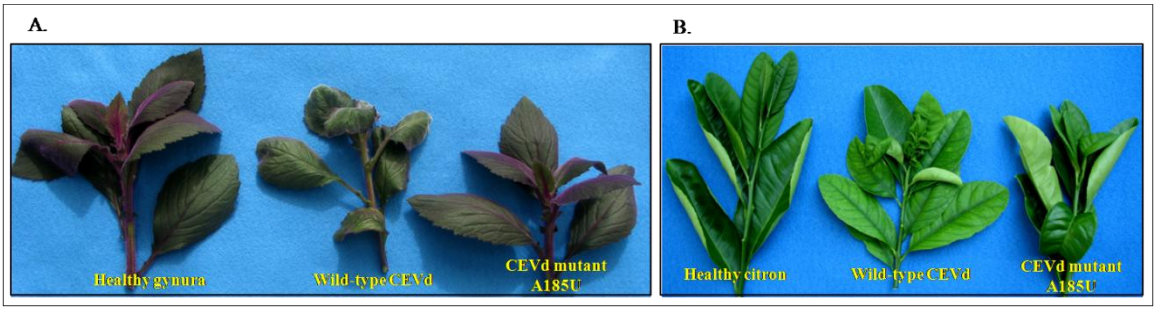

Figure 49. Biological properties of *in vivo* generated CEVd mutant A185U. Mutant induced milder symptoms, compared to the symptoms induced by WT-CEVd, in gynura (A). It induced symptoms like that of WT-CEVd clone, leaf rugosity and epinasty, in citron (B).

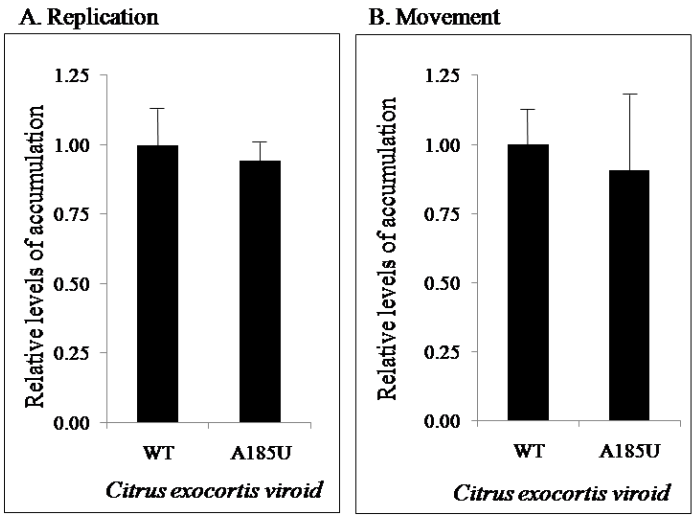

Figure 50. Relative levels of accumulation of wild-type CEVd and *in vivo* generated CEVd mutant A185U in citrus protoplasts (A) and systemic leaves of citron seedling (B).

***Mutants with double mutations*:**

Three CEVd mutants, carrying two mutations on their genome, could not infect the experimental hosts' citron, gynura, and chrysanthemum (Table 10). (i) A mutant generated in citron (*C. medica*) with the transversion mutations (U41A) and (G107U) (Figure 51); (ii) A mutant generated in luffa (*Luffa aegyptiaca*) with two mutations, transition (A61G) and transversion (G107U) (Figure 52); and (iii) A mutant generated in hybrid tomato (*L. esculentum* x *L. peruvianum*) with transversion (C263A) and transition (A155G) (Figure 53). The above mentioned mutants did not replicate in the citrus protoplasts and did not move systemically to the leaves of citron seedlings after 5 dpi (Table 11).

***Mutant U41A/G107U*:**

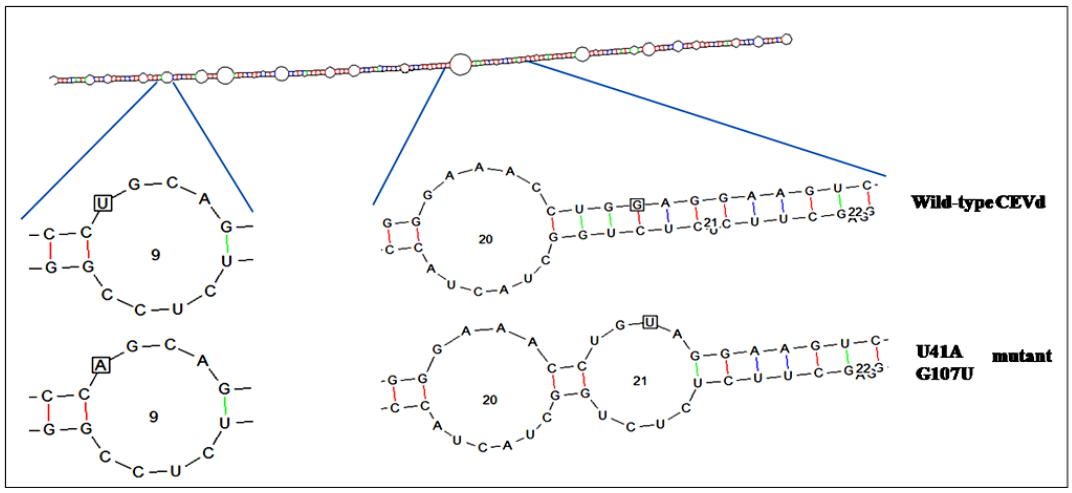

Figure 51. Primary and thermodynamic secondary structures of CEVd RNA (-134.06 at 37 ^{0}C) as predicted by RNAdraw V1.1 RNA secondary structure calculation and analysis algorithm. Mutated nucleotide site is presented in the square box. Two mutations, U41A & G107U, lead to the change in the formation of a new loop in the predicted secondary structure.

***Mutant A61G/G107U*:**

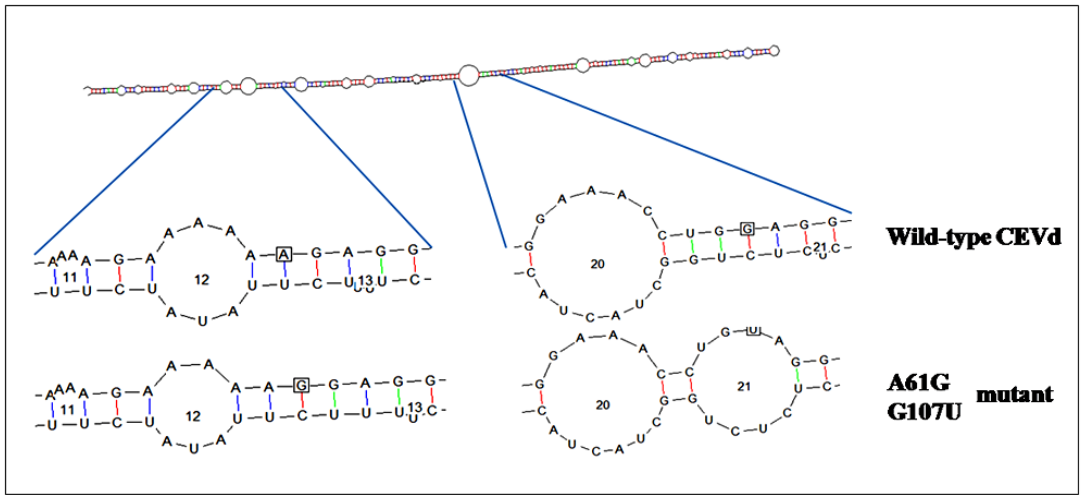

Figure 52. Primary and thermodynamic secondary structures of CEVd RNA (-133.59 at 37 ^{0}C) as predicted by RNAdraw V1.1 RNA secondary structure calculation and analysis algorithm. Mutated nucleotide site is presented in the square box. Two mutations, A61G & G107U, lead to the change in the loop position and formation of a new loop in the predicted secondary structure.

***Mutant C263A/A155G*:**

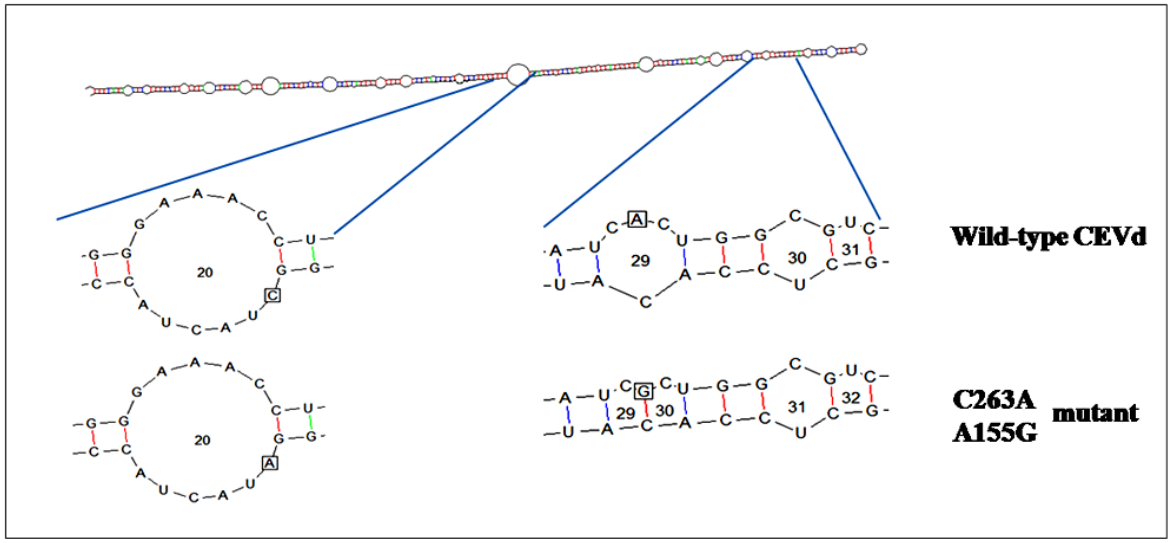

Figure 53. Primary and thermodynamic secondary structures of CEVd RNA (-140.36 at 37 ^{0}C) as predicted by RNAdraw V1.1 RNA secondary structure calculation and analysis algorithm. Mutated nucleotide site is presented in the square box. Two mutations, C263A & A155G, did result in formation of a new loop in the predicted secondary structure.

***Mutant 62A+/U278A*:**

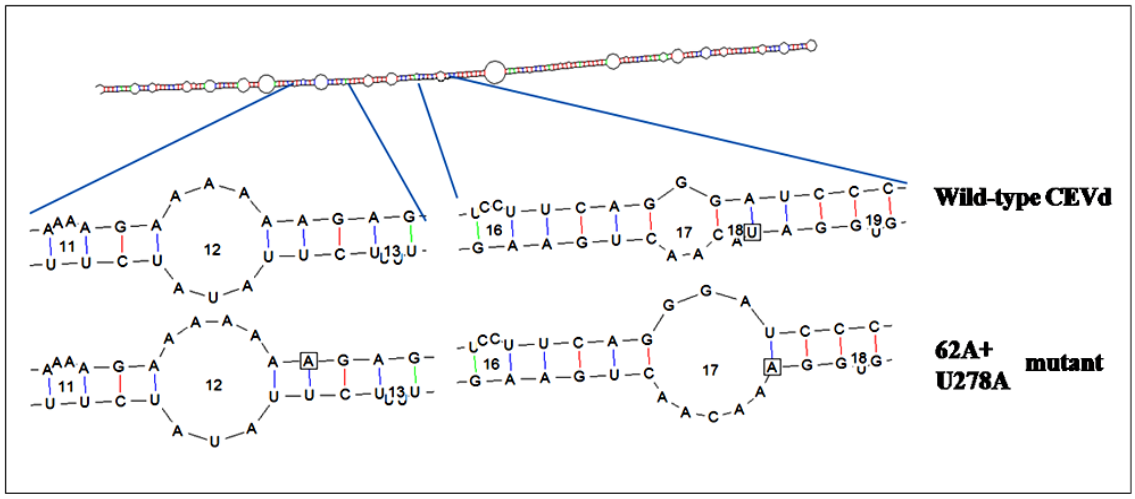

Figure 54. Primary and thermodynamic secondary structures of CEVd RNA (-136.87 at 37 ^{0}C) as predicted by RNAdraw V1.1 RNA secondary structure calculation and analysis algorithm. Mutated nucleotide site is presented in the square box. Two mutations, 62A+ & U278A, lead to the enlargement of loop number 17 in the predicted secondary structure.

A CEVd mutant generated in hybrid tomato (*L. esculentum* x *L. peruvianum*) with two mutations, one addition of adenine (62A+) and one transversion (U278A) (Figure 54), could infect all expermental hosts tested (Table 10). The mutant (62A+/U278A) induced symptoms similar to WT-CEVd in chrysanthemum while it induced severe symptoms in citron and gynura (Figure 55). The levels of accumulations of the mutant (62A+/U278A) in citrus protoplasts was found to be higher than the WT-CEVd after 5 dpi. However, both the mutant and the wild-type accumulated to similar levels in the systemic leaves of citron seedlings after 5 dpi (χ^2=1.66, two-tailed P value=1.96, df=1) (Figure 56).

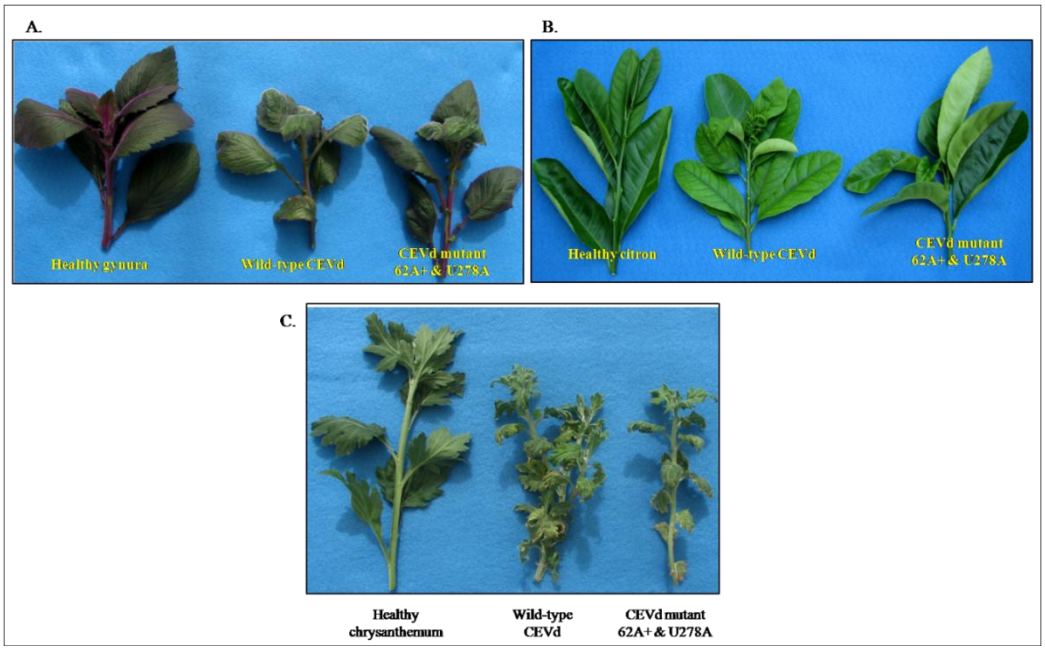

Figure 55. Biological properties of *in vivo* generated CEVd double mutant 62A+ & U278A. Mutant induced symptoms similar to WT-CEVd in chrysanthemum (C) while it induced severe symptoms in citron (B) and gynura(A).

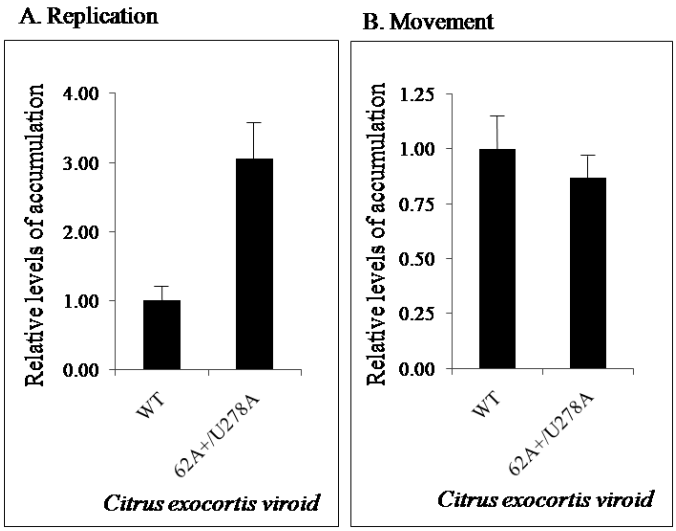

Figure 56. Relative levels of accumulation of wild-type CEVd and *in vivo* generated CEVd mutant 62A+/U278A in citrus protoplasts (A) and systemic leaves of citron seedling (B).

The WT-CEVd was the master sequence as well as the most recent common ancestor in all hosts tested. Viroid processing in citron, gynura, and chrysanthemum resulted in the reversion of the mutations to wild-type sequence. However, the mutations 62A+ and U278A were stabilized in the population separately (Table 12). The difference in the haplotype frequency of the master sequence and the variants in the viroid population was not statistically significant in citron (χ^2= 0.095, two-tailed P value=0.757, df=1). but it was significant in chrysanthemum (χ^2= 6.72, two-tailed P value=0.0095, df=1) and gynura (χ^2= 11.26, two-tailed P value=0.0008, df=1) (Table 12).

A CEVd mutant generated in Rutgers tomato (*L. esculentum*) with two mutations, one transition (U316C) and one transversion (U278A) (Figure 57), could infect all expermental hosts tested (Table 10). The mutant (U316C/U278A) induced symptoms

similar to WT-CEVd in citron, and tomato, and milder in gynura (Figure 58). No significant difference was observed for the levels of accumulations of the mutant (U316C/U278A) and the WT-CEVd in citrus protoplast after 5 dpi (χ^2=0.22, two-tailed P value=0.63, df=1). However, the mutant was not detected systemicaly in the leaves of citron seedlings after 5 dpi (Table 11).

***Mutant U316C/U278A*:**

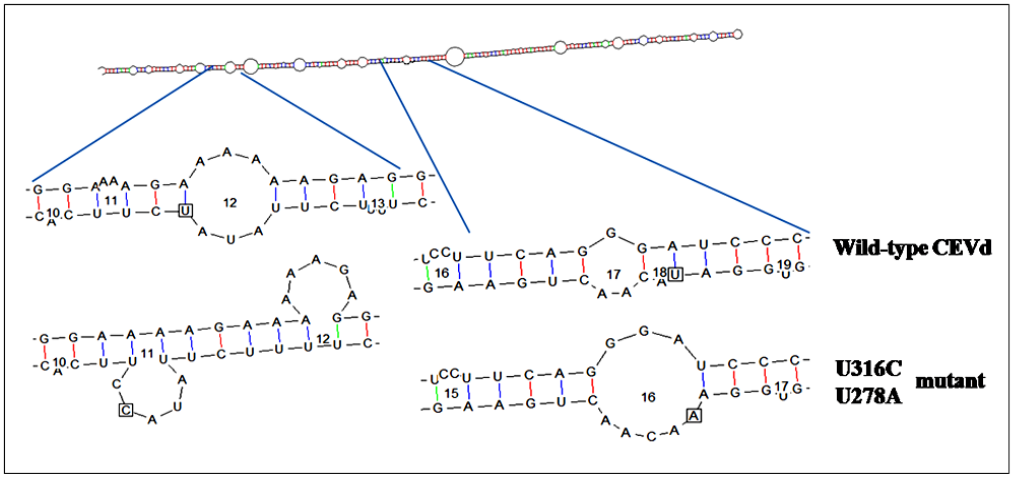

Figure 57. Primary and thermodynamic secondary structures of CEVd RNA (-136.56 at 37 ^{0}C) as predicted by RNAdraw V1.1 RNA secondary structure calculation and analysis algorithm. Mutated nucleotide site is presented in the square box. Two mutations, U316C & U278A, lead to the change in formation and enlargement of new loops in the predicted secondary structure.

The WT-CEVd was the master sequence as well as the most recent common ancestor in all hosts tested. Viroid processing in tomato, citron, and gynura hosts resulted in the reversion of the mutations to wild-type sequence. However, only U278A was stabilized in the progeny population. The difference in the number of master sequences and the variants in the viroid population was not statistically significant in tomato (χ^2=

3.13, two-tailed P value=0.0768, df=1) andgynura (χ^2= 1.97, two-tailed P value=0.159, df=1). However, it was statistically significant in citron (χ^2= 6.095, two-tailed P value=0.0136, df=1) (Table 12).

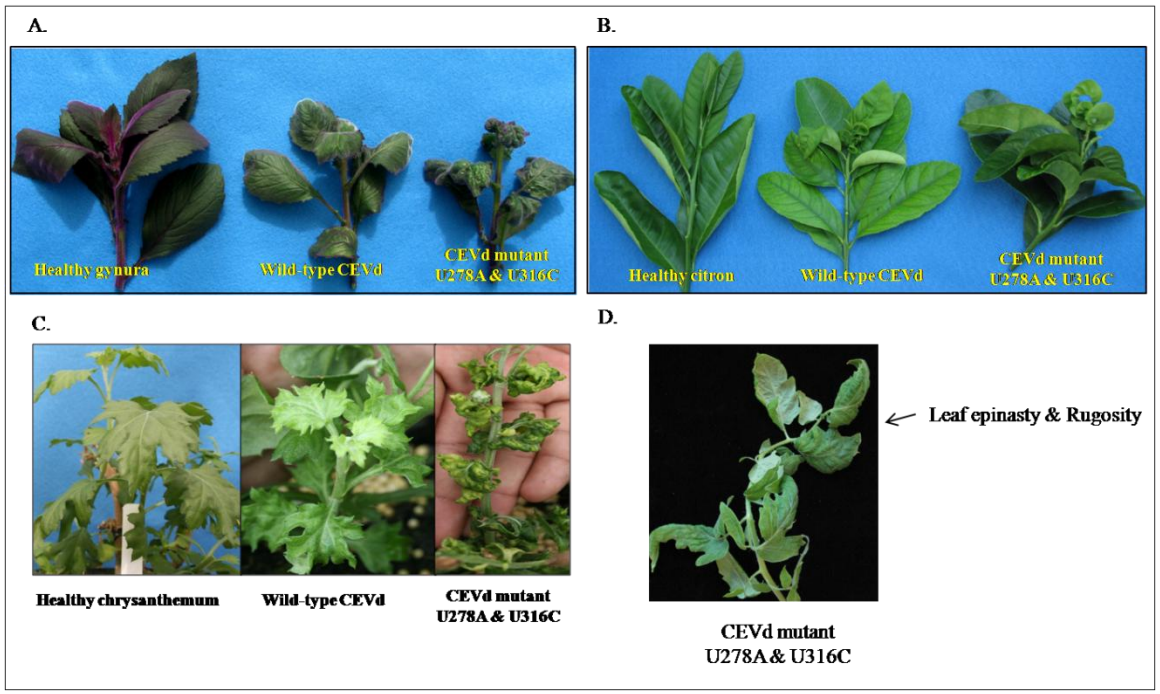

Figure 58. Biological properties of *in vivo* generated CEVd double mutant U278A & U316C. Mutant induced severe symptoms than the WT-CEVd clone, leaf rugosity and epinasty, in gynura (A), citron (B), chrysanthemum (C) and tomato (D).

***Mutants with triple mutations*:**

Mutants, carrying three mutations on their genome, could not infect the experimental hosts - citron, gynura and chrysanthemum (Table 10). (i) A CEVd mutant generated in hybrid tomato (*L. esculentum* x *L. peruvianum*) with three mutations; a transition (A15G) and the transversions (G366U) & (U130A) (Figure 59); (ii) A mutant generated in luffa (*Luffa aegyptiaca*) with the transitions (U19C) & (G67A) and a

transversion (A321U) (Figure 60); and (iii) A mutant generated in Rutgers tomato (*L. esculentum*) with the transversions (G106U) & (C263A) and a transition (A228G) (Figure 61). The above mutants were not detected in citrus protoplasts or systemically in the leaves of citron seedlings after 5 dpi (Table 11).

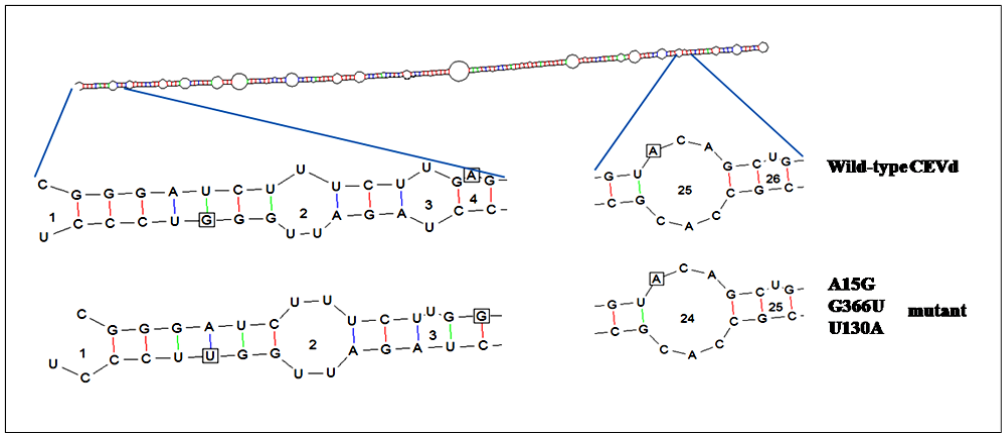

Figure 59. Primary and thermodynamic secondary structures of CEVd RNA (-138.51 at 37 ^{0}C) as predicted by RNAdraw V1.1 RNA secondary structure calculation and analysis algorithm. Mutated nucleotide site is presented in the square box. Three mutations, A15G, G366U & U130A, lead to no major changes in the predicted secondary structure.

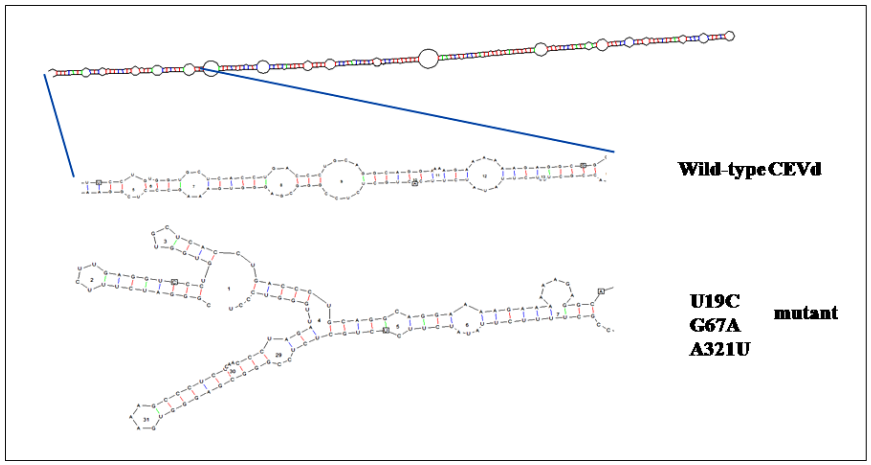

Figure 60. Primary and thermodynamic secondary structures of CEVd RNA (-135.35 at 37 ^{0}C) as predicted by RNAdraw V1.1 RNA secondary structure calculation and analysis algorithm. Mutated nucleotide site is presented in the square box. Three mutations, U19C, G67A & A321U, lead to dramatic change in the predicted secondary structure.

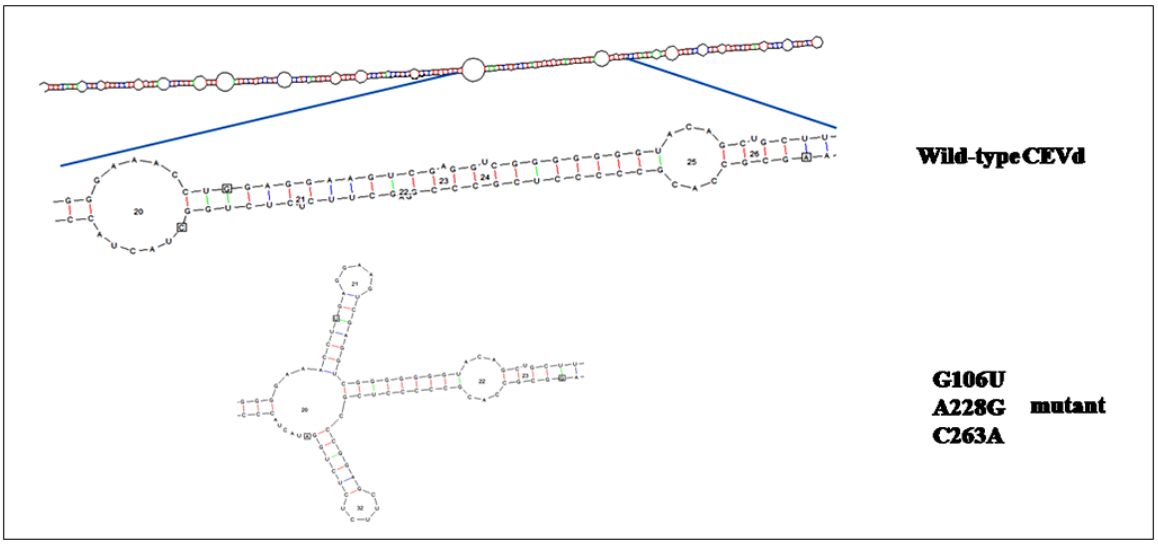

Figure 61. Primary and thermodynamic secondary structures of CEVd RNA (-136.5 at 37 ^{0}C) as predicted by RNAdraw V1.1 RNA secondary structure calculation and analysis algorithm. Mutated nucleotide site is presented in the square box. Three mutations, G106U, A228G & C263A, lead to dramatic change in the predicted secondary structure.

Host range studies of each *in vivo* generated CEVd mutant are summarized in Table 9 and 10. Study of replication and systemic accumulation of mutants is summarized in the Table 11. The effect of host processing on a single sequence variant within a single plant is summarized in Table 12.

Table 9. Host Range studies of *in vivo* generated CEVd mutants with single mutation.

	Original host	Original host		Citron		Gynura		Chrysanthemum	
		Infectivity*	Symptoms	Infectivity	Symptoms	Infectivity	Symptoms	Infectivity	Symptoms
G17A	Sweet Orange	NT	NA	-	NA	-	NA	-	NA
U30C	Eggplant	+	NA	-	NA	-	NA	-	NA
344A-	Datura	+	NA	-	NA	+	mild	-	NA
G50A	Citron	+	mild	+	mild	+	mild	+	mild
62A+	Citron	+	severe	+	severe	+	mild	+	severe
C320U	Hybrid Tomato	NT	NA	-	NA	-	NA	-	NA
108U+	Chrysanthemum	+	mild	+	mild	+	mild	+	mild
U264A	Luffa	NT	NA	-	NA	+	mild	-	NA
A265G	Eggplant	+	NA	+	severe	+	mild	+	severe
U278A	Rutgers Tomato	+	severe	+	severe	+	severe	+	severe
C289U	Sweet Orange	NT	NA	-	NA	-	NA	-	NA
G128A	Rutgers Tomato	-	NA	-	NA	-	NA	-	NA
128G-	Datura	+	NA	-	NA	+	severe	-	NA
U129A	Citron	+	severe	+	severe	+	severe	+	severe
G159U	Citron	-	NA	-	NA	-	NA	-	NA
U182C	Citron	-	NA	-	NA	-	NA	-	NA
A185U	Luffa	-	NA	+	mild	+	mild	-	NA

"+" positive infection, "-" no infection, NT: not tested, NA: not applicable.

Table 10. Host Range studies of *in vivo* generated CEVd mutants with double and triple mutations.

	Original host	Original host		Citron		Gynura		Chrysanthemum	
		Infectivity*	Symptoms	Infectivity	Symptoms	Infectivity	Symptoms	Infectivity	Symptoms
U41A G107U	Citron	-	NA	-	NA	-	NA	-	NA
A61G G107U	Luffa	NT	NA	-	NA	-	NA	-	NA
62A+ U278A	Hybrid tomato	NT	NA	+	severe	+	severe	+	mild
C263A A155G	Hybrid tomato	NT	NA	-	NA	-	NA	-	NA
U316C U278A	Rutgers tomato	+	severe	+	Severe	+	Severe	+	severe
A15G G366U U130A	Hybrid tomato	NT	NA	-	NA	-	NA	-	NA
U19C G67A A321U	Luffa	NT	NA	-	NA	-	NA	-	NA
G106U A228G C263A	Rutgers tomato	-	NA	-	NA	-	NA	-	NA

"+" positive infection, "-" no infection, NT: not tested, NA: not applicable.

Table 11. Citrus Model system used to study the molecular and biological properties of *in vivo* generated CEVd mutants.

Mutant	Citrus Model			
	Protoplast	**Citron seedling**	**Citron/Rough Lemon plant**	
	Replication*	Systemic Accumulation*	Infectivity**	Symptoms[¥]
G17A	no	no	-	NA
U30C	no	no	-	NA
344A-	no	no	-	NA
G50A	↔	↔	+	Mild
62A+	↑	↔	+	Severe
C320U	↓	no	-	NA
108U+	↔	↔	+	Mild
U264A	no	no	-	NA
A265G	↔	↔	+	Severe
U278A	↑	↔	+	Severe
C289U	no	no	-	NA
G128A	↔	no	-	NA
128G-	↔	no	-	NA
U129A	↔	↑	+	Severe
G159U	↔	no	-	NA
U182C	↔	no	-	NA
A185U	↔	↔	+	Milder
U51A G107U	no	no	-	NA
A61G G107U	no	no	-	NA
62A+ U278A	↑	↔	+	Severe
C263A A155G	no	no	-	NA
U316C U278A	↔	↔	+	Severe
A15G G366U U130A	no	no	-	NA
U19C G67A A321U	no	no	-	NA
G106U A228G C263A	no	no	-	NA

* "↑" more than wild-type; "↓" less than wild-type; "↔" same as wild-type
** "+" positive infection; "-" no infection
[¥] NA: not applicable.

Table 12. *De novo* generated viroid progeny population from an *in vivo* generated CEVd mutant within a single-plant.

Host	Mutant	Master sequence	Fitness Peaks	No. of Sequences	Master sequences	Variants	
						Total	Unique[a]
Gynura	344A-	WT		47	34	13	13
	G50A	WT		40	24	16	16
	62A+	61A-	WT,62A+	45	23	22	15
	108U+	WT		44	30	14	12
	U264A	U264A		42	27	15	15
	A265G	WT		43	30	13	13
	U278A	U278A	U129A	40	23	17	16
	128G-	WT		41	29	12	12
	U129A	U129A	WT	28	9	19	12
	A185U	WT		44	28	16	16
	62A+/U278A	WT	62A+,U278A	47	35	12	11
	U316C/U278A	WT	U278A	41	25	16	12
		subtotal		**502**	**317**	**185**	**163**
Citron	G50A	WT		39	23	16	12
	62A+	WT	62A+	47	17	30	12
	108U+	WT		36	27	9	9
	A265G	WT	A265G	40	23	17	17
	U278A	WT	U278A	44	19	25	14
	U129A	WT	U129A	43	23	20	17
	A185U	WT		44	30	14	14
	62A+/U278A	WT	62A+,U278A	42	20	22	16
	U316C/U278A	WT	U278A	42	29	13	13
		subtotal		**377**	**211**	**166**	**124**
Chrysanthemum	G50A	WT		42	18	24	21
	62A+	WT	62A+,61A-	41	8	33	22
	108U+	WT		28	3	25	21
	A265G	WT	A265G	30	3	27	21
	U278A	U278A	131,187	40	4	36	22
	U129A	WT	U129A	46	17	29	23
	62A+/U278A	WT	62A+,U278A	43	13	30	21
	U316C/U278A	WT	U278A	42	20	22	16
		subtotal		**228**	**48**	**180**	**130**
Rutgers tomato	U278A	U278A		43	33	10	7
	U316C/U278A	WT	U278A	46	29	17	15
		subtotal		**89**	**62**	**27**	**22**
Datura	344A-	WT	A130U	43	22	21	20
	128G-	WT		46	32	14	14
		subtotal		**89**	**54**	**35**	**34**
Eggplant	U30C	WT		43	26	17	17
	A265G	WT	108,129	43	30	13	9
		subtotal		**86**	**56**	**30**	**26**
		Total		**1375**	**748**	**627**	**504**

[a] Multiple clones with the same mutations, WT: wild-type CEVd.

De novo generated CEVd progeny population composition, from *in vivo* generated CEVd mutant inoculation, was not altered significantly (χ_2, $p<0.05$) with replication among same host, however, the population profile among the different hosts was significantly altered ($\chi 2= 131.46$, $p<0.01$, $df= 10$) (Table 7). Significant difference (χ_2, $p<0.05$) was observed in the type of mutations generated within a host and also among different hosts. Transition mutations were quite common in the progeny population than the other type of mutations (Table 13). Two or more mutations per genome were quite common in the CEVd progeny populations of chrysanthemum (Table 13).

Table 13. Type of mutations generated by the experimental hosts upon infection with *in vivo* generated CEVd mutants.

Hosts	Number of mutations	Addition		Deletion		Transition		Transversion		2 or more mutations per genome
		No.	%	No.	%	No.	%	No.	%	
Gynura	585	67	11	112	19	223	38	183	31	46
Etrog citron	454	16	4	75	17	184	41	180	40	39
Chrysanthemum	279	32	11	50	18	101	36	96	34	103
Rutgers tomato	122	6	5	0	0	45	37	71	58	7
Datura	95	56	59	2	2	32	34	5	5	5
Eggplant	94	2	2	13	14	70	74	9	10	5
Total	**1639**	**179**		**252**		**655**		**544**		**205**

No significant difference (χ_2, $p<0.05$) was observed for the infectivity of mutants among three experimental hosts (Table 14). Mutants with addition mutation were infective in all three hosts, while mutants with deletion mutation showed no infectivity except gynura (Table 15). Mutants with Transversion mutation showed more infectivity than the transition mutation (Table 15). Mutation residing on type of strand (upper or lower) of viroid secondary structure had no significant (χ_2, $p<0.05$) influence on the infectivity of that mutant (Table 15). Distribution of mutations on the five structural domains of CEVd secondary structure was not even (Figure 62). More than half of the mutations observed were resided in the pathogenic and variable domains. Nucleotide positions on CEVd genome 12, 343 and 367 of left terminal domain; positions 50, 61, 62, 69, 295, 301 and 309 of pathogenic domain; positions 263, 264 and 278 of CCR domain; positions 128, 129, 130 and 234 of variable domain; 157, 160 and 174 of right terminal domain were mutation hot-spots (Figure 63). Nucleotide positions 50 and 130 were prone to mutations both at the cellular and plant levels (Table 5 and Figure 63).

Table 14. Infectivity of 25 *in vivo* generated CEVd mutants in three experimental hosts.

Hosts	Infectivity	No. of Mutants
Citron	Severe	3
	Mild	6
	Non-infectious	16
Gynura	Severe	4
	Mild	8
	Non-infectious	13
Chrysanthemum	Severe	3
	Mild	3
	Non-infectious	19

Table 15. Infectivity based on type of mutation and strand of viroid secondary structure in three experimental hosts.

	Citron	Gynura	Chrysanthemum
Addition	2/2	2/2	2/2
Deletion	0/2	2/2	0/2
Transition	1/5	1/5	1/5
Transversion	3/6	3/6	2/6
Upper strand	4/10	5/10	3/10
Lower strand	3/7	5/7	2/7

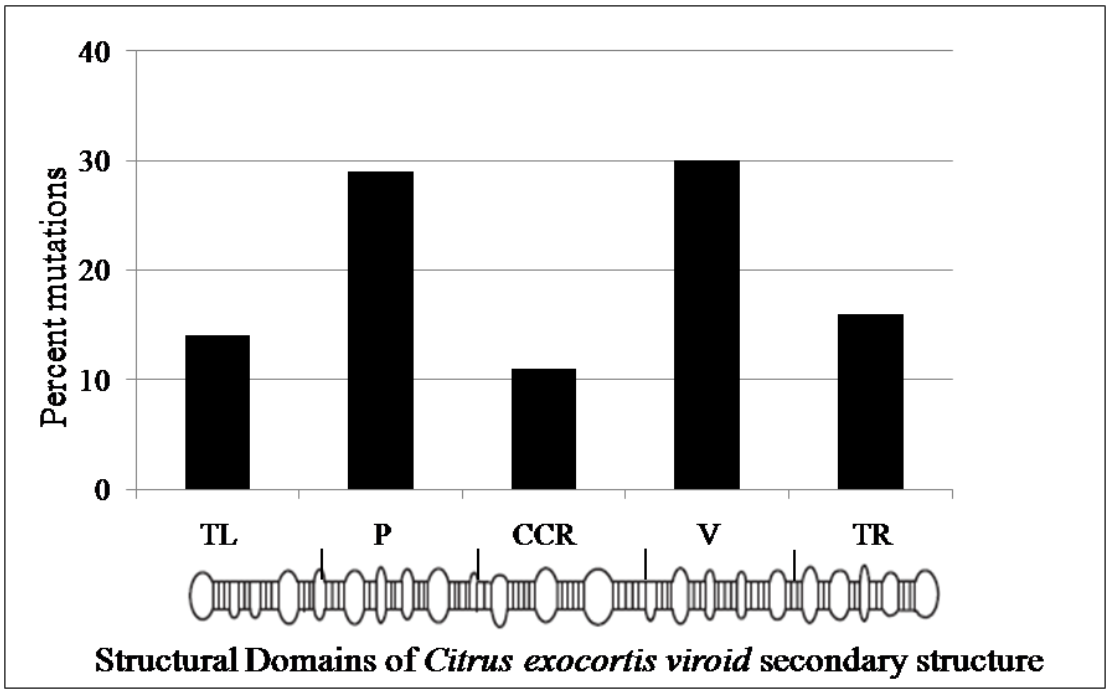

Figure 62. Distribution of the mutations across the five structural domains of the CEVd genome*. TL: Left Terminal, CCR: Central Conserved Region, TR: Right Terminal.
*CEVd genome:371 nt, Primers:33 nt (CCR domain) removed, CEVd genome for analysis:338 nt.

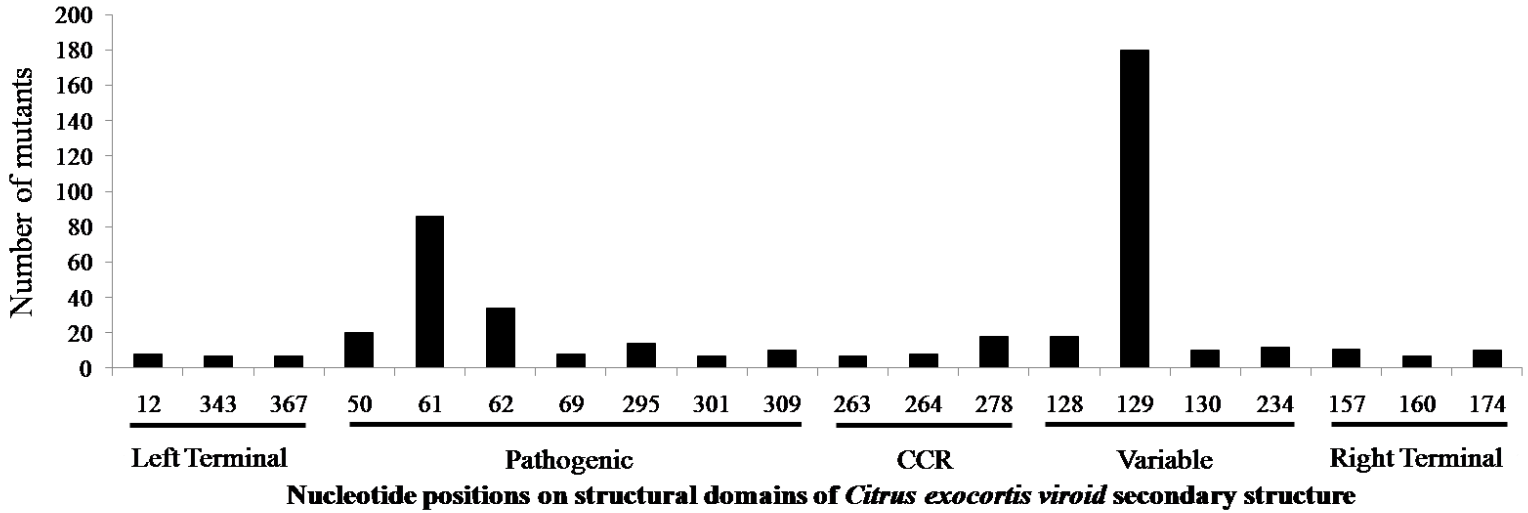

Figure 63. Mutation hot-spots on the *Citrus exocortis viroid* genome across structural domains of secondary structure. CEVd genome is 371 nt long. Primer sequences of 33 nt [lies in Central Conserved Region (CCR) domain] were removed from the analysis and the final CEVd genome size used for analysis was 338 nt.

DISCUSSION

Viroids are non-translated in nature and rely on the host for replication, thus it was critical to characterize a single sequence variant and study the biological interactions of that variant with a particular host. A viroid infection in a single plant results in a progeny population with distinct but closely related sequences composing a quasi-species (Eigen *et al*., 1989; Gandia *et al*., 2000; Owens *et al*., 2000; Gandia and Duran-Vila, 2004). Mutation and selection are the two basic processes of evolution. The observed genetic diversity was the result of both a high mutation rate during replication and competition between the constantly arising sequence variants. In this present study, among the *in vivo* generated CEVd mutants tested, most of the mutants were reverted back to wild-type sequence as a consequence of natural selection on the genetic variation and the fittest genotype was favored.

The left terminal domain possess imperfect palindrome (IP), a rod-like or Y-shaped thermodynamically preferred structure (includes nucleotide positions 16 to 21 and 365 to 369 in CEVd). The nucleotide G17 in CEVd genome seems to be essential for the infectivity in citron, gynura and chrysanthemum hosts. Since, the transition mutation G17A, resides in the IP of the left terminal domain, affected the predicted secondary structure of CEVd and the mutant could not infect the experimental hosts tested. Evidences indicated that the transcription of potato spindle tuber viroid (PSTVd) by RNA polymerase II starts in the left terminal loop (Schindler and Muhlbach, 1992; Kolonko *et al*., 2006). Though the viroids do not have a TATA-box motif as promoter element for

host polymerase II, well defined structural elements as well as nucleotide sequence were found to be critical for viroid transcription (Kolonko *et al*., 2006). Site-directed mutagenesis studies revealed that the disruption or destabilization of the left terminal domain prevented the transcription (Hammond 1994; Hu *et al*., 1997). The viroid processing by the hosts shows that the nucleotides in the left terminal domain are critical for infectivity as the deletion mutant (344A-) and transition mutant (U30C) could not infect the experimental hosts. However, both mutants infected their original hosts and additionally the deletion mutant (344A-) infected gynura (Table 9). But in all these cases, the mutants were reverted back to wild-type sequence and also mutants were eliminated from the progeny profile.

A few sequence changes in the pathogenic domain were sufficient to influence the severity of PSTVd disease symptoms (Schnolzer *et al.*, 1985). However, the CEVd processing in both gynura and citron resulted in reversion of the mutation G50A to wild-type sequence and also it was eliminated from the progeny profile (Table 9). As a consequence of this, mutant G50A behaved like wild-type in protoplasts, citron seedlings as well as at the symptom expression level. A relatively low thermodynamic stability region in the pathogenic domain (nucleotide positions 51 to 61 and 306 to 319 in CEVd) called pre-melting (PM) tend to influence the pathogenicity in viroids (Streger *et al*., 1984). Schnolzer *et al.* (1985) found an inverse correlation between the thermodynamic stability of PM region and virulence of certain naturally occurring strains of PSTVd in tomato. However, Visvader and Symons (1985) failed to find such relationships among a number of CEVd sequence variants.

An addition mutation (62A+) did not affect the thermodynamic stability of the PM region of pathogenic domain in CEVd dramatically, but induced severe symptoms in citron. The severe symptoms induced by the mutant might be due to its increased accumulations in citrus protoplasts than the wild-type. Similar observation was made when enhanced symptoms in citrus cachexia disease correlated with a higher titer of *Hop stunt viroid* (Serra *et al*., 2008). The PM region of pathogenic domain, which has low thermodynamic stability due to the stretch of oligo 'A', might be the reason for replication infidelity and induction of fitness peaks by 61A- mutation in gynura and chrysanthemum. Nearly 20% of the mutations on the entire genome of CEVd observed in the progeny viroid molecules lie in the PM region. Earlier studies have shown that mutations distributed unevenly on the five structural domains in pospivioroids and sequence variability occurs at specific positions of the viroid molecule (Keese & Symons, 1985; Ambros *et al*., 1998; Owens *et al*., 2003; Bernad *et al*., 2009). This variability allows the viroid to adapt to different hosts and environmental changes. The pathogenic domain has been demonstrated to be involved in replication (Qi *et al*., 2004) and systemic movement (Zhong *et al*., 2008) of *Pospiviroid*.

A transition mutation C320U, part of the HP II Loop of CEVd secondary structure, affected the predicted secondary structure. Though the predicted secondary structure of the mutant (C320U) was more stable (-140.34 kJ/mol) than the other mutants of pathogenic domain, G50A (-137.95 kJ/mol) and 62A+ (-138.75 kJ/mol), the mutation abolished the infectivity in the experimental hosts tested suggesting the importance of the cytosine nucleotide at position 320.

Cleavage and ligation are important steps in processing the longer-than-unit strands of replicating viroid molecules. Hairpin I (HP I)/double-stranded structure formed by the upper CCR strand and flanking nucleotides are involved in cleavage, and loop E and flanking nucleotides of both strands engaged in the ligation process (Diener 1986; Gas *et al*., 2007; Gas *et al*., 2008). The HP I stem of the CCR domain in CEVd includes nucleotide positions 81 to 110. Though the mutant (108U+) did not affect the thermodynamic stability of HPI dramatically, but it was eliminated and reverted back to wild-type sequence in all the hosts tested. Mutations predicted to disrupt HPI abolished the infectivity in tomato plant (Hammond and Owens, 1987).

Loop E motif in CCR domain (includes nucleotide sites 97-GGGAAACCU-105 and 261-GGCUACUACC-270 in CEVd) is involved in the processing of longer-than-unit strands of replicating viroid molecules (Baumstark *et al*., 1997; Schrader *et al*., 2003; Gas *et al*., 2007). A transversion mutation U264A, resides in the Loop E motif, did not affect the predicted secondary structure, but found to be non-infective in all experimental hosts tested except gynura. In citron and chrysanthemum hosts, uridine nucleotide seems to be critical for the viroid processing. On contrary, viroid processing in gynura stably preserved the mutation (U264A) in progeny population. However, previous studies on viroid processing in gynura have shown that the host displayed low fidelity in maintaining a mutation (Szychowski *et al*., 2005). Replication of PSTVd was increased by 5 to 10 fold in the cultured cells of tobacco BY2, but not in *N. benthamiana* due to a single nucleotide substitution (C259U) in loop E (Qi and Ding 2002). The U257A substitution engineered in loop E of a PSTVd strain caused flat-top lethal symptoms (Qi

and Ding 2003). Evidences show that the loop E has role in replication (Zhong *et al*., 2006) and host adaptation (Wassenegger *et al*., 1996; Qi and Ding, 2002; Zhu *et al*., 2002).

Nucleotide adenine at position 265 seems to be critical for viroid processing, as the transition mutation A265G (resides in the loop E motif) was reverted back to wild-type in all host plants tested. However, a transversion mutation U278A, part of HP II loop in the CCR domain, was stably maintained in the viroid progeny profile of all the host plants except citron. The mutant U278A induced severe symptoms in all hosts plants (Table 9). The severe symptoms observed in citron plants might be attributed to the 13 fold increase in titer. Previously, a higher titer *Hop stunt viroid* was correlated to the enhanced symptoms in citrus cachexia disease (Serra *et al*., 2008). Nucleotide cytosine at position 289 seems to be critical for viroid infectivity as the transition mutation C289U could not infect the host plants tested.

Nucleotide guanidine at position 128 of variable domain seems to be important for infectivity as the transition mutant (G128A) could not infect the experimental hosts tested. A deletion mutation at 128 (128G-) could infect only gynura and its original host, datura. Mutation was not desired in both hosts and it was reverted back to wild-type. However, a transversion mutation (U129A) was stably maintained in the progeny population of gynura and thereby inducing severe symptoms. Earlier studies have shown that the sequences in the variable domain play an important role in viroid replication (Visvader and Symons, 1986; Sano *et al.*, 1992), and a single transition mutation within

the variable domain of PSTVd was sufficient to influence the infectivity (Owens *et al.*, 1991).

The mutations in the right terminal domain, G159U and U182C, affected the systemic accumulation of the viroid, though they could replicate in the citrus protoplasts. Previous studies have shown that the mutations in the right terminal domain inhibited PSTVd systemic infection (Hammond, 1994; Zhong *et al*., 2008). This is also the region that has been shown to interact with a bromodomain-containing protein, VIRP1, from tomato (Gozmanova *et al*., 2003; Maniataki *et al*., 2003) and recently shown to be important for PSTVd infection (Kalantidis *et al*., 2007).

Mutants with two or more mutations per CEVd genome found to be non-infective except two mutants 62A+/U278A and U316C/U278A. The mutant U41A/G107U and A61G/G107U affected the HP I metastable structure, which is involved in viroid processing. Mutations predicted to disrupt HPI abolished the infectivity in tomato plant (Hammond and Owens, 1987). In this present study, a mutant carrying single mutation at position 108 (108U+) reverted back to wild-type sequence. These results suggest that the nucleotides present in the HP I of CCR domain are conserved and critical for the viroid processing.

The study of the molecular and biological properties of *in vivo* generated CEVd variants revealed the effects of mutation, selection, and genetic drift on the adaptation and extinction of CEVd RNA. The stability of the 62A+, U129A and U278A variants in their respective progeny populations clearly indicates the phenomenon of genetic drift and fixation of a mutation in the population. Genetic structure and diversity of CEVd

progeny population altered significantly with replication in different hosts and understanding these interactions may facilitate the prediction and prevention of emerging virulent strains.

PART B

Nucleotide Sequence and Genome Organization of Dweet mottle virus and Its Relationship to Members of the Family *Betaflexiviridae*

INTRODUCTION

Dweet mottle virus (DMV) was reported from Riverside, California in 1968 during reindexing of a 'Cleopatra' mandarin variety introduced from Florida in the Citrus Variety Improvement Program, the fore-runner of Citrus Clonal Protection Program (CCPP) (Krueger *et al*., 2005). DMV produced leaf mottling symptoms only in 'Dweet' tangor showing certain similarities to the symptoms of psorosis and concave gum (Roistacher & Blue, 1968). A partial sequence analysis showed that DMV has very high sequence homology (over 96%) with the *Citrus leaf blotch virus* (CLBV) (Vives *et al.*, 2004). CLBV was first reported in Spain in an introduction of 'Nagami' kumquat from Corsica (Navarro *et al.*, 1984). Both DMV and CLBV induce mottling in 'Dweet' tangor and stem pitting in 'Etrog' citron (Galipienso *et al*., 2000) however, only CLBV causes vein clearing in 'Pineapple' sweet orange and bud union crease on trifoliate and trifoliate hybrids rootstocks and has been reported to be seed transmitted (Navarro *et al*., 1984; Galipienso *et al*., 2000 & 2001; Vives *et al*., 2004; Guerri *et al.*, 2004).

Experiments with full-genome cDNA clones of CLBV indicated that the bud union crease and vein clearing symptoms might be caused by a different agent associated with 'Nagami' kumquat sources (Vives *et al*., 2008). Since DMV and CLBV have

distinct biological similarities and differences, a direct comparison of the full DMV genome at the genetic level was undertaken. The full genomic sequence and genome organization of DMV is presented here and compared to the members of *Alpha*- and *Beta-flexiviridae* family. The practical implications for citrus germplasm programs and threats to the citrus industry from viruses such as DMV and CLBV are also discussed.

MATERIALS AND METHODS

Virus Source and RNA Isolation. The virus used for the present study was DMV isolate-932 (according to the CCPP citrus disease bank records). Total RNA was extracted with an RNeasy kit (Qiagen, CA) according to manufacturer's instructions from DMV infected plants maintained at the USDA-ARS National Clonal Germplasm Repository for Citrus and Dates, Riverside.

Synthesis and Cloning of DMV cDNAs. Primers were designed using sequence information of CLBV from the online database (NCBI Accession: NC_003877). Primers were designed in such a way that overlapping clones can be generated all along the length of the genome (Table 16). Reverse transcription-polymerase chain reaction (RT-PCR) (Figure 64) was performed with RNA from the DMV infected plants as template (Sambrook & Russell, 2001). RT-PCR products with a 3'-A tail (*Taq* DNA polymerase activity) were cloned into pGEM-T easy vector (Promega Corp. USA) using TA-cloning strategy followed by transformation of *Escherichia coli* DH5-α chemical competent cell (Sambrook & Russell, 2001).

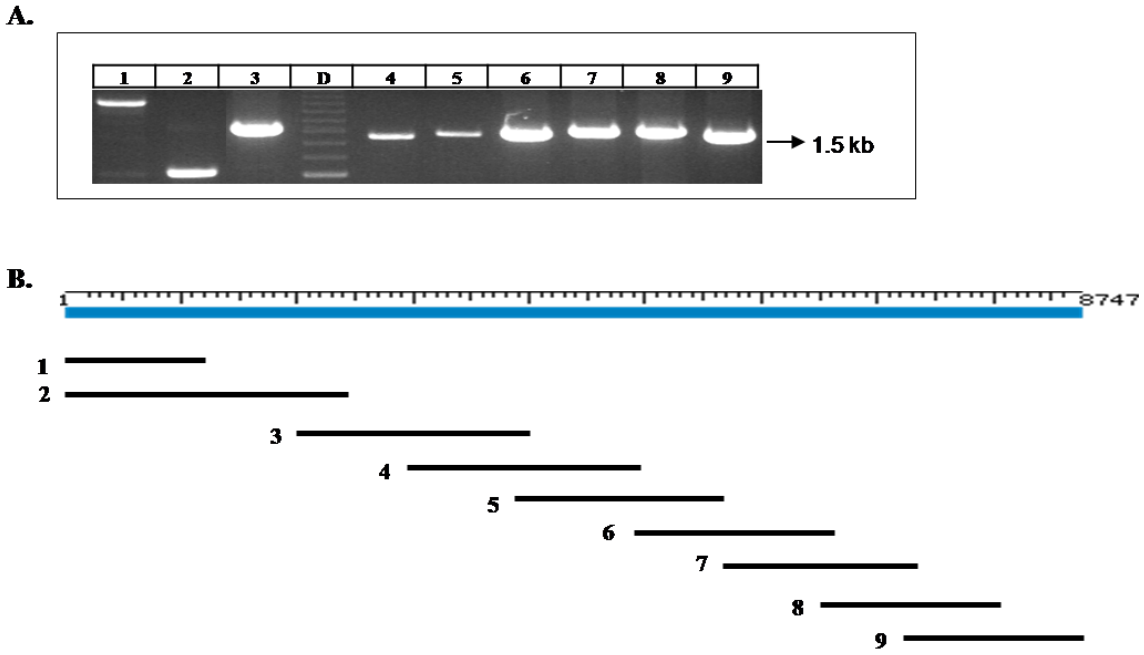

Figure 64. (A) The RT-PCR products of DMV generated from the isolate DMV-932. (B) RT-PCR fragments number 1 to 9 cover the entire length of DMV genome (8747 bp) from 5' to 3' end with sequential overlap. D, DNA Ladder; Fragment (1) 1-2668 nt, (2) 1-880 nt, (3) 2331-4142 nt, (4) 3231-4886 nt, (5) 3901-5616 nt, (6) 4701-6440 nt, (7) 5420-7227 nt, (8) 6232-8029 nt, (9) 7051-8747 nt.

Sequencing and Computer-Assisted Nucleotide and Amino Acid Sequence Analysis.

Transformed *E. coli* colonies were verified for the presence of insert by sequencing with T7 promoter primer from 5'-end and SP6 promoter primer from 3'-end with an automated DNA sequencer (University of California Riverside Core Instrumentation Facility - Keen Hall).

Table 16. Primers Used for Reverse Transcription and PCR Amplification to obtain the overlapping Dweet mottle virus cDNA clones. Nucleotide (nt) position is referred to CBLV sequence (NCBI GenBank accession number NC_003877).

Primer	Polarity	Sequence (5' to 3')	Position (nt)
CIT 120	Sense	GAAAAGCAACGAAAGCAACCTACA	1-24
CIT 131	Sense	GAAAAGCAACGAAAGCAACC	1-20
CIT 133	Sense	ATGGCTTTGATGAGCAACAA	74-93
CIT 134	Anti-Sense	TCAGATATCTTCGTCGGAA	5962-5944
CIT 135	Sense	ATGGCATCCCTGATCAATGT	5962-5981
CIT 136	Anti-Sense	TCACTTGGTTCCAGTGTCA	7050-7032
CIT 137	Sense	ATGAAAATCACCAATGATAA	7115-7134
CIT 138	Anti-Sense	CTACATTTCTAAGAGTTTTG	8206-8187
CIT 145	Sense	AGAACTCGAGCCGAAACAGCTGTTATTG	6301-6328
CIT 146	Anti-Sense	CAATAACAGCTGTTTCGGCTCGAGTTCT	6328-6301
CIT 147	Sense	TTCATGGGTACCTTCTTTAGAAGAGATC	2641-2668
CIT 148	Anti-Sense	GATCTCTTCTAAAGAAGGTACCCATGAA	2668-2641
CIT 149	Anti-Sense	CACTGCGAAGATGTGATG	880-865
CIT 150	Sense	TCACTGTAGTCTATCCAC	702-719
CIT 151	Anti-Sense	CTATCCTCTTTCCCAGCA	1760-1743
CIT 152	Sense	GAATCTGAATGACTATGAC	1540-1559
CIT 153	Anti-Sense	CTGGGCACAGTTGAAATG	2563-2546
CIT 154	Sense	GAGGAGTCACGTTGATTAT	2331-2350
CIT 155	Anti-Sense	TGGCTGCAAATTGAATTTTG	3410-3391
CIT 156	Sense	GAATCTCAATGGCTTTAAGA	3231-3251
CIT 157	Anti-Sense	CAAGGTCAGATTCAACCAA	4142-4124
CIT 158	Sense	ATCAATCCTGACATTTGAAC	3901-3920
CIT 159	Anti-Sense	CAACTAAATGCGCCCTTG	4886-4869
CIT 160	Sense	TGACAGTTATGATAAGGTTC	4701-4721
CIT 161	Anti-Sense	TCATCGAAATCATGACAAAC	5616-5597
CIT 162	Sense	TGCAAATTGGGATGCAAATT	5420-5440
CIT 163	Anti-Sense	GCACCTGAATGCTACCG	6440-6423
CIT 164	Sense	GCAATTAGATCTCTATTACC	6232-6252
CIT 165	Anti-Sense	TGAATTTTCGAATGATGTCAT	7227-7206
CIT 166	Sense	GTATAACGTGTGACTAGTG	7051-7070
CIT 167	Anti-Sense	CCATCAGCTTCAGTTGGA	8029-8011
CIT 168	Sense	GGAAAGATATAGCATATGCA	7931-7947
CIT 169	Anti-Sense	GTCTAAAAGTTCTTAAAAGAC	8747-8727

Nucleotide sequence data were assembled and analyzed using ContigExpress tool (Vector NTI Advance 10- InforMax, USA). Sequence information was used in the Basic Local Alignment Search Tool (BLAST) program to observe the regions of similarity between DMV sequences to the sequence database. Amino acid sequences were analyzed with help of BLAST program (Schaffer *et al*., 2001). ORF Finder of the NCBI was used to search the potential ORFs on the DMV genome. Conserved domains on the amino acid sequences were identified by CD-Search on NCBI (Marchler-Bauer & Bryant, 2004; Marchler-Bauer *et al*., 2009). Oligo calculator (http://mbcf.dfci.harvard.edu/docs/oligocalc.html) was used to calculate the percent G+C content. Molecular weights of the putative proteins encoded by the potential ORFs were calculated by the protein molecular weight calculator (http://www.bioinformatics.org/SMS/prot_mw.html).

***In silico* analysis.**

Sequence-alignment. Comparative analysis of amino acid and nucleotide sequences of the RNA-dependent RNA polymerase (RdRP) domain of the replicase polyprotein and the capsid protein (CP) the DMV was performed with the selected members of *Alpha*- and *Beta-flexiviridae* family. For the comparative analysis, nucleotide and amino acid sequence information were obtained from NCBI data base and used in the Clustal program (Larkin *et al*., 2007). Alignment of amino acid sequence of RdRP domain of selected members of *Alpha- and Beta-flexiviridae family* was generated with GeneDoc and Clustal program (Nicholas & Nicholas, 1997; Larkin *et al*., 2007).

Table 17. Abbreviation, name, taxonomic position and sequence accession numbers of the viruses of family *Alpha-* and *Beta-Flexiviridae* used in the phylogenetic analysis.

Abbreviation	Virus name	Genus*	Accession No
DMV-932	Dweet mottle virus isolate DMV-932	*Citrivirus*	FJ009367
CLBV Spain	*Citrus leaf blotch virus* Spain	*Citrivirus*	NC_003877
CLBV NZ	CLBV isolate New Zealand_G78	*Citrivirus*	EU857540
GarVA	*Garlic virus A*	*Allexivirus*	NC_003375
GarVB	*Garlic virus B*	*Allexivirus*	EF596816
GarVC	*Garlic virus C*	*Allexivirus*	NC_003376
ASGV	*Apple stem grooving virus*	*Capillovirus*	NC_001749
CTLV	*Citrus tatter leaf virus*	*Capillovirus*	FJ355920
PBNLSV	*Pear black necrotic leaf spot virus*	*Capillovirus*	AY596172
NCLV	*Narcissus common latent virus*	*Carlavirus*	NC_008266
PVM	*Potato virus M*	*Carlavirus*	NC_001361
PVS	*Potato virus S*	*Carlavirus*	NC_007289
ASPV	*Apple stem pitting virus*	*Foveavirus*	NC_003462
CGRMV	*Cherry green ring mottle virus*	*Foveavirus*	NC_001946
CNRMV	*Cherry necrotic rusty mottle virus*	*Foveavirus*	NC_002468
PVX	*Potato virus X*	*Potexvirus*	NC_011620
PapMV	*Papaya mosaic virus*	*Potexvirus*	NC_001748
CymMV	*Cymbidium mosaic virus*	*Potexvirus*	NC_001812
ACLSV	*Apple chlorotic leaf spot virus*	*Trichovirus*	NC_001409
CMLV	*Cherry mottle leaf virus*	*Trichovirus*	NC_002500
PMV	*Peach mosaic virus*	*Trichovirus*	NC_011552
GVA	*Grapevine virus A*	*Vitivirus*	NC_003604
GVB	*Grapevine virus B*	*Vitivirus*	NC_003602
GVE	Grapevine virus E	unclassified *Vitivirus*	NC_011106

* Members of *Alphaflexiviridae* are genera *Allexivirus* and *Potexvirus*. Members of *Betaflexiviridae* are genera *Capillovirus*, *Carlavirus*, *Citrivirus*, *Foveavirus*, *Trichovirus* and *Vitivirus*

***Phylogenetic Analysis*.** Phylogenetic and molecular evolutionary analyses were performed using the conserved amino acid sequences of RdRP domain from 6 members of *Alphaflexiviridae* and 17 members of *Betaflexiviridae* family (Table 17) by MEGA

version 4.1 (Tamura *et al*., 2007) and MrBayes (Ronquist & Huelsenbeck, 2003) programs. Neighbor-Joining, Minimum Evolution, Maximum Parsimony, UPGMA (Unweighted Pair Group Method with Arithmetic mean) and Bayesian methods of phylogeny estimation were utilized (Yang & Rannala, 1997). Multiple alignments of amino acid sequences were obtained using ClustalX2 (Larkin *et al*., 2007). Bootstrap values were obtained by including 10,000 replicates in MEGA4.1 program and MrBayes program was run for 2 million generations to estimate the posterior probabilities.

RESULTS

Sequence analysis and Genome organization. Overlapping cDNA fragments ranging from 1 to 2.6 kb (Figure 64) were used to compile the nucleotide sequence of the viral genome. The produced consensus nucleotide sequence of the DMV genome was submitted to GenBank accession FJ009367. The blast analysis showed 98-99% nt nucleotide homology between DMV and CLBV isolates.

The genomic organization of DMV is represented in Figure 65. The complete genome of the virus consists of 8747 nucleotides (nt), excluding the poly (A) tail at the 3' end. The overall A+U and G+C content of DMV genomic RNA was 60% and 40% respectively.

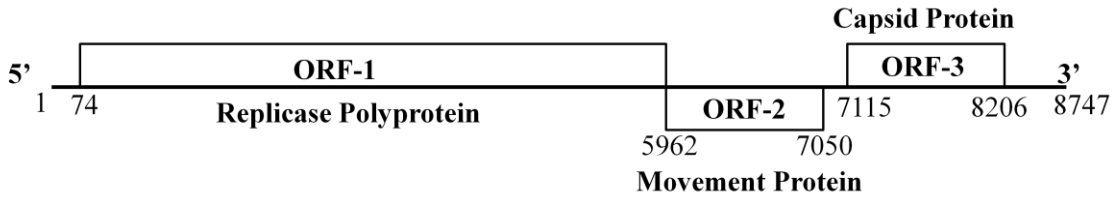

Figure 65. Schematic representation of the genomic organization of DMV. The open reading frames (ORFs) are shown as boxes.

ORF-1, which is at the 5'-proximal region, comprises 5889 nt (position from 74 to 5962 nt) with a translation product of 1962 aa (227.48 kDa), which is a putative polyprotein with replicase activity. ORF-2 is 1089 nt long, and is located at position 5962 to 7050. The putative translation product of ORF-2 is a 362 aa long movement protein (40.25 kDa). The 3'-proximal ORF is located between the residues 7115 and 8206 and encodes a putative coat protein of 363 aa (40.69 kDa). The 5' untranslated region (UTR) is about 74 nt long while the 3' UTR is 541 nt long. Intergenic region of 64 nt is present between ORF-2 and ORF-3. One nucleotide overlap between ORF-1 and ORF-2 indicates a potential +1 frame-shift translation strategy employed by the virus.

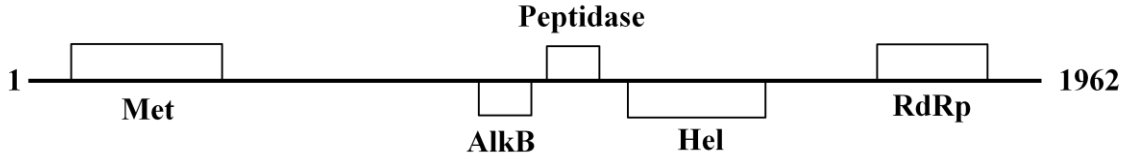

Figure 66. Schematic representation of organization of conserved core domains of replicase polyprotein (1962 aa) of DMV. Met: Methyl Transferase; AlkB: Oxygenase protein; Hel: Helicase; RdRP: RNA-dependent RNA polymerase.

Table 18. Conserved core domains of replicase polyprotein (1962 aa) and their function in virus replication cycle.

Core domain	aa in length	Function of the domain
Met	44-360	Capping Enzyme
AlkB	875-962	Integrity of RNA by oxidative demethylation
Endo-peptidase	978-1065	Auto-proteolysis
Hel	1160-1412	RNA helicase
RdRP	1628-1858	RNA Polymerase

aa: amino acids; Met: Methyl Transferase; AlkB: Oxygenase protein; Hel: Helicase; RdRP: RNA-dependent RNA polymerase

The replicase polyprotein encoded by DMV ORF-1 is represented in figure 66. CD-Search on NCBI revealed conserved core domains on the amino acid sequences of replicase polyprotein (Marchler-Bauer & Bryant, 2004; Marchler-Bauer *et al*., 2009). RdRP, Met and Hel domains are conserved throughout the alphavirus-like superfamily (Koonin & Dolja, 1993) (Table 18). Endopeptidase domain of DMV is similar to Carlavirus peptidase, which is involved in auto-proteolysis of a polyprotein (Lawrence *et al*., 1995). AlkB protein is involved in maintaining the integrity of the viral RNA genome by oxidative demethylation (van den Born *et al*., 2008)

The comparative analysis of amino acid and nucleotide sequence of RdRP and CP reveals the high sequence homology between DMV and CLBV isolates (Table 19). The highest amino acid sequence similarity for the RdRP and CP was between DMV and CLBV isolates (99-100% & 98-99%) followed by *Cherry mottle leaf virus* (60% & 4%) and *Apple stem pitting virus* (55% & 6%) (Table 19). The amino acid sequence

alignment represented in the figure 67 shows conservation of RdRP domain among the members of *Beta-flexiviridae* family.

Table 19. Comparative analysis of amino acid and nucleotide sequences of the RdRP domain of replicase polyprotein and CP of the Dweet mottle virus with the selected members of the family *Alpha-* and *Beta-flexiviridae*. Comparison is shown as percentage identity

	CLBV-Spain	CLBV-NZ	CMLV	ASPV	PVS	GVA	ASGV	GarVA	PVX	
DMV RdRP	100	99	60	55	51	47	25	12	11	% Amino Acid Identity
	99	98	59	57	55	51	36	31	28	% Nucleotide Identity
DMV CP	99	98	4	6	1	1	5	2	2	% Amino Acid Identity
	99	98	14	23	20	13	19	17	16	% Nucleotide Identity

List of Abbreviations, names, taxonomic position and sequence accession numbers of the viruses of *Flexiviridae* family used in the alignment study are provided in Table 17.

Phylogeny: Comparison of DMV to other members of *Alpha- and Beta-flexiviridae*. DMV and CLBV isolates were clustered in a single clade, within the genus *Citrivirus*, of the neighbor-joining and maximum parsimonious topologies (100% bootstrap) with close ancestral relationships with the *Trichovirus* of the *Betaflexiviridae* family (Figure 68 & 69). These phylogenetic relationships were also supported by the minimum evolution, UPGMA, and Bayesian predicted topologies (data not shown).

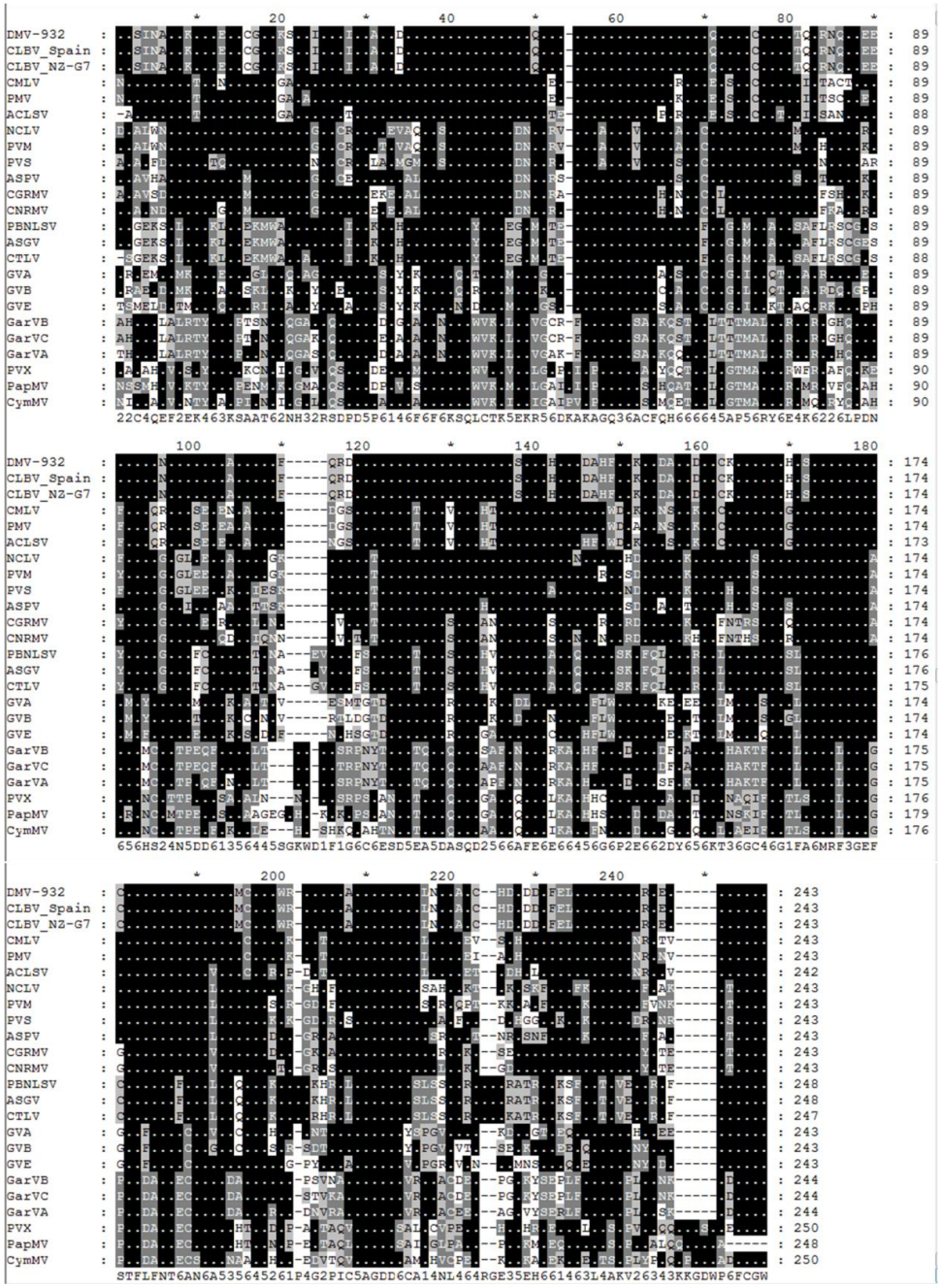

Figure 67. Alignment of amino acid sequence of RdRP domain of selected members of *Alpha-* and *Beta-flexiviridae* family using GeneDoc program (Nicholas & Nicholas, 1997). The black and gray shadows represent the identical and conserved sequences within all aligned sequences. The intensity of the shading represents the degree of conservation. List of Abbreviations, names, taxonomic position and sequence accession numbers of the viruses of *Alpha-* and *Beta-flexiviridae* family used in the alignment study are provided in Table 17.

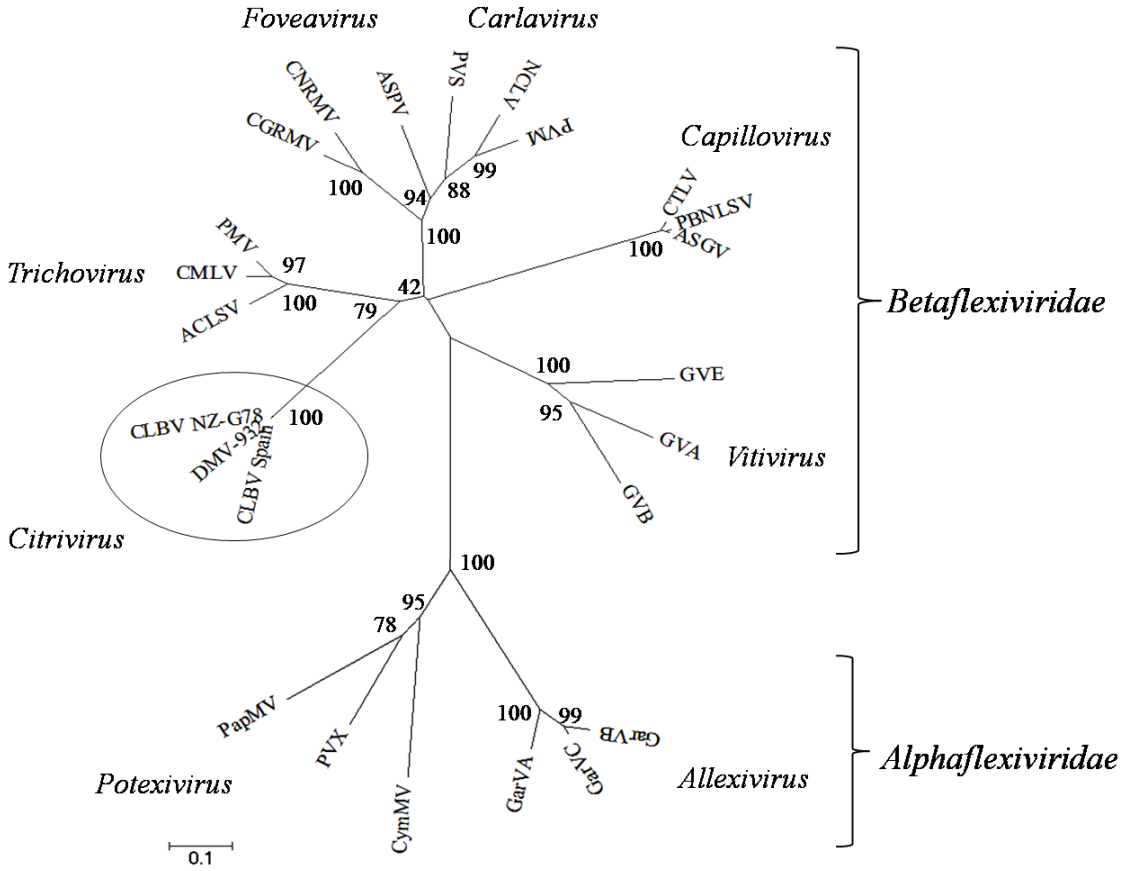

Figure 68. Phylogenetic relantionships of Dweet mottle virus with members of the *Alpha-* and *Beta-flexiviridae* family based on the amino acid sequence of the conserved core RdRP domain of the replicase polyprotein. Presented topologies were reconstructed with the Neighbor-joining method (10,000 bootstraps). The scale bars represent the number of residue substitutions per site. Three viruses from selected genera of the *Alpha-* and *Beta-flexiviridae* families were used for the analysis. List of Abbreviations, names, taxonomic position and sequence accession numbers of the viruses of *Alpha-* and *Beta-flexiviridae* family used in the phylogenetic analysis is provided in Table 17.

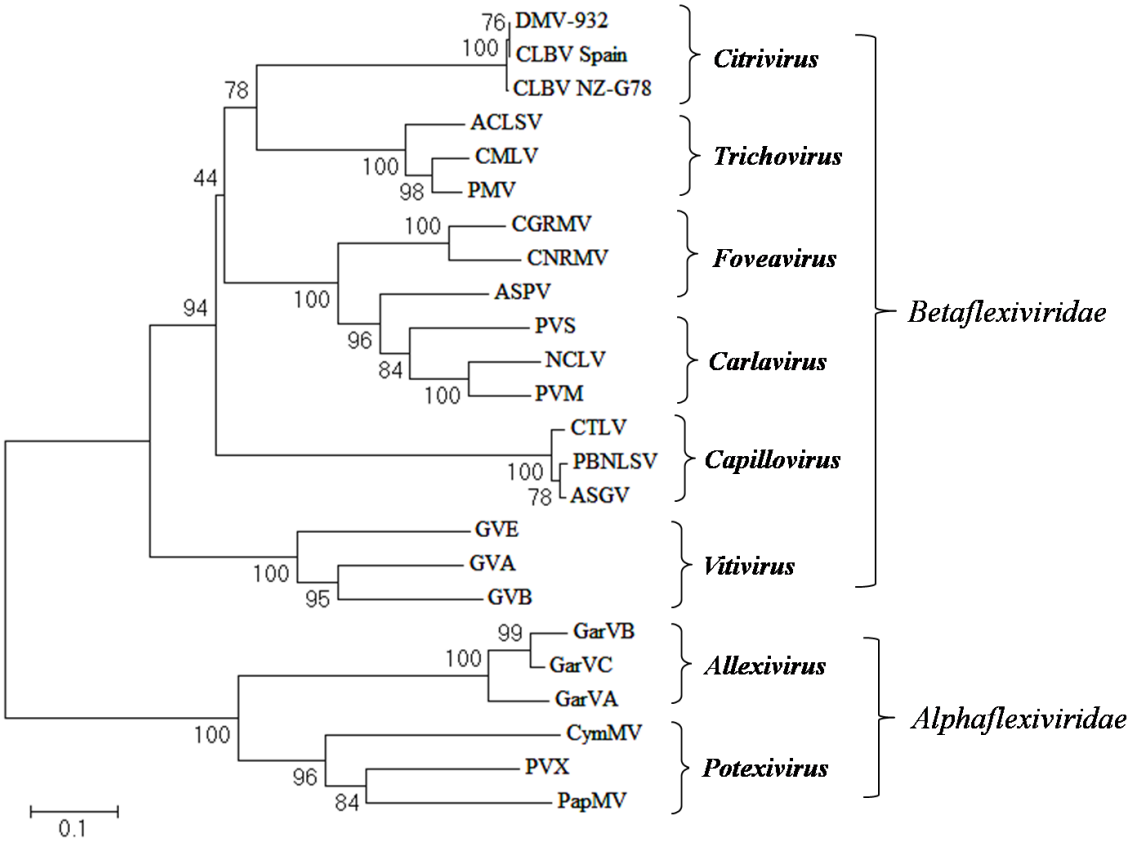

Figure 69. Phylogenetic relantionships of Dweet mottle virus with members of the *Alpha-* and *Beta-flexiviridae* family based on the amino acid sequence of the conserved core RdRP domain of the replicase polyprotein. Presented topologies were reconstructed with the Maximum Parsimony method (10,000 bootstraps). The scale bars represent the number of residue substitutions per site. Three viruses from selected genera of the *Alpha-* and *Beta-flexiviridae* families were used for the analysis. List of Abbreviations, names, taxonomic position and sequence accession numbers of the viruses of *Alpha-* and *Beta-flexiviridae* family used in the phylogenetic analysis is provided in Table 17.

DISCUSSION

The complete nucleotide sequence of DMV was determined and compared to sequences of members of the *Alpha- and Beta-flexiviridae* family. Analyses of the entire nucleotide sequence revealed that the DMV genome is closely related to that of the CLBV with very similar ORFs and protein products. The new virus genus *Citrivirus* to CLBV has been considered for its peculiar biological, structural and molecular characteristics compared to other members of *Betaflexiviridae* (Vives *et al*., 2001; Martelli *et al*., 2007; Carstens, 2010). In addition, Vives *et al.* (2002) compared 14 isolates of CLBV from different geographical regions of the world and found low genetic diversity. The historical background of the California DMV isolate in combination with the complete genome sequence and the phylogenetic analysis presented here strongly supports the inclusion of DMV to the genus *Citrivirus* as its member. According to the molecular criteria for species demarcation within a genus of the *Betaflexiviridae* family, amino acid sequences of polymerase and CP genes must differ by more than 10% (Adams *et al*., 2004). Sequence homology and genome organization support the hypothesis that DMV is a CLBV isolate and not a distinct species however, more information on the biological properties of the DMV (i.e. seed transmission) is necessary for a final conclusion.

An interesting revelation from the study of organization of conserved core domains of replicase polyprotein is AlkB protein (Figure 66). Numerous single-stranded plant RNA viruses encode AlkB-domain, remarkably, majority of which belong to the

Betaflexiviridae family (Aravind & Koonin, 2001; Martelli *et al*., 2007). Bacterial and mammalian AlkB proteins are 2-oxoglutarate (2-OG) and Fe(II)-dependent oxygenase that reverse methylation damage in RNA and DNA (Falnes, 2004; Koivisto *et al*., 2004). AlkB maintains the integrity of the viral RNA genome by oxidative demethylation through repair of deleterious methylation damage (van den Born *et al*., 2008). Interestingly, most of the AlkB-containing viruses infect woody or perennial plants. The long-term survival of viruses within the single infected plant might be attributed to the functional advantages provided by AlkB protein (Martelli *et al*., 2007).

The threat posed to the California citrus industry from viruses such as DMV and CLBV is high. Currently, the majority of California citrus (with the exception of some lemons) is propagated on trifoliate and trifoliate hybrids such as 'Troyer' and 'Carrizo' citrange. Therefore, dispersal of a graft transmissible pathogen causing bud union crease on these rootstocks could potentially cause severe economic losses. The seed transmission of CLBV for 'Troyer' citrange specifically has been estimated at 2.5% (Guerri *et al*., 2004). The effect on citrus nurseries by such transmission rates can be serious for the production of young trees as well as the direct distribution of citrus seeds.

The history of the identification and characterization of CLBV and DMV and the diseases associated with them is an excellent example of the value of the use of biological indexing in the citrus germplasm quarantine, certification, and distribution programs. Unlike the situation in Florida, the spread of DMV in the California orchards was avoided probably because of the practice of using 'Dweet' tangor as the bio-indexing host for DMV. Additional treatments apart from bio-indexing such as thermal therapy

and shoot-tip grafting would eliminate, even if any misidentified positives, before the release. CCPP followed this practice for decades before any laboratory characterization of the virus was available.

REFERENCES

Adams MJ, Antoniw JF, Bar-Joseph M, Brunt AA, Candresse T, Foster GD, Martelli GP, Milne RG, Fauquet CM (2004) The new plant virus family *Flexiviridae* and assessment of molecular criteria for species demarcation. *Arch. Virol.* 149: 1045–1060.

Albiach-Marti, MR, Grosser JW, Gowda S, Mawassi M, Satyanarayana T, Garnsey SM, Dawson WO. 2004. Citrus tristeza virus replicates and forms infectious virions in protoplasts of resistant citrus relatives. *Mol. Breed*. 14: 117-128.

Ambros S, Hernandez C, Desvignes JC, Flores R. 1998. Genomic structure of three phenotipically different isolates of peach latent mosaic viroid: implications of the existence of constraints limiting the heterogeneity of viroid quasispecies. *J. Virol*. 72: 7397–7406.

Ambros S, Hernandez C, Flores R. 1999. Rapid generation of genetic heterogeneity in progenies from individual cDNA clones of peach latent mosaic viroid in its natural host. *J. Gen. Virol*. 80: 2239–2252.

Aoki S, Takebe I. 1969. Infection of tobacco mesophyll protoplasts by tobacco mosaic virus ribonucleic acid. *Virol.* 39: 439-448.

Aravind L, Koonin EV. 2001. The DNA-repair protein AlkB, EGL-9, and leprecan define new families of 2-oxoglutarate-and iron-dependent dioxygenases. *Genome Biol*. 2: research0007.1–research0007.8.

Baumstark T, Schroder ARW, Riesner D. 1997. Viroid processing: a switch from cleavage to ligation is driven by a change from a tetraloop to a loop E conformation. *EMBO J*. 16: 599-610.

Bernad L, Duran-Vila N, Elena SF. 2009. Effect of citrus hosts on the generation, maintenance and evolutionary fate of genetic variability of *Citrus exocortis viroid* (CEVd). *J. Gen. Virol.* 90: 2040.

Candresse T, Gora-Sochacka A, Zagorski W. 2001. Restoration of secondary hairpin II is associated with restoration of infectivity of non-viable recombinant viroid. *Virus Res*. 75: 29–34.

Carstens EB. 2010. Ratification vote on taxonomic proposals to the International. Committee on Taxonomy of Viruses (2009). *Arch. Virol.* 155: 133–146.

Chomczynski P, Sacchi N. 1987. Single-step method of RNA isolation by acid guanidinium thiocyanate-phenol-chloroform extraction. *Anal. Biochem.* 162: 156–159.

Clement M, Posada D, Crandall K. 2000. TCS: a computer program to estimate gene genealogies. *Mol. Ecol.* 9: 1657-1660.

Cocking EC. 1960. Method for the isolation of plant protoplasts and vacuoles. *Nature* 187: 927–929.

Cocking EC. 1966. An electron microscopic study of the initial stages of infection of isolated tomato frit protoplasts by tobacco mosaic virus. *Planta* 68: 206–214.

Codoner FM, Daros JA, Sole RV, Elena SF. 2006. The fittest versus the flattest: Experimental confirmation of the quasispecies effect with subviral pathogens. *PLoS Pathogens* 2: 1187-1193.

Daros JA, Elena SF, Flores R. 2006. Viroids: an Ariadne's thread into the RNA labyrinth. *EMBO Rep*. 7: 593–598.

Diener TO. 1971a. Potato spindle tuber "virus": a plant virus with properties of a free nucleic acid. III. Subcellular location of PSTV-RNA and the question of whether virions exist in extracts or *in situ*. *Virol.* 43: 75–89.

Diener TO. 1971b. Potato spindle tuber "virus" IV. A replicating, low molecular weight RNA. *Virol.* 45: 411-428.

Diener TO. 1979. Viroids: structure and function. *Science* 205: 859-866.

Diener TO. 1986. Viroid processing: a model involving the central conserved region and hairpin I. *Proc. Natl. Acad. Sci. U.S.A.* 83: 58–62.

Diener TO. 1999. Viroids and the nature of viroid diseases. *Arch. Virol. Suppl*. 15: 203-220.

Ding B, Itaya A, Zhong X. 2005. Viroid trafficking: a small RNA makes a big move. *Curr. Opin. Plant Biol*. 8: 606-612.

Ding B. 2009. The biology of viroid-host interactions. *Annu. Rev. Phytopathol*. 47: 105–131.

Domingo E, Holland JJ. 1997. RNA virus mutations and fitness for survival. *Annu. Rev. Microbiol*. 51: 151–178.

Eigen M, McCaskill J, Schuster P. 1989. The molecular quasispecies. *Adv. Chem. Phys.* 75: 149–263.

Eigen M. 1971. Self-organization of matter and the evolution of biological macromolecules. *Naturwissenschaften* 58: 465–523.

Eigen M. 1993. The origin of genetic information: viruses as models. *Gene* 135: 37–47.

Falnes PO. 2004. Repair of 3-methylthymine and 1-methylguanine lesions by bacterial and human AlkB proteins. *Nucleic Acids Res.* 32: 6260–6267.

Felsenstein J. 1989. PHYLIP - Phylogeny Inference Package (Version 3.2). *Cladistics* 5: 164-166.

Felsenstein J. 1991. *PHYLIP*: Phylogenetic Inference Package. University of Washington, Seattle, WA.

Flores R, Gas ME, Molina D, Hernandez C, Daros JA. 2008. Analysis of viroid replication. *Methods Mol. Biol*. 451: 167-183.

Flores R, Hernandez C, Martinez de Alba AE, Daros JA, Serio FDi. 2005. Viroids and viroid-host interactions. *Annu. Rev. Phytopath*. 43: 117-139.

Flores R, Randles JW, Owens RA, Bar-Joseph M, Diener TO. 2005b. Viroids. In: Fauquet C.M., Mayo M.A., Maniloff J., Desselberger U., Ball A.L. (eds). Virus Taxonomy, Eight Report of the International Committee on Taxonomy of Viruses, Elsevier/Academic Press, London, UK, pp. 1145-1159.

Foissac, Duran-Vila N. 2000. Characterization of two citrus apscaviroids isolated in Spain, *Arch. Virol.* 145: 1975–1983.

Gafny R, Mogilner N, Nitzan Y, Ben Shalom J, Bar-Joseph M. 1995. The movement and distribution of citrus tristeza virus and citrus exocortis viroids in citrus seedlings. *Ann. Appl. Biol*. 126: 465-470.

Galipienso L, Navarro L, Ballester-Olmos JF, Pina J, Moreno P, Guerri J. 2000. Host range and symptomatology of a graft-transmissible pathogen causing bud union crease of citrus on trifoliate rootstocks. *Plant Pathol.* 49: 308–314.

Galipienso L, Vives MC, Moreno P, Milne RG, Navarro L, Guerri J. 2001. Partial characterisation of Citrus leaf blotch virus, a new virus from Nagami kumquat. *Arch. Virol.* 146: 357–368.

Gandia M, Bernad L, Rubio L, Duran-Vila N. 2007. Host effect on the molecular and biological properties of a citrus exocortis viroid isolate from *Vicia faba*. *Phytopathol.* 97: 1004–1010.

Gandia M, Duran-Vila N. 2004. Variability of the progeny of a sequence variant of *Citrus bent leaf viroid* (CBLVd). *Arch. Virol* 149: 407–416.

Gandia M, Palacio A, Duran-Vila N. 2000. Variability of *Citrus exocortis viroid* (CEVd). In: *Proc. 14th Conf. Int. Organ. Citrus Virologists*. IOCV, Riverside. pp 265-272.

Gandia M, Rubio L, Palacio A, Duran-Vila N. 2005. Genetic variation and population structure of an isolate of citrus exocortis viroid (CEVd) and the progenies of two infectious sequence variants. *Arch.Virol*. 150: 1945-1957.

Garcia-Arenal F, Fraile F, Malpica JM. 2001. Variability and genetic structure of plant virus populations. *Annu. Rev. Phytopathol.* 39: 157–186.

Gas ME, Hernandez C, Flores R, Daros JA. 2007. Processing of nuclear viroids in vivo: an interplay between RNA conformations. *PLoS Pathog.* 3:e182.

Gas ME, Molina-Serrano D, Hernandez C, Flores R, Daros JA. 2008. Monomeric linear RNA of citrus exocortis viroid resulting from processing in vivo has 5_-phosphomonoester and 3_-hydroxyl termini: implications for the RNase and RNA ligase involved in replication. *J. Virol.* 82: 321−25.

Gora A, Candresse T, Zagorski W. 1994. Analysis of the population structure of three phenotipically different PSTVd isolates. *Arch. Virol.* 138: 233–245.

Gora A, Candresse T, Zagorski W. 1996. Use of intramolecular chimeras to map molecular determinants of symptom severity of potato spindle tuber viroid (PSTVd). *Arch. Virol.* 141: 2045-2055.

Gora-Sochacka A, Kierzez A, Candresse T, Zagorski W. 1997. The genetic stability of potato spindle tuber viroid (PSTVd) molecular variants. *RNA* 3: 68–74.

Gora-Sochacka A. 2004. Viroids: unusual small pathogenic RNAs. *Acta Biochim. Pol.* 51: 587-607.

Gozmanova M, Denti MA, Minkov IN, Tsagris M, Tabler M. 2003. Characterization of the RNA motif responsible for the specific interaction of potato spindle tuber viroid RNA (PSTVd) and the tomato protein Virp1. *Nucleic Acids Res.* 31: 5534–5543.

Gross HJ, Domder H, Lossow C, Jank P, Raba M, Alberty H, Sanger HL. 1978. Nucleotide sequence and secondary structure of potato spindle tuber viroid. *Nature* 273: 203-208.

Grosser JW, Gmitter Jr. FG. 1990. Protoplast fusion and citrus improvement, *Plant Breed. Rev.* 8: 339–374.

Gruner R, Fels A, Qu F, Zimmat R, Steger G, Riesner D. 1995. Interdependence of pathogenicity and replicability with potato spindle tuber viroid. *Virol.* 209: 60–69.

Guerri J, Pina JA, Vives MC, Navarro L, Moreno P. 2004. Seed Transmission of Citrus leaf botch virus: Implications in Quarantine and Certification Programs. *Plant Dis*. 88: 906.

Hammond RW, Owens RA. 1987. Mutational analysis of potato spindle tuber viroid reveals complex relationships between structure and infectivity. *Proc. Natl. Acad. Sci*. 84: 3967–3971.

Hammond RW. 1994. *Agrobacterium*-mediated inoculation of PSTVd cDNAs onto tomato reveals the biological effects of apparently lethal mutations. *Virol*. 201: 36-45.

Henco K, Sanger H L, Riesner D. 1979. Fine structure melting of viroids as studied by kinetic methods. *Nucleic Acids Res*. 6: 3041-3059.

Holland JJ, Spindler K, Horodyski F, Grabau E, Nichol S, Vanderpol S. 1982. Rapid evolution of RNA genomes. *Science* 215: 1577–1585.

Hu Y, Feldstein PA, Bottino PJ, Owens RA. 1996. Role of the variable domain in modulating potato spindle tuber viroid replication. *Virol*. 219: 45–56.

Hu Y, Feldstein PA, Hammond J, Hammond RW, Bottino PJ, Owens RA. 1997. Destabilization of potato spindle tuber viroid by mutations in the left terminal loop. *J. Gen. Virol*. 78: 1199-1206.

Ito T, Ieki H, Ozaki K. 2000. A population of variants of a viroid closely related to citrus viroid-I in citrus plants. Arch. Virol. 145: 2105-2114.

Kalantidis K, Denti MA, Tzortzakaki S, Marinou E, Tabler M, Tsagris M. 2007. Virp1 is a host protein with a major role in Potato spindle tuber viroid infection in Nicotiana plants. *J. Virol*. 81: 12872–12880.

Keese P, Symons RH. 1985. Domains in viroids: evidence of intermolecular RNA rearrangements and their contribution to viroid evolution. *Proc. Natl. Acad. Sci*. 82: 4582–4586.

Kingman, J. F. C. 1982a. The coalescent. *Stochastic Processes Appl*. 13: 235-248.

Kingman, J. F. C. 1982b. On the genealogy of large populations. *J. Appl. Probab*. 19A: 27-43.

Kofalvi S, Marcos J, Canizares C, Pallas V, Candresse T. 1997. *Hop stunt viroid* (HSVd) sequence variant from prunus species: Evidence for recombination between HSVd isolates. *J. Gen. Virol.* 78: 3177-3186.

Koivisto P, Robins P, Lindahl T, Sedgwick B. 2004. Demethylation of 3-methylthymine in DNA by bacterial and human DNA dioxygenases. *J. Biol. Chem.* 279: 40470–40474.

Kolonko N, Bannach O, Aschermann K, Hu KH, Moors M, Schmitz M, Steger G, Riesner D. 2006. Transcription of potato spindle tuber viroid by RNA polymerase II starts in the left terminal loop. *Virol.* 347: 392–404.

Koonin EV, Dolja VV. 1993. Evolution and taxonomy of positive-strand RNA viruses: implications of comparative analysis of amino acid sequences. *Crit. Rev. Biochem. Mol. Biol.* 28: 375–430.

Krueger RR, Bash JA, Lee RF. 2005. Dweet mottle virus and Citrus leaf blotch virus. *Topics in Subtropics Newsletter* 3: 1.

Larkin MA, Blackshields G, Brown NP, Chenna R, McGettigan PA, McWilliam H, Valentin F, Wallace IM, Wilm A, Lopez R, Thompson JD, Gibson TJ, Higgins DG. 2007. Clustal W and Clustal X version 2.0. *Bioinformatics* 23: 2947-2948.

Lawrence DM, Rozanov MN, Hillman, BI. 1995. Autocatalytic processing of the 223-kDa protein of blueberry scorch carlavirus by a papainlike proteinase. Virol. 207: 127–135.

Li H, Roossinck MJ. 2004. Genetic bottlenecks reduce population variation in an experimental RNA virus population. *J. Virol*. 78: 10582-10587.

Librado P, Rozas J. 2009. DnaSP v5: A software for comprehensive analysis of DNA polymorphism data. *Bioinformatics* 25: 1451-1452.

Loss P, Schmitz M, Steger G, Riesner D. 1991. Formation of a thermodynamically metastable structure containing hairpin II is critical for infectivity of potato spindle tuber viroid RNA. *EMBO J*. 10: 719–727.

Mandahar CL. 2006. Multiplication of RNA plant viruses. ISBN 978-1-4020-4724-4. Springer. pp 99-100.

Maniataki E, Martinez de Alba AE, Sagesser R, Tabler M, Tsagris M. 2003. Viroid RNA systemic spread may depend on the interaction of a 71-nucleotide bulged hairpin with the host proteinVirP1. *RNA* 9: 346–354.

Marchler-Bauer A, Anderson JB, Chistaz F, Derbyshire MK, DeWeese-Scott C, Fong JH, Geer LY, Geer RC, Gonzales NR, Gwadz M, He S, Hurwitz DI, Jackson JD, Ke Z, Lanczycki CJ, Liebert CA, Liu C, Lu F, Lu S, Marchler GH, Mullokandov M, Song JS, Tasneem A, Thanki N, Yamashita RA, Zhang D, Zhang N, Bryant SH. 2009. CDD: specific functional annotation with the Conserved Domain Database. *Nucleic Acids Res.* 37: 205-10.

Marchler-Bauer A, Bryant SH. 2004. CD-Search: protein domain annotations on the fly. *Nucleic Acids Res.* 32: 327-331.

Martelli GP, Adams MJ, Kreuze JF and Dolja VV. 2007. Family *Flexiviridae*: a case study in virion and genome plasticity. *Annu Rev. Phytopathol*. 45: 73–100.

Matzura O, Wennborg A. 1996. RNAdraw: An integrated program for RNA secondary structure calculation and analysis under 32-bit Microsoft Windows. *Comput. Appl. Biosci.* 12: 247–249.

Muhlbach HP, Sanger HL. 1979. Viroid replication is inhibited by α-amanitin. *Nature* 278: 185–188.

Murakishi HH, Hartmann JX, Pelcher LE, Beachy RN. 1970. Improved inoculation of cultured plant cells resulting in high virus titre and crystal formation. *Virol.* 41: 365–367.

Murashige T, Skoog F, 1962. A revised medium for rapid growth and bioassays with tobacco tissue cultures. *Physiologia Vivorum* 56: 75–79.

Navarro L, Pina JA, Ballester JF, Moreno P and Cambra M. 1984. A new graft transmissible disease found in 'Nagami' kumquat. *Proc 9th Conf In Org Citrus Virologists* 234-240.

Navarro L, Roistacher CN, Murashige T. 1975. Improvement of shoot-tip grafting *in vitro* for virus-free citrus. *J. Amer. Soc. Hort. Science* 100: 471-479.

Nicholas KB, Nicholas HB Jr. 1997. GeneDoc: Analysis and Visualization of Genetic Variation. *EMBNEW. NEWS* 4: 14.

Owens RA, Chen W, Hu Y, Hsu YH. 1995. Suppression of potato spindle tuber viroid replication and symptom expression by mutations which stabilize the pathogenicity domain. *Virol*. 208: 554-564.

Owens RA, Steger G, Hu Y, Fels A, Hammond RW, Riesner D. 1996. RNA structural features responsible for potato spindle tuber viroid pathogenicity. *Virol.* 222: 144-158.

Owens RA, Thompson SM, Steger G. 1991. Effects of random mutagenesis upon potato spindle tuber viroid replication and symptom expression. *Virol.* 185: 18–31.

Owens RA, Thomson SM, Kramer M. 2003. Identification of neutral mutants surrounding two naturally occurring variants of Potato spindle tuber viroid. *J. Gen. Virol*. 84: 751–756.

Owens RA, Yang G, Gundersen-Rindal D, Hammond RW, Candresse T, Bar Joseph M. 2000. Both point mutation and RNA recombination contribute to citrus viroid III sequence diversity. *Virus Genes* 20: 243-252.

Palacio-Bielsa A, Foissac X, Duran-Vila N. 1999. Indexing of citrus viroids by imprint hybridization. *Eur. J. Plant Pathol*. 105: 897-903.

Palacio-Bielsa A, Romero-Durban J, Duran-Vila N. 2004. Characterization of citrus HSVd isolates, *Arch. Virol.* 149: 537–552.

Palukaitis P. 1987. Potato spindle tuber viroid: Investigation of the long-distance. intra-plant transport route. *Virol*. 158: 239-241.

Polivka H, Staub U, Gross HJ. 1996. Variation of viroid profiles in individual grapevine plants: novel grapevine yellow speckle viroid 1 mutants show alterations of hairpin I. *J. Gen. Virol*. 77: 155–161.

Price M, Schell J, Grosser J, Pappu SS, Pappu HR, Febres V, Manjunath KL, Niblett CL, Derrick KS, Lee RF. 1996. Replication of Citrus Tristeza Closterovirus in Citrus Protoplasts. *Phytopathol.* 86: 830-833.

Qi Y, Ding B. 2002. Replication of Potato spindle tuber viroid in cultured cells of tobacco and *Nicotiana benthamiana*: the role of specific nucleotides in determining replication levels for host adaptation. *Virol*. 302: 445–456.

Qi Y, Ding B. 2003. Inhibition of cell growth and shoot development by a specific nucleotide sequence in a noncoding viroid RNA. *Plant Cell* 15: 1360–74.

Qi Y, Pelissier T, Itaya A, Hunt E, Wassenegger M, Ding B. 2004. Direct role of a viroid RNA motif in mediating directional RNA trafficking across a specific cellular boundary. *Plant Cell* 16: 1741–1752.

Rackwitz HR, Rohde W, Sanger HL. 1981. DNA-dependent RNA polymerase II of plant origin transcribes viroid RNA into full-length copies. *Nature* 291: 297-301.

Rakowski AG, Symons RH. 1989. Comparative sequence studies of variants of avocado sunblotch viroid. *Virol. 73*:352–356.

Riesner D, Henco K, Rokohl U, Klotz G, Kleinschmidt AK, Domdey H, Jank P, Gross HJ, Sanger HL. 1979. Structure and structure formation of viroids. *J. Mol. Biol*. 133: 85-115.

Rigden JE, Rezaian MA. 1993. Analysis of sequence variation in grapevine yellow speckle viroid 1 reveals two distinct alternative structures for the pathogenic domain. *Virol.* 193: 474–477.

Roistacher CN, Blue RL. 1968. A psorosis-like virus causing symptoms only on Dweet tangor. *Proc 4th Conf Int Org Citrus Virologists* 13-18.

Ronquist F, Huelsenbeck JP. 2003. MRBAYES 3: Bayesian phylogenetic inference under mixed models. *Bioinformatics* 19: 1572-1574.

Sambrook J, Russell DW. 2001. *Molecular cloning. A laboratory manual*. Third edition. Cold Spring Harbor Laboratory Press, Cold Spring Harbor, New York.

Sanger HL, Klotz G, Riesner D, Gross HJ, Kleinschmidt A. 1976. Viroids are single-stranded covalently closed circular RNA molecules existing as highly base-paired rod-like structures. *Proc. Natl. Acad. Sci*. 73: 3852–3856.

Sano T, Candresse T, Hammond RW, Diener TO, Owens RA. 1992. Identification of multiple structural domains regulating viroid pathogenicity. *Proc. Natl. Acad. Sci*. 89: 10104–10108.

Satyanarayana T, Gowda S, Ayllon MA, Albiach-Marti MR, Dawson WO. 2002b. Mutational analysis of the replication signals in the 3'-nontranslated region of *Citrus tristeza virus*. *Virol*. 300: 140–152.

Satyanarayana T, Gowda S, Boyko VP, Albiach-Marti MR, Mawassi M, Navas-Castillo J, Karasev AV, Dolja V, Hilf ME, Lewandowski DJ, Moreno P, Bar-Joseph M, Garnsey SM, Dawson WO. 1999. An engineered closterovirus RNA replicon and analysis of heterologous terminal sequences for replication. *Proc. Natl. Acad. Sci*. 96: 7433–7438.

Schaffer A, Aravind A, Madden TL, Shavirin S, Spouge JL, Wolf YI, Koonin EV, Altschul SF. 2001. Improving the accuracy of PSI-BLAST protein database searches with composition-based statistics and other refinements. *Nucleic Acids Res.* 29: 2994-3005.

Schindler IM, Muhlbach HP. 1992. Involvement of nuclear DNA-dependent RNA polymerases in potato spindle tuber viroid replication: a reevaluation. *Plant Sci* 84: 221–229.

Schmitz A, Riesner D. 1998. Correlation between bending of the VM region and pathogenicity of different potato spindle tuber viroid strains. *RNA* 4: 1295–1303.

Schneider WL, Roossinck MJ. 2001. Genetic diversity in RNA viral quasispecies is controlled by host-virus interactions. *J. Virol*. 75**:** 6566-6571.

Schnolzer M, Haas B, Ramm K, Hofmann H, Sanger HL. 1985. Correlation between structure and Pathogenicity of *Potato spindle tuber viroid* (PSTV). *EMBO J*. 4: 2181–2190.

Schrader O, Baumstark T, Riesner D. 2003. A mini-RNA containing the tetraloop, wobble-pair and loop E motifs of the central conserved region of potato spindle tuber viroid is processed into a minicircle. *Nucleic Acids Res.* 31: 988–998.

Semancik JS, Roistacher CN, Rivera-Bustamante R, Duran-Vila N. 1988. Citrus cachexia viroid, a new viroid of citrus: Relationship to viroids of the exocortis disease complex. *J. Gen. Virol*. 69: 3059-3068.

Semancik JS, Weathers LG. 1972. Exocortis disease: evidence for a new species of "infectious" low molecular weight RNA in plants. *Nat. New Biol*. 237:242–44

Semancik JS. 1986. Separation of viroid RNA by cellulose chromatography indicating conformational distinctions. *Virol*. 155: 39-45.

Serra P, Gago S, Duran-Vila N. 2008. A single nucleotide change in *Hop stunt viroid* modulates citrus cachexia symptoms. *Virus Res.* 138: 130–134.

Steger G, Hoffmann H, Fortsch J, Gross HJ, Randles JW, Sanger HL, Riesner D. 1984. Conformational transitions in viroids and virusoids: Comparison of results from energy minimization algorithm and from experimental data. *J. Biomol. Struct. Dyn.* 2: 543-571.

Styer L. 1995. RNA in eukaryotic cells is synthesized by three types of RNA polymerases. Page 853. Chapter 33, RNA synthesis and Splicing. In: *Biochemistry*. Fourth edition. W.H. Freeman and Company, New York.

Sztuba-Solinska J, Bujarski JJ. 2008. Insights into the single-cell reproduction cycle of members of the family bromoviridae: lessons from the use of protoplast systems. *J. Virol*. 82: 10330-40.

Szychowski JA, Vidalakis G, Semancik JS. 2005. Host directed processing of citrus exocortis viroid. *J. Gen. Virol.* 86: 473 – 477.

Tabler M, Tsagris M. 2004.Viroids: petite RNA pathogens with distinguished talents. *Trends Plant Sci*. 9: 339–348.

Takebe I, Otsuki Y. 1969. Infection of tobacco mesophyll protoplasts by tobacco mosaic virus. *Proc. Nat. Acad. Sci.* 64: 843–848.

Tamura K, Dudley J, Nei M, Kumar S. 2007. *MEGA4*: Molecular Evolutionary Genetics Analysis (MEGA) software version 4.0. *Mol. Biol. Evol.* 24: 1596-1599.

Templeton AR, Crandall KA, Sing CF, 1992. A cladistic analysis of phenotypic associations with haplotypes inferred from restriction endonuclease mapping and DNA sequence data. III. Cladogram estimation. *Genetics* 132: 619–633.

Templeton AR, Sing CF. 1993. A gladistic analysis of phenotypic associations with haplotypes inferred from restriction endonuclease mapping. IV. Nested analysis with cladogram uncertainty and recombination. *Genetics* 134: 659-669.

Thompson J D, Gibson TJ, Plewniak F, Jeanmougin F, Higgins DG. 1997. The ClustalX windows interface: flexible strategies for multiple sequence alignment aided by quality analysis tools. *Nucleic Acids Res.* 24: 4876-4882.

Tommasini L, Roose M, Federici C, Ramadugu C, Fenton R, Nothnagel EA, Close TJ. 2009. Molecular mechanisms underlying rind separation in mandarin (*Citrus reticulata* B.) (Manuscript under preparation).

van den Born E, Omelchenko MV, Bekkelund A, Leihne V, Koonin EV, Dolja VV, Falnes PO. 2008. Viral AlkB proteins repair RNA damage by oxidative demethylation. *Nucleic Acids Res*. 36: 5451-5461.

Visvader J, Symons RH. 1985. Eleven new sequence variants of citrus exocortis viroid and the correlation of sequence with pathogenicity. *Nucleic Acids Res*. 13: 2907–2920.

Visvader JE, Symons RH. 1986. Replication of in vitro constructed viroid mutants: location of the pathogenicity-modulating domain in citrus exocortis viroid. *EMBO J*. 13: 2051–2055.

Vives MC, Galipienso L, Navarro L, Moreno P, Guerri J. 2001. The Nucleotide Sequence and Genomic Organization of Citrus Leaf Blotch Virus: Candidate Type Species for a New Virus Genus. *Virol*. 287: 225-233.

Vives MC, Martin S, Ambros S, Renovell A, Navarro L, Pina JA, Moreno P, Guerri J. 2008. Development of a full-genome cDNA clone of Citrus leaf blotch virus and infection of citrus plants. *Mol. Plant Pathol.* 9: 787-97.

Vives MC, Pina JA, Juárez J, Navarro L, Moreno P, Guerri J. 2004. Dweet mottle disease is probably caused by Citrus leaf blotch virus. Abstracts, *16th Conf Int Soc Citrus Virologists*, 98.

Vives MC, Rubio L, Galipienso L, Navarro L, Moreno P, Guerri J. 2002. Low genetic variation between isolates of Citrus leaf blotch virus from different host species and different geographical origins. *J. Gen. Virol*. 83: 2587-2591.

Warren GS, Hill SJL. 1989. Infection of suspension-cultured cells of carrot with tobacco mosaic virus. *Physiol. and Mol. Plant Pathol.* 35: 287-292.

Warrilow D, Symons RH. 1999. *Citrus exocortis viroid* RNA is associated with the largest subunit of RNA polymerase II in tomato in vivo. *Arch. Virol*. 144: 2367–2375.

Wassenegger M, Spieker RL, Thalmeir S, Gast F-U, Riedel L, Sanger HL. 1996. A single nucleotide substitution converts *Potato spindle tuber viroid* (PSTVd) from noninfectious to an infectious RNA for *Nicotiana tabacum*.*Virol.* 226: 191–197.

White PR. 1943. *A Handbook of Plant Tissue Culture*. The Jaques Cattell Press, Lancaster, Penn, 277 p.

White PR. 1963. *The cultivation of animal and plant cells*. Ronald Press Co, New York, 228 p

Widholm JM. 1972. The use of fluorescein diacetate and phenosafranine for determining viability of cultured plant cells. *Stain Technol*. 47: 189–194.

Yang Z, Rannala B. 1997. Bayesian phylogenetic inference using DNA sequences: a Markov chain Monte carlo method. *Mol. Biol. Evol.* 14: 717-724.

Zar JH. 1984. Biostatistical analysis. Second edition. Prentice Hall, Englewood Cliffs, New Jersey.

Zhong X, Archual AJ, Amin AA, Ding B. 2008. A genomic map of viroid RNA motifs critical for replication and systemic trafficking. *Plant Cell* 20: 35–47.

Zhong X, Itaya A, Ding B. 2005. Transfecting protoplasts by electroporation to study viroid replication, *Current Protocols in Microbiology 16D.4.1–16D.4.11*, John Wiley & Sons Inc.

Zhong X, Leontis NB, Qian S, Itaya A, Qi Y, Boris-Lawrie K, Ding B. 2006. Tertiary structural and functional analyses of Loop E motif in viroid RNA reveal its essential role in RNA-templated RNA replication by the nuclear transcription machinery. *J. Virol.* 80: 8566–8581.

Zhu Y, Green L,Woo Y-M, Owens R, Ding B. 2001. Cellular basis of potato spindle tuber viroid systemic movement. *Virol.* 279: 69–77.

Zhu Y, Qi Y, Xun Y, Owens R, Ding B. 2002. Movement of potato spindle tuber viroid reveals regulatory points of phloem-mediated RNA traffic. *Plant Physiol*. 130: 138–146.